TECHNISCHE UNIVERSITÄT WIEN
Vienna University of Technology

PAUL SCHERRER INSTITUT
PSI

Masterarbeit

Catalytic Hydrothermal Gasification of Microalgae: Start-up of a New Process Demonstration Unit

ausgeführt zum Zwecke
der Erlangung des akademischen Grades
eines Diplomingenieurs

genehmigt durch
Univ.Prof. Dipl.-Ing. Dr.techn. Hermann Hofbauer
E166 – Institut für Verfahrenstechnik,
Umwelttechnik und Technische Biowissenschaften

durchgeführt am Paul Scherrer Institut unter der Leitung von
Prof. Dr. Frédéric Vogel
Labor für Bioenergie und Katalyse,
Gruppe Katalytische Verfahrenstechnik

eingereicht an der Technischen Universität Wien
Fakultät für Maschinenwesen und Betriebswissenschaften

von
Jakob Breinl
0925342

Wien, März 2015

Acknowledgement

The present work was implemented within the scope of a cooperation project between Vienna University of Technology (TU Vienna) and the Paul Scherrer Institute (PSI). It could not have been carried out without the support of a couple of people.

First of all, I want to thank Prof. Hermann Hofbauer (TU Vienna) and Prof. Frédéric Vogel (PSI) for making this cooperation official.

Moreover, I want to thank Prof. Alexander Wokaun, who helped me to extend my status as an Erasmus exchange student, which allowed me to stay in a student apartment.

Further on, I want express my gratitude to Prof. Frederic Vogel (PSI) for accepting me in his working group and providing me the opportunity to work on such an exciting project. Whenever I worried about not solving problems or not getting enough results for my thesis, he assured me having valuable information at the end and encouraged me to continue along the path.

In addition, I want to thank whole-hearted my colleagues in Fredi's group. I was very lucky having Gael Peng as my supervisor, who immediately helped me out when I needed his assistance. Albert Schuler conducted the ICP analysis and created interesting scientific discussions by taking a look at things from a different view. Peter Hottinger set up the LabVIEW software and fixed all the problems that occurred therein. Erich de Boni and Lorenz Bäni did a great job in constructing the plant and assisting me whenever I faced a mechanical issue. Especially Erich invested a lot of time in this project and could be seen as the driving force.

Moreover, I want to warmly thank my girlfriend Teresa Turk. She was able to cheer me up, whenever I felt depressed because of things not working they way I wanted them to work, and made me see things a bit more relaxed.

Last but not least, I want to express my gratitude to my parents Yvonne and Eckart Breinl. They supported me during the whole period of my studies socially and financially, which allowed me to concentrate on my academic education. Without them I would not be at the point that I have reached now.

Abstract

A new PDU (Process Demonstration Unit) for continuous catalytic hydrothermal gasification of wet biomass was developed. The plant, which had a capacity of 1 kg/h, consisted of six main sections: a feeding section, a salt separator for hydrothermal liquefaction and salt separation, a salt removal section, a catalytic reactor for hydrothermal gasification, a pressure control section and a phase separator. This work aimed at assessing and improving the stability of the new PDU for the production of methane. The assessment was conducted by an experimental approach including salt separation tests with model solutions and liquefaction- and gasification tests of microalgae (*Phaeodactylum tricornutum*).

At first, salt separation tests with model solutions were conducted. The aim was to get familiar with the new pilot plant and its equipment and to investigate the performance of the salt separator. The model solutions were aqueous salt solutions of Na_2SO_4 (0.1 mol/kg) and K_2SO_4 (0.05 mol/kg) with and without the addition of isopropanol (10 wt%). The experiments were performed at a nominal pressure of 280 bar and a temperature profile for the salt separator of about 240 °C at the bottom and 430 °C at the top. The mass flow rate of feed and brine effluent were in the range of 16.5-18.2 g/min and 1.6-3.2 g/min. Measurement of the electrical conductivity and sulfur analysis of brine- and reactor effluent showed that the salts could be separated and concentrated very efficiently. The addition of isopropanol did not have a significant effect on the separation efficiency. However, the mass balance with respect to sulfur could not be closed indicating salt deposition inside the salt separator.

As a next step, liquefaction tests of microalgae were carried out. The aim was to study the salt separator when working with microalgae. For those tests the catalytic reactor was not needed and bypassed. The feed contained about 8-13 wt% Ph. tricornutum, its mass flow rate was 17.5-19.7 g/min and the working pressure was set to 280 bar. The temperatures at the bottom and the top of the salt separator were in the range of 180-300 °C and 390-430 °C. In all tests the reactor effluent contained a tarry and an aqueous phase and its electrical conductivity reached significantly high values. When the temperature at the bottom of the salt separator was rather high, the brine effluent had a clear orange-brown color and tar could be found on the filter. When the temperature at the bottom of the salt separator was rather low, the brine effluent had a muddy green-brown color and non-liquefied feed could be found on the filter. Measurement of the electrical conductivity and sulfur analysis indicated more efficient salt separation for harsher conditions inside the salt separator with respect to temperature. Visual inspection of the interior of the salt separator proved the expectation of salt deposition.

Furthermore, liquefaction tests of microalgae with subsequent S-adsorption were conducted. The aim was to assess the suitability of ZnO as a S-adsorber and to determine its catalytic activity regarding hydrothermal gasification. Therefore, the catalytic reactor was filled with ZnO and not bypassed anymore. In parallel, the conditions in the salt separator should be improved. The feed contained about 6.5-8.6 wt% Ph. tricornutum, its mass flow rate was 18.9-

23.0 g/min and the working pressure was set to 280 bar. The temperatures at the bottom and the top of the salt separator were in the range of 230-250 °C and 400-420 °C. The temperature inside the reactor was in the range of 380-410 °C. As in the previous algae tests, the reactor effluent contained a tarry and an aqueous phase. However, the aqueous phase was a little bit clearer indicating some catalytic activity of ZnO. Indeed, a gas containing mostly H_2 and CO_2 was produced, but the carbon gasification efficiency was only around 5%. Moreover, sulfur analysis suggested ZnO being a promising S-adsorber under hydrothermal conditions. Again, the electrical conductivity of the reactor effluent was very high and most of the times higher than the one of the brine effluent. It was not possible to reach an operating point for the salt separator, where neither tar nor non-liquefied feed was found on the filter of the brine effluent. It was concluded that the temperature at the bottom of the salt separator had to be at least 280 °C for complete liquefaction and some tar in the brine effluent had to be accepted.

Finally, hydrothermal gasification tests of microalgae were carried out. The aim was to reach stable working conditions for a continuous production of methane. The lower section of the reactor was filled with ZnO for S-adsorption, whereas the higher section was filled with the catalyst (5%-Ru/C) for subsequent gasification. The feed contained 9.0-10.5 wt% Ph. tricornutum, its mass flow rate was about 17 g/min, the WHSV was up to 0.24 $g_{Org}/g_{Cat}-h$ and the working pressure was set to 280 bar. The temperatures at the bottom and the top of the salt separator were in the range of 280-310 °C and 420-440 °C. The temperature inside the reactor was in the range of 375-410 °C. In contrast to the previous algae tests, the reactor effluent was clear and colorless throughout the tests indicating high gasification efficiency. The TOC content stayed below 1000 mg/L and a gas containing mostly CH_4 (57 vol%) and CO_2 (36 vol%) could be produced. No catalyst deactivation could be detected while processing microalgae for 6.4 h. The carbon content in the brine effluent was low, too (1300-1500 mg/kg), although tar could be found on the filer again. The nitrogen concentration of brine- and reactor effluent reached values close to the nitrogen concentration of the feed. The pH values of brine- and reactor effluent were 5.94 and 8.44, respectively. The presence of ammonia in the reactor effluent could be expected. ICP analysis showed that K, Na, P and S could be separated and concentrated in the brine effluent very efficiently. An elemental separation efficiency in the following order could be identified: K > Na > P > S. Although none of those elements could be found in the reactor effluent, its electrical conductivity reached again very high values.

In summary, the overall goal of starting up the new PDU and reaching a stable operating point for a continuous production of bio-methane from microalgae could be achieved. Nevertheless, a number of unsolved issues could be identified leaving room for process optimization.

Contents

List of Figures

List of Tables

1. Introduction

1.1. Motivation

The world's energy demand is increasing constantly. In 2012 the primary energy supply accounted for more than 13 300 Mtoe[1]; about 80% were delivered by fossil fuels (natural gas, oil, coal) [15]. Since these energy resources are non-renewable, i.e. natural regeneration takes much longer than anthropogenous utilization, the atmospheric carbon dioxide concentration is rising (Figure 1.1). This reinforces the greenhouse effect causing many environmental stresses.

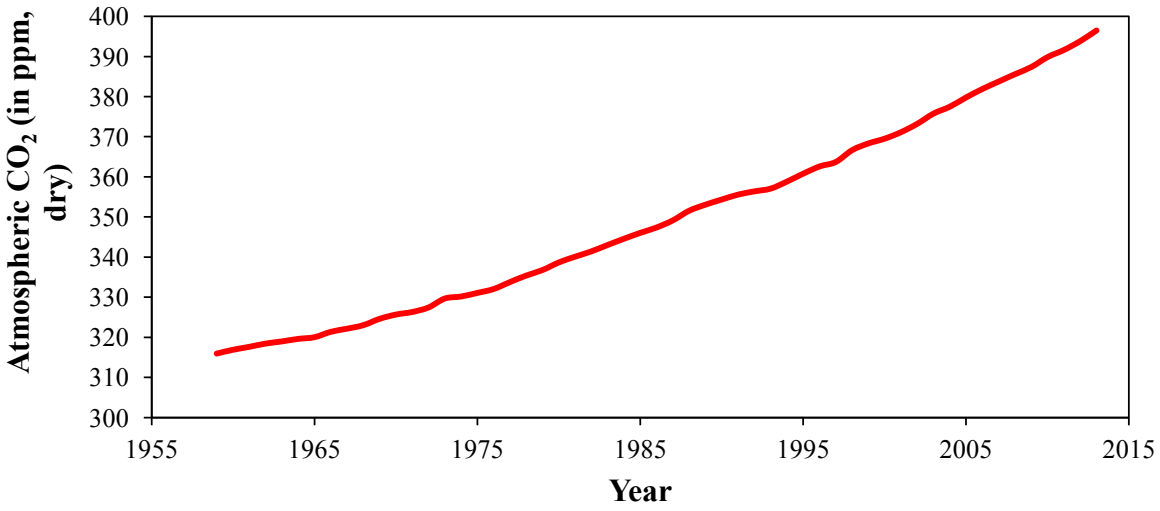

Figure 1.1: Atmospheric CO_2. Data from [3].

In September 2013 the Fifth Assessment Report of IPCC's Working Group I was published including the following conclusions [16]:

- "Warming of the climate system is unequivocal, and since the 1950s, many of the observed changes are unprecedented over decades to millennia. The atmosphere and ocean have warmed, the amounts of snow and ice have diminished, sea level has risen, and the concentrations of greenhouse gases have increased [. . .]."
- "Human influence on the climate system is clear. This is evident from the increasing greenhouse gas concentrations in the atmosphere, positive radiative forcing, observed warming, and understanding of the climate system."
- "Continued emissions of greenhouse gases will cause further warming and changes in all components of the climate system. Limiting climate change will require substantial and sustained reductions of greenhouse gas emissions."

[1] 1 Mtoe = 41.87 PJ

This energy and climate question is not only an environmental problem but also a political and economical issue. For 2020 the EU enacted the "20-20-20" targets (20% reduction of greenhouse gas emissions compared to 1990, 20% share of EU's energy consumption from renewable resources, 20% higher energy efficiency) through the climate and energy package [17]. According to Figure 1.2, the supply of renewable energy between 2012 and 2020 has to be doubled (keeping the demand constant) to fulfill at least the second target.

The European Renewable Energy Council (EREC) reports a "[...] pathway towards a 100% renewable energy supply system by 2050 and clearly shows that it is not a matter of technology, but rather a matter of making the right choices today [...]" [18]. In addition, this report demonstrates the significance of biomass (biofuels) for a sustainable transport sector and demonstrates EU's long-term economical, environmental and social benefits of such a system.

Further research in the fields of renewable energy is of great importance to develop more efficient and competitive solutions to meet the EU targets for 2020 and to generate a sustainable energy system.

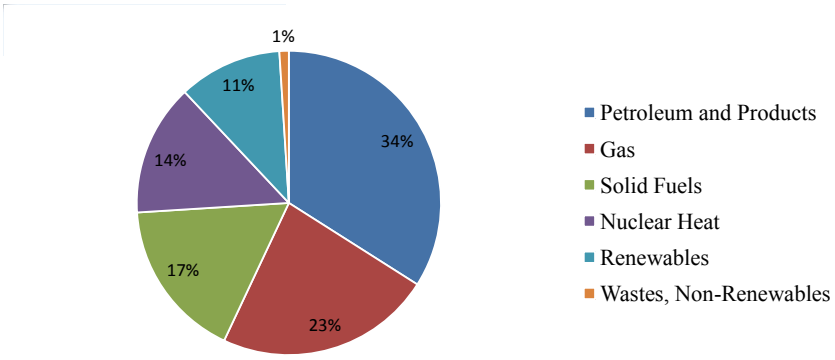

Figure 1.2: EU-28 Gross Inland Consumption - Energy Mix 2012 (Total: 1682 Mtoe). Data from [4].

1.2. Methane from biomass

1.2.1. Comparison of present technologies

The European Commission defined biomass as "[...] the biodegradable fraction of products, waste and residues from biological origin from agriculture (including vegetal and animal substances), forestry and related industries including fisheries and aquaculture, as well as the biodegradable fraction of industrial and municipal waste [...]" [17]. This wide range of possible feedstocks has led to the development of different conversion technologies depending on the desired products. They can be grouped in thermal, biological and mechanical conversion processes. Table 1.1 shows which product is obtained through which process and in which form it can be sold on the market.

Table 1.1: Biomass conversion pathways. Adapted from [11].

		Thermal conversion				**Biological conversion**		**Mechanical conversion**
		Pyrolysis	Liquefaction	Gasification	Combustion	Fermentation	Anaerobic digestion	Oil milling
Product	Charcoal	x						
	Bio-oil	x	x					
	Plant oil							x
	Organic solvents/acids/alcohols					x		
	Fuel-gas	x		x				
	Bio-gas						x	
	Heat				x			
Market	Chemicals	x	x	x		x		
	Heat	x	x	x	x			
	Electricity	x	x	x	x		x	x
	Transport fuel, etc.	x	x	x			x	x

Methane is produced via pyrolysis, gasification (high-temperature, hydrothermal) and anaerobic digestion. In the case of gasification it is called *bioSNG* (biological Synthetic Natural Gas) and in the case of anaerobic digestion *biogas* [19].

Pyrolysis is a thermo-chemical process where the feed is heated up to temperatures up to 600 °C in the absence of oxygen. After the evaporation of free and bound water (i.e. drying period from 0 to 200 °C), the long-chain organic compounds are decomposed to gaseous and liquid compounds. Charcoal is formed, too, and partial oxidation occurs if the feed contains oxygen [20]. Depending on the feed composition, heating rate, final temperature and residence time, the product yields will be different. Nevertheless, the yield of gaseous products like methane will be poor [21–23]. Therefore, pyrolysis is mainly used for the production of liquid fuels and charcoal.

Table 1.2: Main characteristics of some processes for biomass conversion to methane. Partly adapted form [12].

Characteristic	Conventional gasification & methanation	Anaerobic digestion	Hydrothermal gasification
Feed type	Wood, grass (dry)	Manure, household residues, sewage sludge, marine algae	Most wet types
Residence time	< 10 min	< 50 days	< 30 min
Advantages	High efficiency for dry biomass, close to commercialization	Commercially available, fertilizer as by-product	High efficiency, fertilizer as by-product
Disadvantages	Low efficiency for wet biomass	Organic residues, low efficiency, plant size	Technical and economical barriers
Technological readiness	Good (1 MW_{SNG} PDU in Güssing, Austria 2008)	Very good (commercially available)	R&D

High-temperature gasification (conventional gasification) is a follow-up process of pyrolysis and takes place at temperatures between 500 and 1300 °C (mainly between 700 and 1200 °C). The pyrolysis products are reacting with each other under aerobic conditions through the addition of oxygen, air or steam. The air-fuel equivalence ratio (i.e. ratio of the fuel-to-oxidizer ratio to the stoichiometric fuel-to-oxidizer ratio) is between 0 and 1. The new product is a gas mixture containing carbon monoxide, carbon dioxide, hydrogen, methane, steam and – if gasified with air – nitrogen. Undesired side products are tar, ash and dust. The composition of the gas depends on the feed composition and on the choice of gasification agent, reactor, heat transfer, temperature and pressure [20]. After cleaning and conditioning, the gas is treated in a heterogeneously catalyzed process where hydrogen and carbon monoxide are converted to methane [24, 25]. The thermal efficiency of high-temperature gasification is only high (up to 70-80%) if the feed is dry. It drops drastically with increasing water content [26].

Anaerobic digestion is a state-of-the-art biological technology for the production of methane from wet biomass (dry matter < 15%). A microbial conversion of the organic matter takes

place at temperatures between 20 and 60 °C in the absence of oxygen. The produced biogas contains methane (45-75%), carbon dioxide (25-55%), steam (2-7%) and trace elements like hydrogen sulfide, nitrogen, oxygen and hydrogen. One drawback of this process is the very long necessary residence time (up to 50 days in a continuously stirred tank reactor, CSTR), which causes the digesters to become huge (up to 8000 m^3) [20]. This is why more and more emphasis is put on developing new processes, especially solid-state processes (dry matter > 15%), to densify the feed [27,28]. Another drawback is that not the entire organic fraction can be digested by the microorganisms. Some organic parts stay in the residual sludge together with the nutrients [29].

Hydrothermal gasification is another technology that is suitable for producing methane from high-moisture biomass like manure, sewage sludge, wet wastes and algae. The organic matter is (nearly) fully converted catalytically at temperatures and pressures around the critical point of water (374 °C, 22.1 MPa). Salts contained in the feed can be recovered for the reuse as nutrients due to their low solubility in supercritical water. The absence of a drying step and low residence times result in a very energy-efficient process [10,30,31]. A detailed description of the hydrothermal gasification technology will be given in Section 2.

In Table 1.2 the main technical and economical aspects of conventional gasification, anaerobic digestion and hydrothermal gasification for the production of methane are summarized.

1.2.2. Potential of microalgae as a sustainable biomass source

Microalgae are all kind of unicellular and simple multicellular photosynthetic micro-organisms like prokaryotes and eukaryotes. In contrast, macroalgae are composed of multiple cells which organize to structures like roots, stems, and leaves of higher plants [32,33]. Microalgae can be either autotrophic, heterotrophic or both (i.e. mixotrophic). Autotrophic microalgae use sunlight to convert inorganic carbon from atmospheric carbon dioxide to organic matter; this is the well-known process of photosynthesis. Heterotrophic microalgae consume organic carbon produced by other organisms in the environment [34]. Photosynthesis is a two-stage process with a light-dependent and a light-independent step. Initially, energy carrier molecules are produced through the consumption of sunlight and water and the release of oxygen. Then the energy carrier molecules are converted to organic matter through the Calvin-Benson cycle (see Figure 1.3) [5]. The product composition depends on the type of microalgae, the light intensity, carbon dioxide- and oxygen concentration and the nutrients. A detailed description of microalgae is presented by Richmond [35].

Microalgae can be cultivated in a variety of systems. There is no global (technical and economical) optimum; the cultivation system has to be designed for each strain individually. Basically, microalgae can be produced either in open systems, like lakes and ponds, or in closed systems called photo-bioreactors [36]. A more detailed description and a comparison of the different systems can be found elsewhere [37–40].

For the production of biofuels microalgae show a couple of advantages compared to higher plants like palm oil, rape, sunflower, soybeans, corn, etc. [32, 41–43]:

- Microalgae have a very high growth rate (e.g. 1-3 doublings/day) and make it possible to meet fuel demand with limited land use (see Table 1.3).
- Microalgae can be cultivated in all kind of waters (fresh/brackish/saline) and consume less water than land crops. Therefore, microalgae can be cultivated in areas that are not suitable for conventional agriculture provided that water is available.
- Microalgae utilize nitrogen and phosphorus providing an additional way of wastewater treatment.
- Energy production from microalgae does not compete with conventional agriculture, which is a big issue in the case of other energy crops (see [44]).
- Very efficient carbon dioxide mitigation is possible due to the tolerance of microalgae to high carbon dioxide concentrations (1 kg of microalgae requires about 1.8 kg of CO_2).
- In photo-bioreactors microalgae can be cultivated throughout the year leading to a high productivity.

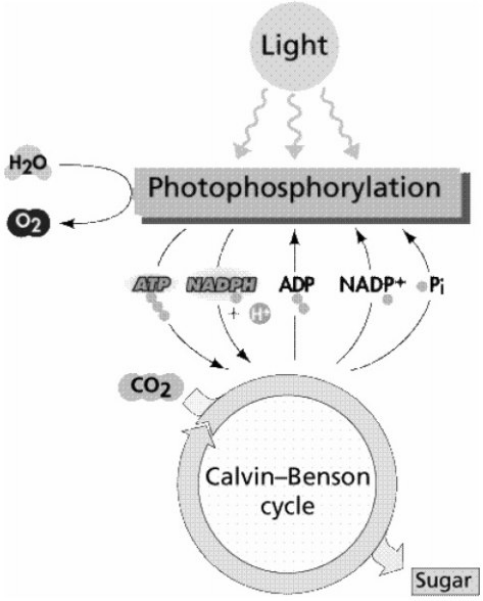

Figure 1.3: Overview of the two phases during photosynthesis [5].

These features led to a growing interest of algal biomass as a promising renewable energy source in the last few years and the consideration of algal fuels as the 3rd generation of biofuels [45].

Despite those very promising aspects, recent techno-economic studies demonstrated that bio-energy production from microalgae is not yet cost-competitive with energy production from other biomass- or fossil sources [13, 46–49]. Particularly the necessity to grow microalgae

in artificial culture systems contributes the most to investment and production costs [49]. However, it is believed that there is room for significant cost reduction through both biological and engineering improvement opportunities [47].

Table 1.3: Energy productivity of some biomass feedstocks [13].

Plant source	Energy productivity (in GJ/ha-year)
Algae	704.44 - 905.71
Corn	198.13 - 317.00
Canola	144.09 - 176.11
Switchgrass	150.95 - 243.85

1.2.3. Reasons for methane

Although different liquid and gaseous fuels can be produced out of biomass, methane is a very interesting option due to the following aspects:

- Transportation- and distribution infrastructure is available [10].
- Its use as a heating fuel is accepted and well-established [10].
- It can be used as a fuel for CNG (Compressed Natural Gas) cars and for power generation in a gas turbine [10].
- Compared to diesel- and gasoline cars, CNG cars show the lowest emissions with respect to NMHC (non-methane hydrocarbons), NO_x (nitrogen oxide) and fine particles [50].

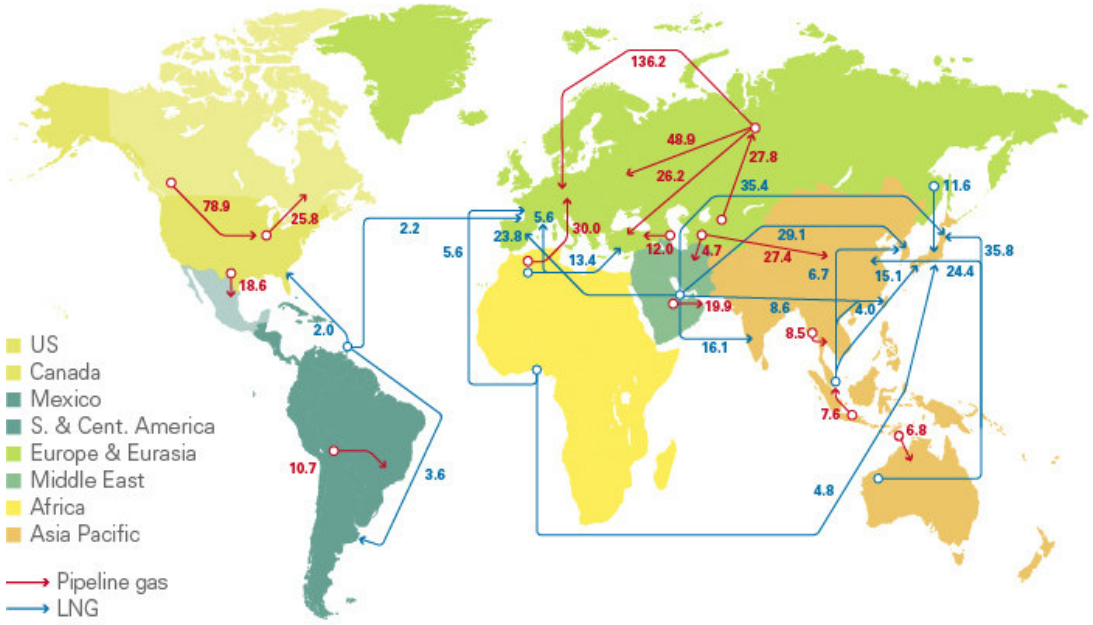

Figure 1.4: Natural gas major trade movements in 2013 (in billion cubic meters) [6].

Moreover, the use of renewable methane (bioSNG or biomethane) would allow many countries to become less economical and political dependent on natural gas exporting countries (see Figure 1.4).

2. Theoretical background and literature review

2.1. Properties of pure sub- and supercritical water

2.1.1. Phase diagram

The p,T- and the ρ,T-phase diagram of water are depicted in Figure 2.1. The curve in the p,T-diagram is called saturation curve [9] and shows the dependence of the vapor pressure on the temperature during an isochoric heat-up. For a specific temperature and pressure, liquid water is in equilibrium with its vapor. With increasing temperature the vapor pressure and the density of the vapor increase, whereas the density of the liquid decreases. At a certain point, the critical point (T_c = 374 °C, p_c = 22.1 MPa, ρ_c = 322 kg/m^3), liquid and vapor reach the same density and become a single homogeneous fluid. Water at $T > T_c$ and $p > p_c$ is called *supercritical* water, otherwise *subcritical* water. The extrapolation of the saturation curve (dashed black line) is the *pseudo-critical line*. It connects the *pseudo-critical points*, which are the points above the critical point of water where the specific (isobaric) heat capacity shows a maximum (see section 2.1.2). Water above the pseudo-critical line has a higher density (HD) and is more liquid-like, whereas it has a lower density (LD) and is more gas-like below the pseudo-critical line [51].

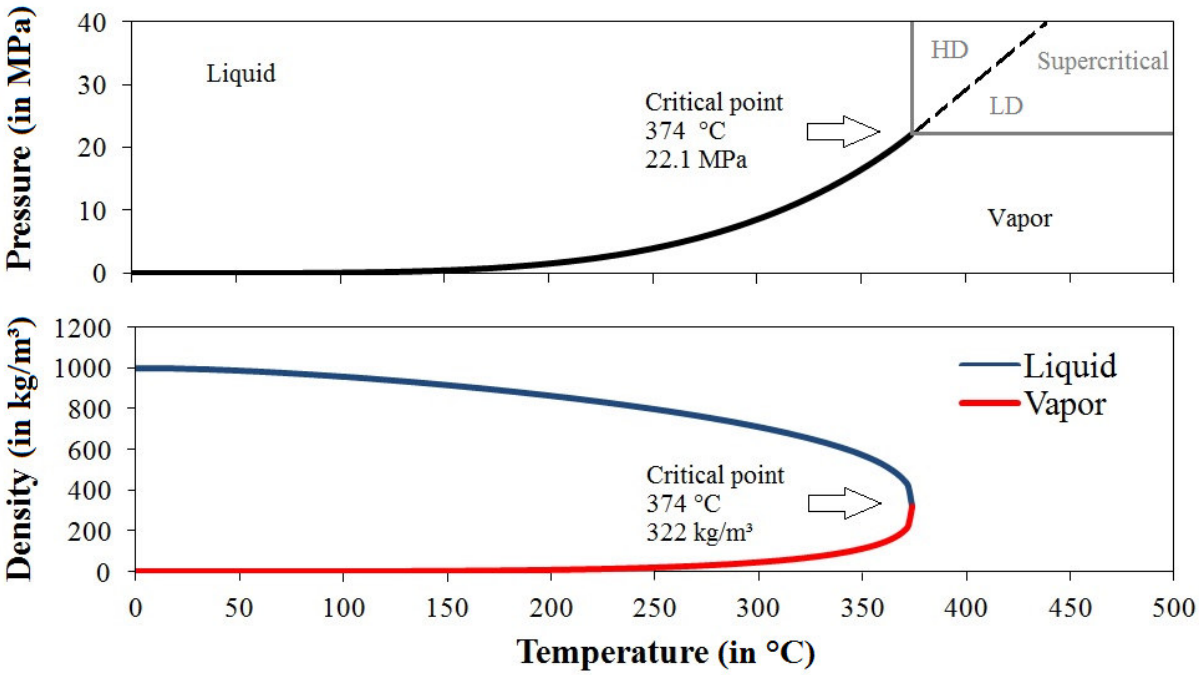

Figure 2.1: Top: phase diagram of water. Bottom: density of the liquid- and the vapor phase during isochoric heat-up. Data from [7].

2.1.2. Specific enthalpy and specific heat capacity

The dependence of the specific enthalpy and the specific (isobaric) heat capacity on temperature and pressure can be seen in Figure 2.2. If subcritical water is heated up under isobaric conditions, at a certain temperature (i.e. the boiling point) the liquid-vapor phase change occurs, which causes the specific enthalpy to increase abruptly. With increasing pressure this "enthalpy jump" moves towards higher temperatures, becomes smaller and turns into a smooth s-shape in the supercritical region. In general, the specific isobaric heat capacity is defined as the partial derivative of the specific enthalpy with respect to temperature at constant pressure [52]. Therefore, the specific heat capacity represents the slope of the specific enthalpy. The temperature in the supercritical regime, where the specific heat capacity shows a maximum corresponding to an s-shaped enthalpy curve, is called *pseudo-critical temperature* [10].

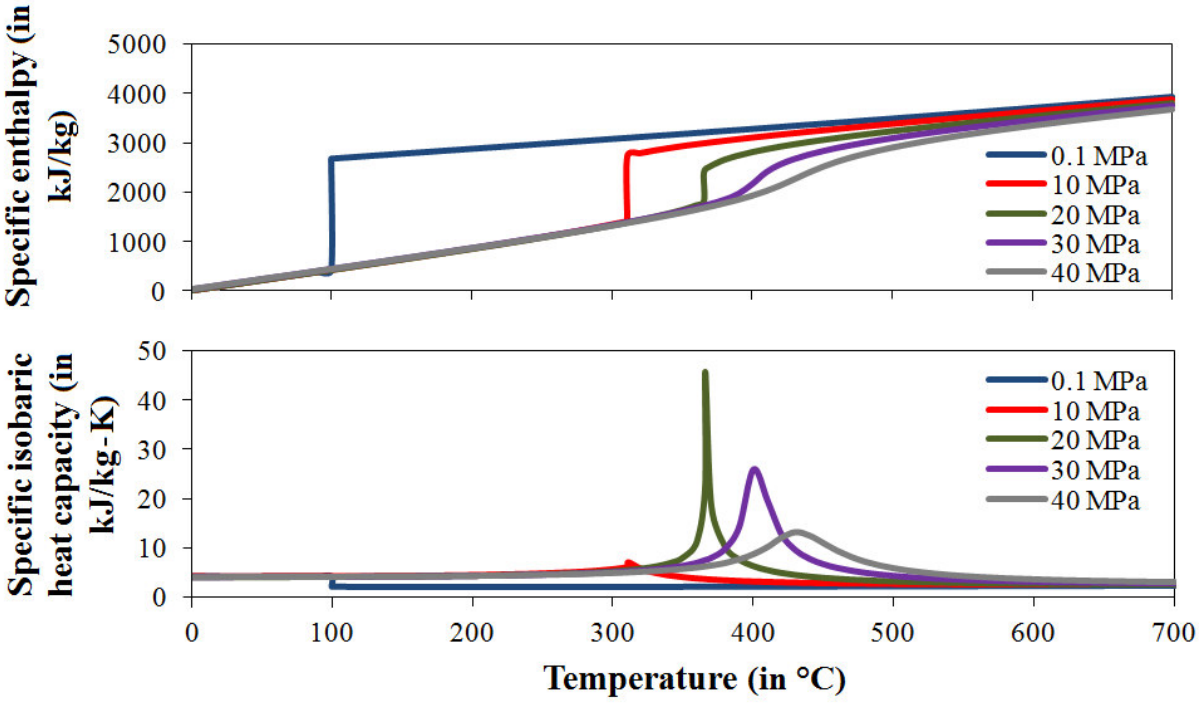

Figure 2.2: Specific enthalpy and specific (isobaric) heat capacity of water during isobaric heat-up at different pressures. Data from [7].

2.1.3. Density and relative permittivity

The relative permittivity is a dimensionless parameter that describes the polarity of a dielectric compared to vacuum [53]. The static (zero-frequency limit) relative permittivity is a measure of the electrostatic interactions between ionic solutes and the solvent [8]. Figure 2.3 shows the dependence of the static relative permittivity and the density of water on temperature and pressure. Both parameters decrease monotonically with increasing temperature independently from pressure. The curves show characteristics similar to the ones of the specific enthalpy

and the specific isobaric heat capacity. The change of the static relative permittivity and the density during phase transition is more distinct for subcritical- than for supercritical water. In comparison, methanol has a static relative permittivity of about 33, acetone of about 21 and diethylether of about 4 at ambient conditions [54].

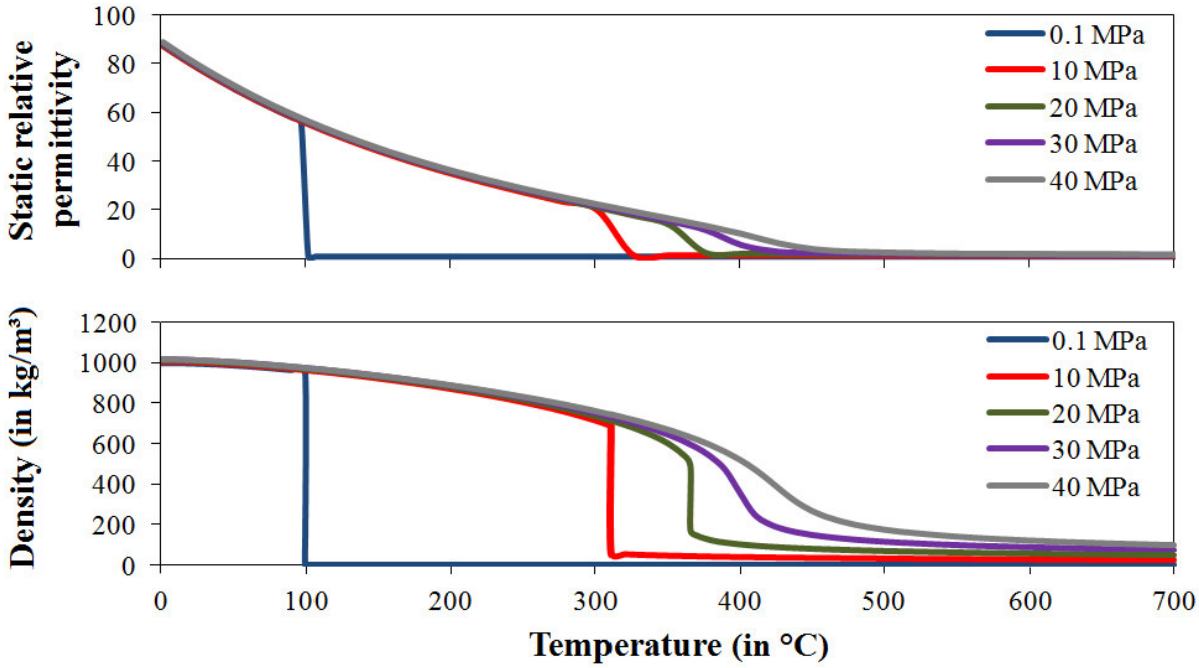

Figure 2.3: Static relative permittivity and density of water during isobaric heat-up at different pressures. Data from [7,8].

2.1.4. Viscosity

The temperature dependence of the dynamic viscosity of water at different pressures is depicted in Figure 2.4. The viscosity is decreasing with increasing temperature independently from pressure and there is no abrupt change during transition from the sub- to the supercritical regime for $p > p_c$.

2.1.5. Ionization constant

The ionization constant of pure water is the defined as the product of its ion concentrations resulting from self-dissociation [31]:

$$K_W = [H_3O^+][OH^-] \tag{2.1}$$

In Figure 2.5 the decadal logarithm of the ionization constant is plotted as a function of temperature at 0.1, 25 and 50 MPa. In the subcritical area the ionization constant increases with

increasing temperature and reaches a maximum with a value of about three orders of magnitude higher than at ambient temperature. After the phase change to supercritical water the ionization constant decreases again. The extent of the decline depends strongly on the pressure. At pressures close to p_c the ionization constant drops to values of some orders of magnitude lower compared to elevated pressures [9].

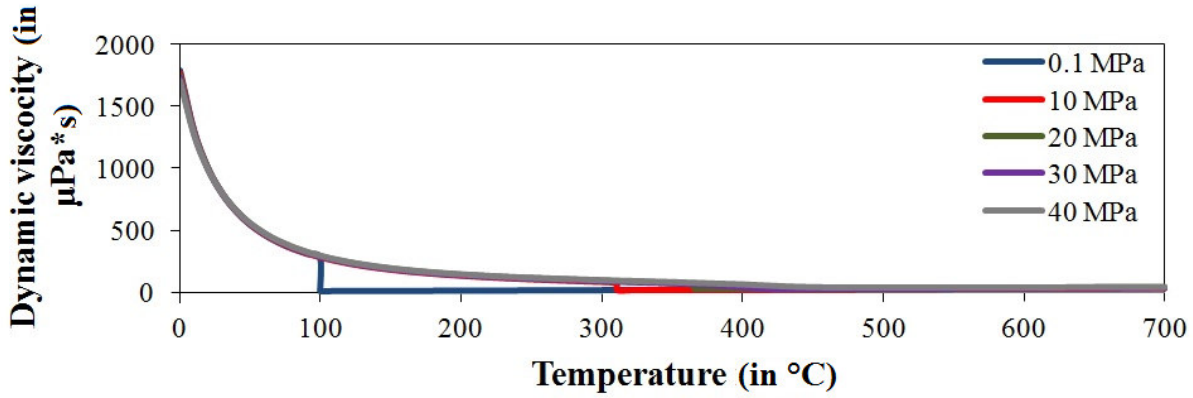

Figure 2.4: Dynamic viscosity of water during isobaric heat-up at different pressures. Data from [7].

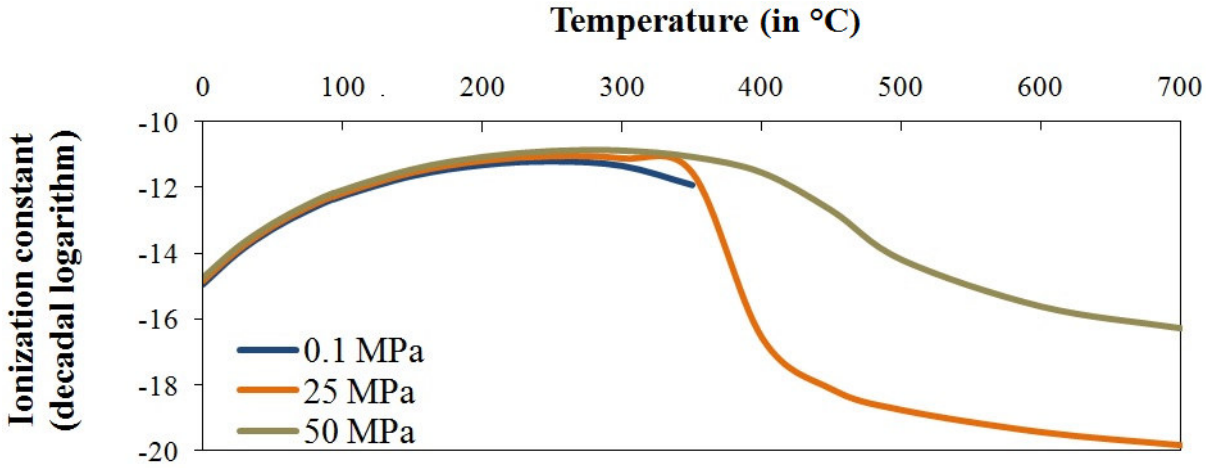

Figure 2.5: Ionization constant of water during isobaric heat-up at different pressures. Data from [9].

2.1.6. Consequences

The different properties of water above and below the critical point bring out many aspects that are of interest for hydrothermal treatment of biomass:

- The great influence of temperature and pressure near the critical point of water allow adjustment of the properties according to the requirements of interest [55].

- A low (static) relative permittivity of water under supercritical conditions, similar to those of non-polar organic solvents under ambient conditions, results in poor solubility of salts and improved solubility of organic substances and gases [10, 56]. This makes the formation of tar and coke less possible [57, 58] and a separation of salts sufficient [59–62].
- The high density (compared to gases) and the low viscosity (compared to liquids) of supercritical water accelerate heat and mass transfer [10, 63].
- The ion product and the density of water have a big influence on ionic reactions, like acid- and base catalyzed reactions, and free radical reaction pathways [55, 64].
- Pressurized aqueous solutions can be heated in a way so that no latent heat of vaporization has to be supplied [10, 31].

2.2. Hydrothermal gasification of biomass

2.2.1. General aspects of biomass reactions in sub- and supercritical water

Hydrothermal treatment of biomass comprises processes in water slurries at elevated pressures and temperatures, where organic materials are converted into useful fuels or chemicals. The conversion takes place either under sub- or under supercritical conditions. The two main technologies for fuel production are hydrothermal liquefaction and gasification. Hydrothermal liquefaction is the appropriate process if liquid fuels are the desired products. The wet biomass is treated under subcritical conditions at temperatures typically between 250 and 370 °C and at pressures between 4 and 22 MPa long enough to break down the solid bio-polymeric structure to mainly liquid components. If gaseous fuels are the desired products, hydrothermal gasification is the chosen path. The wet biomass is usually processed under supercritical conditions, but – with a sufficient catalyst – gasification is also possible below the critical point of water. The wet biomass is not only broken down to liquid components, but rather gasified subsequently [30]. Osada *et al.* [65] defined three regions for hydrothermal gasification: High-temperature supercritical water gasification, low-temperature supercritical water gasification, subcritical water gasification.

Compared to other technologies, the feed does not have to be dried for hydrothermal treatment. To the contrary, water plays an important role as a solvent, a catalyst, a catalyst precursor and a reactant [58].

The ionization constant of water under subcritical and under HD-supercritical conditions reaches values of some orders of magnitude higher than under ambient or LD-supercritical conditions (see sections 2.1.1 and 2.1.3). Therefore, ionic reactions, like acid- and base catalyzed reactions, are favored in this region. In contrast, in LD-supercritical water free radical reactions are favored [64, 66].

The low relative permittivity of water in near- and supercritical water (see section 2.1.3) allows miscibility of water and non-polar organic substances. This makes reactions like hydrolysis of fats and proteins in aqueous media possible. Moreover, the relative permittivity has an influence on the reaction rates. If the transition state of a certain reaction is more polar than its reactants, a high relative permittivity lowers the activation energy leading to an increased reaction rate [55, 67]. The change of the (static) relative permittivity around the critical point is related to the drastic change in density (see Figure 2.3). Thus, density, which is strongly depending on pressure and temperature, can be used as a lever for manipulating the relative permittivity and can boost reaction kinetics [67].

In the following sections the general events during hydrothermal gasification will be discussed. The transformation of wet biomass into gaseous products takes place in two main steps: Degradation of biomass to smaller compounds (liquefaction) and gasification of these fragments. The second step differentiates hydrothermal gasification from hydrothermal liquefaction [31].

2.2.2. Biomass degradation to smaller molecules in sub- and near-critical water

Carbohydrates, lignin, fats and proteins are the main building blocks of typical biomass feedstocks with varying compositions. At the first conversion step (i.e. liquefaction), the polymers are decomposed to smaller compounds [68]. The wide range of different materials makes it very difficult to identify the exact reaction pathways and their kinetics. Many reactions can occur simultaneously, which compete with each other and depend strongly on feed composition, temperature, pressure, residence time, pH, reactor design and catalytic effects. However, a number of representative key compounds have been chosen and investigated to get an idea of the chemical processes during hydrothermal conversion of biomass [66]. The findings of the numerous studies are summarized in a few excellent reviews [31, 55, 66, 68]. The general reaction patterns concerning hydrothermal liquefaction described therein will be briefly discussed now:

- Reaction pathways:

  The main reactions are: Hydrolysis, dehydration, decarboxylation, decarbonylation, deamination, isomerization, condensation (e.g. aldol condensation, Friedel-Crafts alkylation/acylation), aldol splitting, Canizzaro reaction, Diels-Alder reaction, rearrangement, oxidation/reduction and organometallic reactions.

- Conversion of carbohydrates:

  Hydrolysis breaks the ether- and ester bonds of polysaccharides (cellulose, hemicellulose, starch) resulting in the formation of HMF (5-hydroxymethylfurfural) and sugars like glucose, fructose, maltose, xylose, mannose and galactose. They degrade further to different alcohols, furans, acids, aldehydes and aromatic compounds.

- Conversion of lignin:

  Various phenols and methoxy phenols are formed by hydrolysis of the ether bonds of lignin.

- Conversion of fats:

  Chemically, fats and oils are triacylglycerides (TAGs), i.e. triesters of glycerol and fatty acids. Under hydrothermal conditions the TAGs are split to form free fatty acids and glycerol. Glycerol degrades further to different alcohols and aldehydes (methanol, acetaldehyde, propionaldehyde, acrolein, allyl alcohol, ethanol, formaldehyde), whereas the fatty acids produce long-chain hydrocarbons.

- Conversion of proteins:

  In hydrothermal systems the peptide bond is hydrolyzed, which is the C-N bond of proteins linking the amino acids together. The free amino acids decompose to different hydrocarbons, amines, aldehydes and acids. Some products are similar to the ones of the saccharides degradation.

- Byproducts:

  Gases like CO, CO_2, H_2 and CH_4 are produced during liquefaction, too. Additionally, the formation of tars and solid residue is often not avoidable.

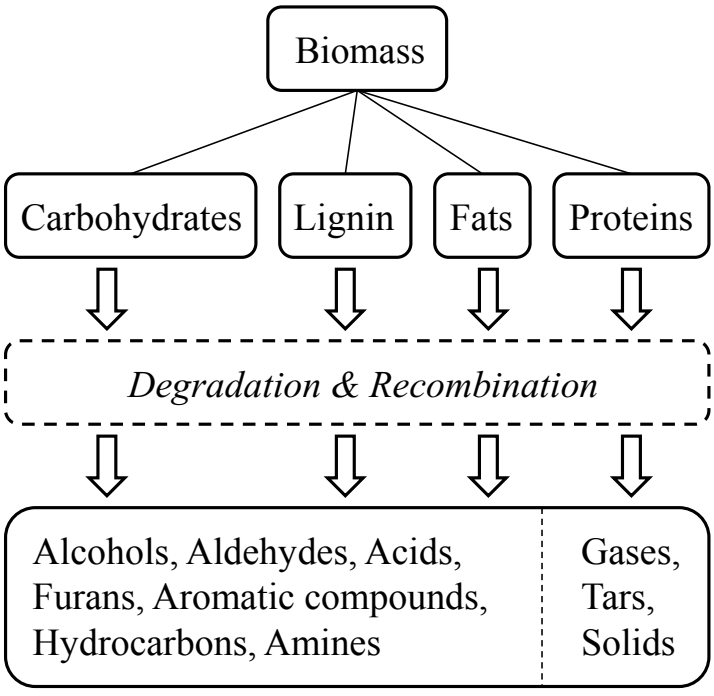

Figure 2.6: Simplified conversion route of carbohydrates, lignin, fats and proteins during hydrothermal liquefaction.

The conversion of carbohydrates, lignin, fats and proteins can be summarized as shown in Figure 2.6.

In addition:

- Hydrolytic reactions are believed to liberate heteroatoms from organic compounds such as P (PO_4^{3-}, HPO_4^{2-}, $H_2PO_4^-$, H_3PO_4), S (S_2^-, HS^-, H_2S, SO_4^{2-}), N (NH_4^+, NH_3) and Cl (Cl^-, HCl) [2].
- The degradation products of carbohydrates and proteins can react with each other to N-heterocyclic compounds in a Maillard reaction, which easily form rather stable free radical cations acting as free radical scavengers during later gasification [58, 69].
- To the best of our knowledge, no work has been reported so far describing the degradation of nucleic acids and chlorophyll of algae.
- Algaenans are aliphatic non-hydrolyzable macromolecules that can be found in green microalgae [70]. Not much information is available about their conversion [71]. However, they seem to be very stable compounds and are believed to be directly converted to hydrocarbons with variable length (alkanes and alkenes) and alkyl-aromatics [72].

2.2.3. Biomass gasification – main reactions and thermodynamic equilibrium

The fragments, which are produced during the degradation of biomass, are further decomposed to gaseous products. The main gasification reactions can be described as follows [73, 74]:

$$CH_xO_y + (2-y)H_2O \leftrightarrow CO_2 + (2-y+x/2)H_2 \quad ... \quad \triangle H_R^\circ > 0 \tag{2.2}$$

$$CH_xO_y + (1-y)H_2O \leftrightarrow CO + (1-y+x/2)H_2 \quad ... \quad \triangle H_R^\circ > 0 \tag{2.3}$$

$$CO + H_2O \leftrightarrow CO_2 + H_2 \quad ... \quad \triangle H_R^\circ = -41\,\text{kJ/mol} \tag{2.4}$$

$$CO + 3H_2 \leftrightarrow CH_4 + H_2O \quad ... \quad \triangle H_R^\circ = -211\,\text{kJ/mol} \tag{2.5}$$

$$CO_2 + 4H_2 \leftrightarrow CH_4 + 2H_2O \quad ... \quad \triangle H_R^\circ = -233\,\text{kJ/mol} \tag{2.6}$$

Reactions 2.2 and 2.3 describe the breakdown of the degradation products to CO, CO_2 and H_2 via steam reforming. The conversion of larger aromatic molecules (e.g. phenols) proceeds in several steps by production and further decomposition of lower molecular intermediates [10]. The water-gas shift (WGS) reaction (Reaction 2.4) and the methanation reactions of CO (Reaction 2.5) and CO_2 (Reaction 2.6) express the equilibrium between CO, CO_2, CH_4, H_2 and H_2O. Reactions 2.2 and 2.3 are endothermic, Reaction 2.4 is slightly exothermic and Reactions 2.5 and 2.6 are strongly exothermic. Furthermore, the volume decreases during the two methanation reactions. Thus, the following conclusion can be drawn according to Le Chatelier's principle: Low temperature and high pressure result in a high yield of CH_4 (see Figure 2.7), whereas high

temperature and low pressure increase the yield of H_2 [58]. These expectations are confirmed by numerous studies on thermodynamics of hydrothermal gasification reactions. In addition, they show that higher feed concentrations favor the formation of CH_4 [10, 75–79]. Besides the gases mentioned above, traces of hydrocarbons (like C_nH_{n+2}) are produced, too [73].

2.2.4. Heterogeneous catalysis promoting CH_4 formation

Below 600 °C the product composition is not close to the thermodynamic equilibrium without the use of catalysts. Reasons are the possible formation of polymeric materials and coke from organic substances with a very low reactivity and the slow methanation reactions [31]. If methane is the desired product, a catalyst that enhances steam reforming, WGS and methanation is needed. The catalytic performances of many metals (e.g. Ru, Ni, Fe, Co, Rh, Pd, Pt, Ir) and activated carbon have been investigated. The results are summarized in a few outstanding reviews [10, 65, 73, 80–83]. Ru and Ni have been identified as the most active and selective catalysts for hydrothermal gasification and methanation at temperatures of 350-450 °C [10]. However, Ru is more stable than Ni due to its higher resistance against oxidation and thermal sintering [82] and became the metal of choice for many working groups despite its high price (approx. 2025 $/kg [84]).

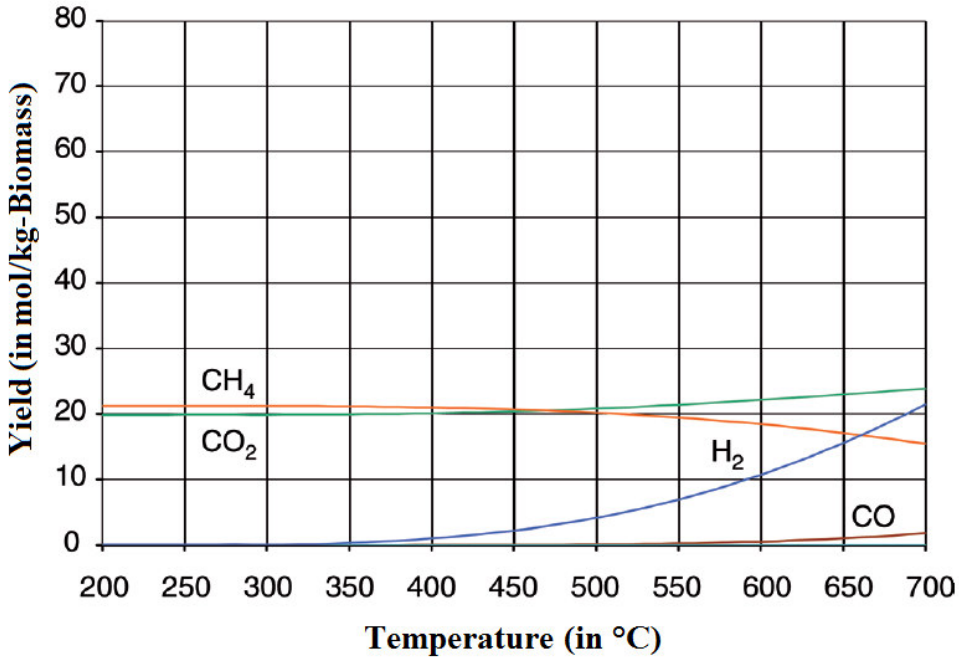

Figure 2.7: Molar yields of gaseous products at thermodynamic equilibrium for a mixture of 20 wt% $CH_{1.50}O_{0.67}$ and 80 wt% H_2O at 300 bar. Solid carbon was excluded from the products. Calculation performed with Aspen Plus® (Version 2006). Adapted from [10].

2.2.5. Potential catalyst supports

A catalyst support should maximize the surface-to-volume ratio of the active phase, provide access to the dispersed crystallites (open pores), improve performance and minimize costs. The support may also influence the overall chemistry of the catalytic process by exhibiting acidic or basic sites or by manipulating the electronic and chemical properties of the active metal [10,85]. For example, formaldehyde was found to decompose to CO and H_2 with a TiO_2 support (acidic), whereas it is mainly converted to methanol with a ZrO_2 support (basic) [86].

However, only a few materials are suitable as supports showing sufficient stability in near- and supercritical water. The most common ones include carbon (activated, graphitic, pyrolytic, nanotubes), ZrO_2 (monoclinic), TiO_2 (rutile) and α-Al_2O_3 [10,82,83]. Elliott *et al.* [87] conducted long-term experiments with ruthenium on ZrO_2, TiO_2 and carbon in a continuous tubular micro-scale reactor. A 10 wt% phenol-water mixture was used as the feed. The gasification efficiency was 94.00% after 3 weeks with 5%-Ru/ZrO_2, 99.99% after 6 weeks with 8%-Ru/C and 99.99% after 19 weeks with 3%-Ru/TiO_2 (rutile). Additionally, the 5%-Ru/C showed "... extremely high activity". A skeptical reader could wonder if carbon itself may be gasified according to the water-gas-reaction:

$$C + H_2O \leftrightarrow CO + H_2 \tag{2.7}$$

In the case of coconut shell activated carbon, this effect becomes significant at temperatures above 600 °C [88, 89]. At lower temperatures, where the production of methane is thermodynamically favored, it seems that the carbon support is not attacked as long as the metal sites are "busy" gasifying the feed molecules [10].

2.2.6. Catalytic effects of salts and reactor walls

During degradation and gasification, salts, such as alkali hydroxides and alkali carbonates, contained in the biomass may act as a catalyst. Alkali salts promote base-catalyzed reactions like hydrolysis, dehydration, aldol splitting, aldol condensation and Cannizzaro reaction [66]. Moreover, they catalyze C-C bond splitting and the WGS reaction [58, 66]. In general, alkali salts increase the yields of oil (during liquefaction) and gas (during gasification) and suppress coke and tar formation [58, 68, 83].

At this point it should be stated that the exclusive use of homogeneous catalysts is not attractive for hydrothermal gasification of biomass. They offer worse selectivity, can be recycled more difficulty and are often less eco-friendly than heterogeneous catalysts [81].

Most of the reactors and vessels for hydrothermal treatment of biomass are made of Inconel and Hastelloy, which are alloys with a high nickel content. Obviously, the nickel at the inner wall attributes to catalytic processes, which makes it difficult to separate between wall effects

and effects of intended catalysts [31, 81]. However, it is believed that at temperatures below 500 °C the product distribution is mainly determined by the added catalyst [31]. Waldner *et al.* [90] performed a batch experiment with a 10 wt% sawdust slurry at 409 °C in a 316 stainless steel tube and reached a carbon gasification efficiency of 21%. By contrast, Boukis *et al.* [74] reached conversion efficiencies of about 86% during gasification of a 5 wt% methanol solution at 600 °C in a tubular Inconel alloy 625 reactor. After H_2O_2 conditioning of the reactor, which had exposed the NiO at the inner reactor wall, the conversion efficiency reached values of more than 99%.

2.2.7. Sulfur poisoning

The sensitivity of metal catalysts towards contaminants is a very important issue in heterogeneous catalysis. Sulfur, which is found in organic and inorganic forms in all biomass types due to its metabolic pathways [91], is a well-known poison for catalysts. Especially ruthenium has been reported being prone to sulfur poisoning [12, 92–98]. Under hydrothermal conditions sulfide, sulfite, sulfate, thiosulfate and elemental sulfur may coexist [10]. Although earlier studies had expected that any sulfur compound could poison the catalyst [95], S^{2-} was identified as the relevant poisoning sulfur species. Moreover, it was concluded that sulfur poisoning is an irreversible process and that regeneration can be only possible by chemical treatment of the S-poisoned catalyst [99, 100]. Oxidative treatment of spent Ru/C and Ru/TiO_2 catalyst with H_2O_2 was successful; unfortunately, the activity was not long-term stable [98, 100–102].

2.2.8. Formation of carbon particles and tars

Solid carbon particles and tarry substances are undesired side-products during hydrothermal gasification. They decrease the gasification efficiency and can lead to blocking of the plant. Two reaction pathways exist for the formation of carbon particles: char formation by devolatilization leading to a crystalline structure similar to the original biomass (but with a higher porosity), coke formation by polymerization of intermediates leading to microspheres. Unless the biomass is "hard" with high lignin content, coke formation is the dominant pathway [103].

Tars are aromatic, non-volatile molecules of higher molecular mass and soluble in polar organic solvents like methanol or acetone. They are very unstable, tend to polymerize and are believed to be coke precursors [104].

As already mentioned in Section 2.1.6, near- and supercritical water dissolves organic substances due to its low relative permittivity. In the presence of an active catalyst the dissolved oily compounds can reach the catalytic sites, where they are gasified. Therefore, tar and coke formation is not expected during hydrothermal gasification. Nevertheless, tar and coke can be formed during heating-up of the feedstock crossing the subcritical area [10].

2.2.9. Salt management

Besides their positive (catalytic) effects during hydrothermal conversion of biomass, salts can have a negative influence, too. They may lead to the following problems:

- Salts can enhance corrosion in various ways [105–107].
- Under supercritical conditions, salts precipitate due to their lower solubility (see Section 2.1.6) leading to plugging of the plant [58, 96].
- Salts may deactivate the catalyst through fouling [31, 92, 93].
- Some salt components may deactivate the catalyst through poisoning (see Section 2.2.7).

In addition to process stability and catalyst life time, recovery of salts has an economic motivation, too. Some inorganic substances (especially nitrogen, potassium and phosphorus) have a high commercial and environmental value if they can be recovered in biologically available forms for the use as fertilizers [31, 108]. Particularly phosphorus recovery has become very important due to its slow natural cycle [109]. The salts contained in biomass and formed during hydrothermal reactions of heteroatoms are often present as ions (NH_4^+, NO_3^-, K^+, PO_4^{3-}, etc.), which lose their solubility in supercritical water [31].

In general, different water-salt systems behave differently under hydrothermal conditions showing various phase equilibria and immiscibility phenomena. Valyashko [110] classified the phase behavior of binary water-salt systems into two main categories, type 1 and type 2. Saturated type 1 salts, like $NaNO_3$ and KH_2PO_4, feature an increasing solubility with increasing temperature up to the melting point of the salt, whereas diluted type 1 salts also show a low solubility in the range of the (pseudo-)critical point of water. In contrast, the solubility of type 2 salts (diluted or saturated), like Na_2SO_4 and K_2SO_4, decreases with increasing temperature up to the critical point of water. Noteworthy is the work of Schubert [59–62], who investigated continuous precipitation and separation of different water-salt systems.

2.3. Previous studies on continuous catalytic hydrothermal gasification of algal biomass

To the best of our knowledge, only two studies have been published so far describing catalytic hydrothermal gasification experiments of algal biomass using a continuous test rig. Their setup and main observations will be summarized in the next two sections.

2.3.1. Elliott's work [1]

Elliott's continuous-flow reactor system consisted of a feeding unit (feed tank, high-pressure feed pump), a CSTR (Continuously Stirred Tank Reactor), a mineral separation unit, a sulfur stripping unit, a tubular reactor and a phase separator. The CSTR (volume: 1 L, SS316) functioned as a preheater and brought the feed to the reaction temperature. As a result, the organics in the biomass were liquified and inorganic components were formed and precipitated as solids. In the mineral separator (volume: 1 L, SS316), which was a simple dip leg vessel, the solids fell to the bottom and the liquids passed overhead through a filter to the sulfur stripper (volume: 1 L, SS316). The process continued in the gasification reactor (volume: 1 L, inner diameter: 1 in, SS304) and finished at the liquid/gas phase separator after cooling. A dome-loaded diaphragm back-pressure regulator was positioned before the phase separator and controlled the pressure. Eight experiments were run at nominally 350 °C and 21 MPa (subcritical region) with different algae types and concentrations. The sulfur scrubber was filled with pelletized Raney nickel and the reactor with 500 g of 7.8 wt% ruthenium metal on a partially graphitized carbon extrudate. The main process parameters and results are shown in Table 2.1.

Table 2.1: Summary of Elliott's main experimental parameters and results [1].

Type of algae	algae mix, Spirulina, Chara, Nannochloropsis salina
Nominal temperature (in °C)	350
Nominal pressure (in MPa)	21
Time on stream (in h)	3.5 - 11.2
Feed concentration (in wt%)	8.0 - 25.0
Feed rate (in L/h)	1.0 - 1.5
LHSV[(a)]	1.2 - 1.9
Carbon conversion to gas (in wt%)	40 - 106
COD conversion (in wt%)	96.60 - 99.96
CH_4 in gaseous product (in vol%)	49.1 - 62.5
CO_2 in gaseous product (in vol%)	36.5 - 48.3
H_2 in gaseous product (in vol%)	0.9 - 3.3
CO in gaseous product (in vol%)	0.0
C_2H_6 in gaseous product (in vol%)	0.0 - 2.5

[(a)]LHSV = liquid hourly space velocity used in units of hourly rate of liters of slurry processed over the liters of catalyst bed.

In general, the tests showed good short-term stability and minimal poisoning effects and high conversions were achieved. A couple of trace elements, including Na, K, S, P, Mg, and Ca, precipitated in the mineral separator. Na and K were found in the aqueous product in significant amounts, too. Furthermore, high amounts of ammonia (in one test up to 19 367 mg/L) were detected in the aqueous product. Analysis of spent sulfur scrubber and catalyst beds showed

insufficient sulfur capture by Raney nickel and catalyst deactivation. Therefore, long-term experiments would not have been stable.

2.3.2. Brandenberger's work [2]

One experiment was performed with a laboratory plant at the PSI. It consisted of a feeding section (feed tank, high-pressure pump), a preheater (SS316L, length: 1.70 m, inner diameter: 12 mm), a salt separator (length: 0.694 m, inner diameter: 12 mm; fabricated by Sitec, Switzerland), a catalytic reactor (SS316L , length: 1.40 m, inner diameter: 12 mm), a cooling section, a pressure regulator and a liquid/gas phase separator. The main differences to Elliott's setup were that the preheater was not a CSTR but rather a tubular reactor, that the precipitated salts were removed continuously as brine and that no sulfur stripper was used. The temperature setpoints of the preheater, the salt separator and the reactor were 360 °C, 470 °C and 420 °C. The pressure of the plant was about 323 bar and the reactor was filled with 118 g of 2 %-Ru/C (BASF). In Table 2.2 the main process parameters and results are listed.

Table 2.2: Summary of Brandenberger's main experimental parameters and results [2].

	Glycerol	Phaeodactylum tricornutum
Nominal temperature - preheater (in °C)	360	360
Nominal temperature - salt separator (in °C)	470	470
Nominal temperature - reactor (in °C)	420	420
Plant pressure (in MPa)	32.3 ± 0.6	32.3 ± 0.6
Time on stream (in min)	110	380
Feed concentration (in wt%)	5	6.5
Feed rate (in kg/h)	0.804	0.770
WHSV (in g_{Org}/g_{Cat}-h)[(a)]	0.34	0.42
Carbon conversion to gas (in wt%)	100 ± 2.3	31.3 ± 0.9
CH_4 in gaseous product (in vol%)	53.8 ± 1.1	12.5 ± 0.7
CO_2 in gaseous product (in vol%)	40.9 ± 1.2	41.3 ± 1.8
H_2 in gaseous product (in vol%)	5.2 ± 0.7	26.4 ± 1.3
CO in gaseous product (in vol%)	0.0 ± 0.0	0.1 ± 0.04
C_2H_6 in gaseous product (in vol%)	0.0 ± 0.07	11.5 ± 0.8
C_3H_8 in gaseous product (in vol%)	0.0 ± 0.02	8.2 ± 0.1

[(a)]WHSV = weight hourly space velocity used in units of hourly rate of algae (dry matter) processed over the grams of catalyst.

In the first 110 min a 5 wt% glycerol solution was pumped through the test rig, for the remaining experimental time (about 380 min) a 6.5 wt% microalgae (Phaeodactylum tricornutum) slurry. Complete and stable gasification of glycerol was possible. The concentrations of CO_2 and CH_4

matched with thermodynamic calculations done with Aspen Plus®, whereas H_2 did not. When the feed was switched to microalgae, the methane concentration in the gaseous product dropped and reached a value of about 12.5% at steady state. By contrast, the concentration of hydrogen, ethane and propane increased suggesting deactivation of the catalyst. The carbon gasification decreased to about 31.3% and the liquid product turned from clear and transparent to milky and separated into an oily and an aqueous phase. Moreover, the electrical conductivity of the liquid product was three times higher than the one of the brine indicating insufficient salt separation. Analysis of the spent catalyst (BET, chemisorption) showed a decreased surface area, likely due to coking, and catalyst poisoning. Additionally, SEM-EDX mapping of fresh and spent catalyst was carried out showing deposition of several elements on the catalyst surface including S, Mg, Ca and P. Finally, strong coking was confirmed by TEM-EDX pictures.

2.4. Scope of this work

The previous sections illustrated that hydrothermal gasification of microalgae is a promising technology for a sustainable production of methane. However, there are still some challenges that have to be overcome. For a better understanding more continuous experiments at laboratory scale have to be performed before scale-up to an industrial process. In the frame of the SunCHem project [2,12] a new continuous test rig for hydrothermal gasification of wet biomass was designed and built based on the experience of Prof. Vogel's group gained in the last few years. In August 2014 a long-term experiment (approx. 100 h) at the ZHAW (Wädenswil, Switzerland) was planned. Since no experiments with the new plant had been conducted yet, the test rig had to be started up and to get going. The final gasification tests of the microalgae *Phaeodactylum tricornutum* should be performed at 280 bar and 400 °C, nominally, with the use of 5%-Ru/C as a catalyst. To prevent the catalyst from poisoning and to ensure long-time activity, zinc oxide should be tested as a sulfur adsorber. This work aimed at assessing and improving the stability of the new PDU (Process Demonstration Unit) for the production of methane. During the experiments, the behavior and sensitivity of the plant towards process parameters (feed type, temperature, flow rate, ...) should be observed. In addition, the weak points should be identified and corrected if possible.

3. Experimental setup and analysis

3.1. Continuously operated laboratory plant (KONTI-C)

The experiments were carried out at PSI's new laboratory plant (*KONTI-C*) for continuous hydrothermal gasification of wet biomass with a capacity of 1 kg/h. A simplified flow-scheme is depicted in Figure 3.1; a more detailed flow diagram can be found in Appendix A. The plant was installed in a shipping container (6640 x 2438 x 2896 mm) and consisted of six main sections: feeding section, salt separator, salt removal section, reactor, pressure control, phase separator.

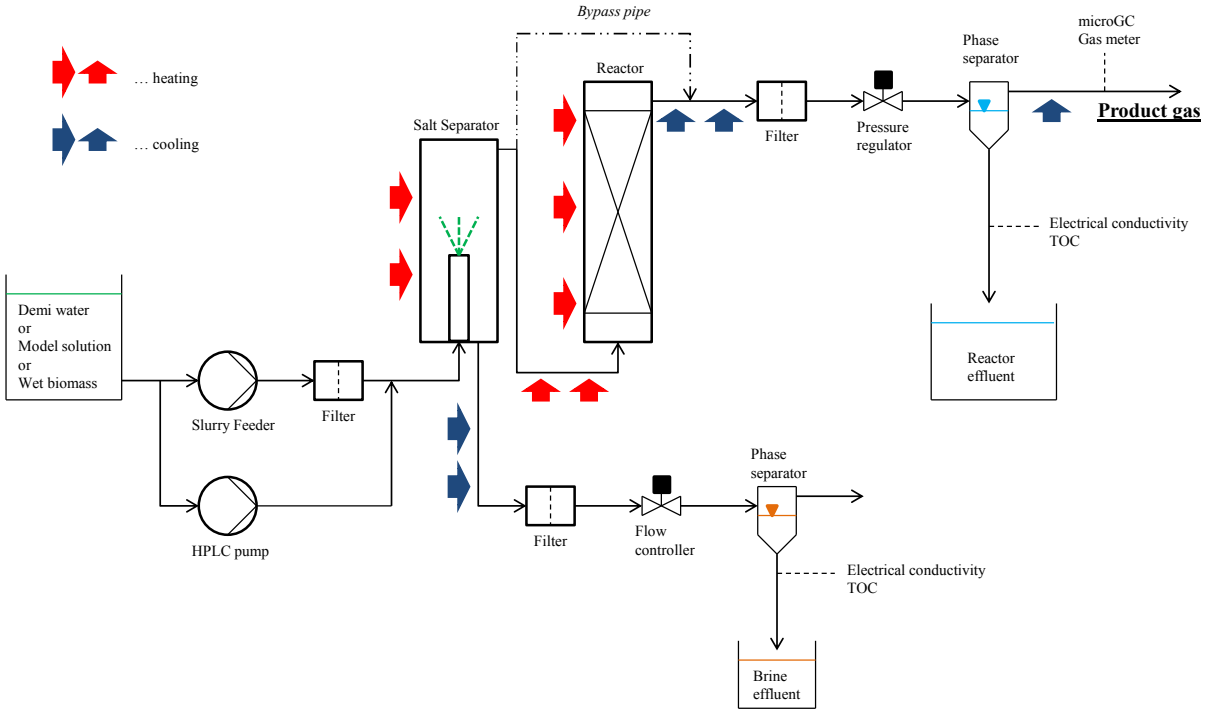

Figure 3.1: Simplified flow-scheme of KONTI-C.

The feeding section held tanks for deionized (DI) water and feed, two pumps and a balance. One pump was an HPLC pump (Varian PrepStar SD-1 Solvent Delivery System) for feeding water and model solutions, the other one was a piston pump (*Slurry Feeder*) for feeding wet biomass. The Slurry Feeder consisted of two cylinders (SS316LN) with a working volume of 2.6 L each and could be operated at a frequency of 0-50 Hz. It had been designed and constructed in-house; a detailed description can be found elsewhere [98]. The balance (KERN & SOHN GmbH, IFS 60K0.5DL) could be used to trace the mass flow rate of the feed during an experiment.

After the feed had been pressurized by one of the two pumps and had passed a filter (pore size: first 250 µm, later 25 µm), it was sprinkled into the salt separator (SITEC, steel grade: 1.4980, inner length: 300 mm, inner diameter: 40 mm) via a standpipe (steel grade: 1.4404), which

extended 100 mm into the salt separator. The standpipe had an inner diameter of 3 mm and an orifice of 1 mm at the end. The salt separator could be heated electrically by two heating blocks to generate a certain temperature profile inside. The temperature was measured at the inner wall at different heights by thermocouples as well as along the axis by an in-house constructed temperature lance, which was dipped into the salt separator from the top. The aim of the salt separator was to heat up and liquify the feed (according to Section 2.2.2) and to separate minerals from organic substances. This could be achieved by establishing a supercritical zone at the top, where most likely organic matter should be dissolved, and a subcritical zone at the bottom, where salts would be dissolved preferably, precipitate or settle by density (compare Section 2.1.6 and [59]). The salt separator had two outlets, one for delivering the liquified, desalinated feed to the reactor, the other one for extracting concentrated brine continuously.

After cooling to 20-30 °C (Huber, Unichiller MPC006), the brine effluent passed a particle trap, a filter (pore size: 25 µm) and a mass flow rate controller (Bronkhorst®, Liquiflow), which was located right before a pressure relief valve. The flow controller, in the following called *Liquiflow*, could be varied between 0 and 100% and was calibrated for a flow between 0 and 3.2 g/min. After pressure relief, the brine effluent entered a liquid/gas phase separator in case of degassing. The carbon content in the liquid could be measured on-line by a TOC analyzer (GE Analytical Instruments, Sievers InnovOx On-Line TOC Analyzer). The liquid phase was collected in a tank, which was positioned on a balance (KERN & SOHN GmbH, IFS 30K0.2DL) for monitoring its mass flow rate. No equipment was pre-installed for continuously capturing or analyzing a possible gas phase.

The liquified, desalinated stream at the top of the salt separator was transferred via a heated tube (steel grade: 1.4404, approx. length: 1600 mm, inner diameter: 0.25 in) to the catalytic reactor (SITEC, steel grade: 1.4435, inner length: 1515 mm, inner diameter: 36 mm), where the liquified organic compounds were gasified. The reactor could be heated electrically by two heating blocks to reach a certain temperature inside. The temperature was measured along the axis by an in-house constructed temperature lance, which was dipped into the reactor from the top. Information regarding reactor fillings will be given later.

After cooling (20-30 °C), particles in the reactor effluent were withheld by a particle trap and further downstream by a filter (pore size: 25 µm). There were actually two parallel filters so that it could be easily switched from one to the other by a three-way-valve in case of plugging. The reactor effluent was depressurized to atmospheric pressure by a manually adjustable spring-loaded relief valve (SITEC). A control valve (Kämmer) combined with a pressure controller (Flowserve) located upstream of the relief valve regulated the pressure in a range of about 5 MPa.

The depressurized fluid was directed to a liquid/gas phase separator (borosilicate glass, 2000 mL), which was fixed at a digital spring balance (HiTec Zang GmbH, GraviDos®). The gas phase leaving the separator at the top was cooled to 8 °C (JCT Analysetechnik GmbH, JCP-S) and its flow was measured by a gas meter (Wohlgroth). Moreover, its composition could be measured

on-line by a microGC (INFICON, 3000 Micro GC). Up until then, the produced gas was emitted to the environment but would be burnt in the future. The carbon content in the liquid phase could be measured by the TOC analyzer, too. Finally, the liquid phase was collected in a tank, which was positioned on a balance (KERN & SOHN GmbH, IFS 60K0.5DL) for monitoring its mass flow rate.

Table 3.1: Abbreviations of temperature-, pressure- and electrical conductivity measurements.

Abbreviation	Unit	Location
TTR 2-1	°C	Feed filter
TTRC 2-(7 or 8)	°C	Heating blocks of salt separator
TTR 2-(2. . . 6)	°C	Inner wall of salt separator[(a)]
TLTR 2-(9. . . 14)	°C	Temperature lance of salt separator[(b)]
TTRC 4-(2 or 21)	°C	Heating blocks of reactor
TLTR 4-(5. . . 20)	°C	Temperature lance of reactor[(c)]
PTR 1-(1 or 2)	barg	Hydraulic system of Slurry Feeder cylinder 1 or 2
PTR 1-(3 or 4)	barg	Feed in Slurry Feeder cylinder 1 or 2
PTR 1-5	barg	Upstream of feed filter
PTR 2-2	barg	Downstream of feed filter
PTR 2-3	barg	Vertical center of salt separator
PTR 4-1	barg	Reactor top
PTR 5-1	barg	Upstream of reactor effluent filter
PTRC 5-3	barg	Downstream of reactor effluent filter (Flowserve)
ECTR 3-1	µS/cm	Brine effluent upstream of collecting tank
ECTR 6-1	µS/cm	Reactor effluent upstream of collecting tank

[(a)]Vertical distance from the top outlet of the salt separator: -290, -217, -145, -72, 0 mm.

[(b)]Vertical distance from the orifice of the standpipe: 10, 40, 70, 100, 130, 160 mm.

[(c)]Vertical distance from the inlet of the reactor: -30, 120, 270, 420, 520, 620, . . . , 1420, 1495, 1595 mm.

In addition to the above mentioned equipment, the pressure was measured at several points of KONTI-C, facilitating the localization of any potential plugging, and the electrical conductivities of brine- and reactor effluent were measured by conductivity meters (SCHOTT®, Handylab pH/LF12). Furthermore, up to nine liquid samples of each brine- and reactor effluent for off-line analysis could be withdrawn automatically by an auto-sampler (in-house constructed, included VICI valve C25-6180 EMH). All temperatures, pressures, balance signals, electrical conductivities of the effluents, carbon content in brine- and reactor effluent, gas composition and the amount of gas produced were monitored on-line. The laboratory plant could be operated by remote control using a LabVIEW-based control program (see Appendix B).

KONTI-C had been equipped with the above described tools and functions for ideally working gasification processes. Since this work mostly involved start-up experiments, not the entire equipment was used for each experiment. In the next section, this will be explained in more detail.

A number of abbreviations for the temperature-, pressure- and electrical conductivity measurements will be used in graphs and text in Sections 4 and 5. They are summarized in Table 3.1.

3.2. Experimental schedule

As already described in Section 2.4, the aim of this project was to start up KONTI-C for continuous conversion of microalgae to methane. To protect the catalyst from sulfur poisoning (see Section 2.2.7), ZnO was used as a sulfur adsorber upstream of the catalyst.

In conclusion, the experimental pathway was given as:

1. Perform salt separation tests with model solutions to get familiar with KONTI-C and investigate the performance of the salt separator.
2. Perform liquefaction tests with algal biomass to check successful biomass degradation and investigate the performance of the salt separator.
3. Observe the sulfur removal efficiency and the catalytic activity of ZnO during hydrothermal gasification of microalgae.
4. Perform catalytic gasification tests with 5%-Ru/C for the production of methane.

As a result, three experiments were run for item 1 and two experiments for each item 2, item 3 and item 4. The model solutions were aqueous salt solutions of Na_2SO_4 (0.1 mol/kg) and K_2SO_4 (0.05 mol/kg), two of them contained 10 wt% isopropanol, too. The feed for the experiments with real biomass nominally contained 10 wt% of Phaeodactylum tricornutum.

Not the entire KONTI-C equipment, as described in Section 3.1, was used for each experiment:

- The auto-sampler was only used for the salt separation tests.
- For one experiment of item 1 and for the experiments of item 2 the reactor was circumvented by a bypass pipe (steel grade: 1.4404, approx. length: 2200 mm, inner diameter: 0.25 in).
- On-line TOC analysis was only conducted for the reactor effluent during the gasification experiments (item 4).
- On-line gas analysis of the product gas was only conducted during the gasification experiments (item 4).

3.3. General procedure

3.3.1. Procedure of the experiments with model solutions

- Feed preparation:

  For each test 4 kg of a salt solution were prepared. Two 2000 mL volumetric flasks were filled with 0.2 mol (28.408g) of Na_2SO_4 and 0.1 mol (17.426 g) of K_2SO_4. For the two experiments with isopropanol 200 g of isopropanol and 1754.166 g of DI water, for the experiment without isopropanol 1954.166 g of DI water were added to each flask. Then the flasks were put on a heated magnetic stirrer, heated up to about 40 °C and stirred until all salt particles were dissolved. Finally, the solutions were poured into a clean tank and the electrical conductivity was measured with a conductivity meter.

- KONTI-C preparation:

  On the previous day KONTI-C was started, including all the needed instruments, pressurized and heated up to the desired settings with DI water to check correct performance of the instruments and the absence of a leakage. Afterwards KONTI-C was cooled down and rinsed overnight leading to very low electrical conductivities in brine- and reactor effluent (To be consistent with the nomenclature of previous studies of Prof. Vogel's group, *reactor effluent* refers to either the stream coming out of the reactor or the stream being bypassed depending on the use of the reactor or the bypass pipe.). On the next day KONTI-C was pressurized and heated up again to the desired settings using the HPLC pump. The setpoint of the mass flow rate could be defined at the pump. During heat-up, which took about 2-3 h, the auto-sampler was prepared. This included rinsing of all the hoses of the auto-sampler with DI water and providing 40 mL glass vials for the samples. Each hose that connected the auto-sampler and one vial was fixed by a needle stung into the septum of the cap of the vial.

- Experimental procedure:

  When steady-state was reached with respect to temperature in the salt separator, the HPLC pump was stopped for one or two seconds, the hose of the HPLC pump was taken out of the DI water tank and put into the tank with the model solution and the HPLC pump was started again. Samples of brine- and reactor effluent were withdrawn every 20 min by the auto-sampler long enough to have the vials filled at least half-full. When the tank with the model solution was nearly empty, the hose of the HPLC pump was put into the DI water tank again. KONTI-C was cooled down and rinsed with DI water overnight.

For the first two tests with model solutions there was no bypass pipe for the reactor available yet. Therefore, the top outlet of the salt separator went through the unheated reactor, which was filled with activated carbon. For the third test a bypass pipe was used.

3.3.2. Procedure of the experiments with algal biomass

- Feed preparation:

  Frozen Phaeodactylum tricornutum was received from Subitec in packages/tanks of 2 to 10 kg with different dry matter content (13-25 wt%). The packages were kept in a freezer at −20 °C and – if needed for an experiment a few days later – put into a fridge at 2 °C for defrosting. For each experiment at least 7 kg of a 10 wt% solution were prepared by mixing the defrosted microalgae with the appropriate amount of DI water. The dry matter content stated on the Subitec packages was checked for the first used package by leaving a sample in a vacuum oven at 60 °C and 300 mbar until the mass did not change anymore. Since the determined dry matter value coincided with the value stated on the package, no additional dry matter determination was conducted for the other packages. During feed preparation care was always taken regarding settling of microalgae in the packages/tanks leading to dilution/concentration effects. If there was feed from a previous test left, the freshly prepared feed was added to the "old" feed. The feed tank was permanently kept in a fridge at 2 °C unless it was used during an experiment.

- KONTI-C preparation:

  On the previous day KONTI-C was started, including all the needed instruments, pressurized and heated up to the desired settings with DI water to check correct performance of the instruments and the absence of a leakage. Afterwards KONTI-C was cooled down and rinsed overnight leading to very low electrical conductivities in brine- and reactor effluent. On the next day KONTI-C was pressurized and heated up again to the desired settings using the HPLC pump. The setpoint of the mass flow rate was set to a value close to the mass flow rate of the Slurry Feeder later on and could be defined at the HPLC pump. During heat-up, which took about 2-3 h, the feed was either prepared or the feed tank was taken out of the fridge (2 °C). The Slurry Feeder was filled, emptied and filled again with feed to get a representative feed sample due to small dilution/concentration effects inside the Slurry Feeder caused by slurry in dead zones from previous operation. If the TOC analyzer was required, it was turned on, flushed and started. If the microGC was needed, it was calibrated with standard gas and started as well.

- Experimental procedure:

  When steady-state was reached with respect to temperature in the salt separator (and in the reactor), the Slurry Feeder was started. By the time the pressure inside the Slurry Feeder reached the pressure downstream, the outlet valve of the Slurry Feeder opened and started pumping algal feed into the plant. The HPLC pump – still delivering KONTI-C with DI water – was stopped at the same time. The brine effluent collecting bottle and the reactor effluent collecting tank were positioned as well. Samples of brine- and reactor effluent were manually withdrawn every 20 min long enough to have the (plastic) vials filled at least half-full. Throughout the experiment, the temperatures and pressures were

watched indicating the need for readjustment of the settings or possible plugging. When the feed tank was nearly empty or a mechanical issue abandoned the experiment, the Slurry Feeder was stopped and the HPLC pump was started again delivering DI water. The residual feed in the Slurry Feeder was pumped back into the feed tank and a feed sample was taken. The brine effluent collecting bottle and the reactor effluent collecting tank were replaced by waste tanks. If TOC- and microGC measurements were running, they were stopped. KONTI-C was cooled down and rinsed with DI water overnight.

- KONTI-C post-processing:

  On the day after an experiment, KONTI-C was depressurized and the filters were removed, inspected and washed with water and ethanol. Then the filters were installed again and the whole plant was rinsed with ethanol using the HPLC pump until the outlets became clear, which took usually a whole day. Finally, KONTI-C was rinsed with DI water again for a couple of hours until the electrical conductivity reached very low values.

3.3.3. Reactor charge and discharge

KONTI-C had two reactors, an operating one and an extra one. Before one of the two reactors could be discharged and charged with a different filling, the current filling had to be dried. This was achieved by heating up the reactor to 80 °C and blowing pressurized air through overnight. Then the reactor was dismounted from KONTI-C and fixed with the bottom side down at a wooden construction made in-house by Erich de Boni and Lorenz Bäni. The bottom screw-cap was removed and the dry filling fell out easily by its own. As a next step, the reactor was flipped having the top side down. Since the temperature lance was fixed at the top of the reactor, the reactor had to be charged this way (see Figure 3.2). Charging the reactor was done in the following way:

1. The bag that contained either ZnO or 5%-Ru/C was weighed.
2. A metal frit (SS316L) was threaded on the lance and pushed to the end of the reactor to cover the filling at the top side.
3. A metal pipe with an inner diameter a little bit bigger than the diameter of the lance was threaded on the lance to keep the flexible lance in axial position during the following charge.
4. The filling was carefully poured in the reactor. Meanwhile, the metal pipe was pulled out step by step and the reactor was knocked with a hammer to avoid blocking and empty zones. From time to time the filling was compressed a little bit with a metal rod.
5. When the reactor was nearly full, another metal frit was threaded on the lance to cover the filling at the bottom side.
6. The bottom screw-cap was screwed on again.

7. The bag with the residual ZnO or 5%-Ru/C was weighed and thus the mass of the reactor filling determined.

Whenever a reactor with a new filling was mounted at KONTI-C, the plant was pressurized and heated up with DI water to rinse the reactor and to check for leaks.

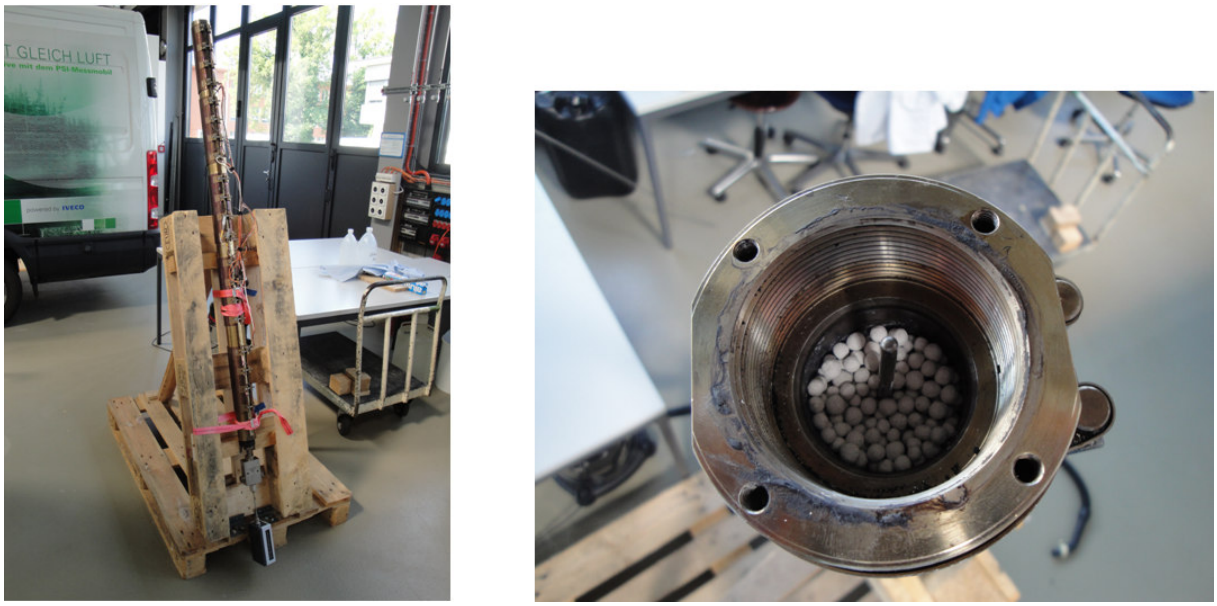

Figure 3.2: Left: Reactor fixed at wooden construction for charge and discharge. Right: Look into filled reactor (bottom side).

3.4. Materials and analytical tools

Table 3.2 lists the materials that were used for the experiments with KONTI-C in the course of this project.

Table 3.2: Materials used for the experiments.

Substance	CAS number	Supplier
Phaeodactylum tricornutum	-	Subitec
Deionized water	-	In-house DI water grid
Sodium sulfate (>99.0%)	7757-82-6	Merck KGaA
Potassium sulfate (>99.0%)	7778-80-5	Sigma-Aldrich
Isopropanol (99.8%)	67-63-0	VWR BDH Prolabo
Ethanol (99.8%)	64-17-5	Thommen-Furler AG
Katalco™ 32-5 (ZnO + cement)	-	Johnson Matthey Catalysts
5%-Ru/C	-	BASF

All of them were used as they had been delivered except for Ru/C. Before utilization the

catalyst was put in a vacuum oven (65 °C, 300 mbar) overnight to remove the moisture. The characteristics of Phaeodactylum tricornutum and the ruthenium catalyst can be found in Appendices C and D.

In Table 3.3 it is summarized which of the following analytical tools was used for which experiment with algal biomass. The samples of the tests with model solutions, which had been withdrawn by the auto-sampler, were only analyzed by the CNS analyzer (Section 3.4.1) with respect to sulfur.

Table 3.3: Overview of the analytical tools' usage for the experiments with algal biomass.

Experiment	Stream	CNS	TOC (on-line)	microGC (on-line)	GC (offline)	ICP-OES
Liquefaction I	Feed	x				
	Brine effluent	x				
	Reactor effluent	x				
Liquefaction II	Feed	x				
	Brine effluent	x			x	
	Reactor effluent				x	
Liquefaction III (+ ZnO)	Feed	x				
	Brine effluent	x				
	Reactor effluent					
Liquefaction IV (+ ZnO)	Feed	x				
	Brine effluent	x				
	Reactor effluent	x			x	
Gasification I	Feed	x				
	Brine effluent	x				
	Reactor effluent	x	x			
Gasification II	Feed	x				x
	Brine effluent	x				x
	Reactor effluent	x	x	x		x

3.4.1. Carbon-, nitrogen- and sulfur elemental analyzer (off-line)

Carbon, nitrogen and sulfur in the samples withdrawn during the KONTI-C experiments were measured with a Vario ELcube CNS analyzer from Elementar using a thermal conductivity detector for CO_2 and N_2 and an infrared detector for SO_2. The samples were burnt at 1150 °C in a chamber under helium- (234 mL/min) and oxygen (35-38 mL/min) atmosphere over a WO_3 catalyst. Nitrogen oxides were reduced to N_2 in a subsequent chamber at 850 °C by a copper catalyst. The remaining gas stream contained only the components CO_2, H_2O, SO_2 and N_2 in the carrier gas (He). The steam was removed in a pipe filled with Sicapent® before measurement.

The analyzer could be run either in liquid or in solid mode. For handling reasons the first measurements were done in liquid mode. However, most of the later measurements were carried out in solid mode due to numerous mechanical and analytical problems in liquid mode. The main issues were as follows:

- Short-term stability of the septum of the combustion chamber (compare [2])

- Fracture of the injection syringe due to inaccurate automatic positioning
- Very slow response regarding sulfur measurement
- Very frequent renewal of the drying pipe

Liquid mode:

Only the samples of one of the experiments with a model solution (second salt separation test) were analyzed in liquid mode. Standard solutions of 0.01 & 0.005 mol/kg, 0.1 & 0.05 mol/kg and 1.0 & 0.5 mol/kg with respect to Na_2SO_4 & K_2SO_4 were prepared for calibrating the analyzer. Regarding the experiments with model solutions, only sulfur analysis was of interest. Whenever a new measurement series was started, a so-called *daily factor* was determined by analyzing one of the standard solutions to determine the current error of the analyzer. The samples were filled into standard 1.5 mL vials and were automatically injected into the combustion chamber using the Vario Liquid Sampler (VLS). For each sample, injections of 20 µL were accomplished until the SD (standard deviation) was low and the last three measurements were used for evaluation. The samples' densities were determined, too, for a later conversion of mg/L to mg/kg.

Solid mode:

Calibration of the analyzer had already been done with the use of Sulfanilamide (CAS: 63-74-1, Sigma-Aldrich). However, a daily factor was determined again whenever a new measurement series was started. This was done by flushing the analyzer with air and analyzing four 2-3 mg Sulfanilamide samples using the last three samples for evaluation. The daily factor for N, C and S was always in the range of ±10%. Analysis of the samples from the KONTI-C experiments was done in the following way:

1. The 50 µL tin capsules, where the samples would be filled in, were weighed.
2. Each sample was homogenized using a sample shaker (Müller+Krempel), filled in four tin capsules under helium atmosphere and the capsules were closed using a special apparatus from Elementar.
3. The filled capsules were weighed again and thus the sample amount in each capsule was determined.
4. The capsules were put on the sample plate of the analyzer, the sample weights were typed in the software of the analyzer and a series measurement was started.
5. The last three measurements of each sample, which had a low SD, were used for evaluation.

3.4.2. Carbon analyzer (on-line)

During the gasification experiments the carbon content in the reactor effluent was measured on-line by Sievers InnovOx Total Organic Carbon Analyzer (GE Analytical Instruments). Samples were withdrawn automatically from the bottom of the phase separator every 9 min. The instrument determined first the TIC (Total Inorganic Carbon) content, then the TC (Total Carbon) content and finally calculated the TOC (Total Organic Carbon) content by subtracting TIC from TC. For the TIC measurement the analyzer mixed the sample with acid (6M phosphoric acid) and deionized water. The substances in the sample containing inorganic carbon reacted with the acid forming CO_2 and by-products. A non-dispersive infrared (NDIR) detector measured the CO_2 concentration subsequently and the TIC concentration was calculated. For the TC measurement the analyzer mixed the sample with acid, oxidizer (300 g/L sodium persulfate) and deionized water. The substances in the sample containing inorganic carbon reacted with the acid forming CO_2 and by-products. In parallel, the mixture was heated up and pressurized to 375 °C and 22.1 MPa resulting in supercritical water oxidation of the substances containing organic carbon. The NDIR detector measured the CO_2 concentration subsequently and the TC concentration was calculated.

The instrument was calibrated for TOC and TIC. For the TOC calibration a blank solution and KHP (potassium hydrogen phthalate) standard solutions of 1000, 5000 and 20 000 mg/L from GE Analytical Instruments (CSTD 68450-01) were used. TIC calibration was first done with a blank solution and a standard solution of 25 mg/L from GE Analytical Instruments. As it will be discussed in Sections 5.6 and 5.7, this range was too low. For the second TIC calibration a blank solution and solutions of 113 and 1130 mg/L Na_2CO_3 were used.

3.4.3. Gas Chromatography (on-line)

During the two gasification experiments the product gas was analyzed for H_2, O_2, N_2, CO, CO_2, CH_4 and C_2H_6 by the 3000 micro GC Gas Analyzer (INFICON GmbH). Samples were withdrawn automatically every 5 min downstream of the gas cooler and upstream of the gas meter. They passed two parallel channels (A and B), where the gaseous components were separated at 80 °C based on their retention and adsorption property with the stationary phase material of the column. When the separated samples left the columns, they were analyzed by a TCD (Thermal Conductivity Detector) using argon as a reference gas and re-injected upstream of the gas meter. The analyzer had always been heated overnight (at 160 °C) and its accuracy checked by measuring a standard gas (Messer Schweiz AG; 40% CO_2, 40% CH_4, 10% H_2, 5% N_2, 1% CO, 0.5% C_2H_6, 3.5% Ar) before the measurement of a KONTI-C experiment was started.

3.4.4. Gas Chromatography (off-line)

Off-line gas analysis was performed by a GC (Agilent 6890 Gas Chromatograph). The gas samples taken during the experiments were collected in a sampling bag (volume: 1L, SKC) and injected into the GC with a 250 µL gas-tight syringe (SGE, Australia). Helium was used as a carrier gas at a flow rate of 4.5 mL/min and a two-column-switching-system separated the gas components of the sample. CO_2 was cut off in the first column (HP-Plot Q, 30 m x 0.53 mm x 40 µm film thickness), the other gases (Ar, N_2, H_2, CO, CO_2, CH_4) in the second column (HP-Plot Molecular Sieve 5A, 30 m x 0.53 mm x 50 µm film thickness). A TCD, which was heated to 250 °C, measured the concentrations of the separated gases. The temperature program during analysis was as follows: 0-3.3 min at 45 °C, heat up to 70 °C at 10 °C/min (no holding time at 70 °C), further heat up to 100 °C at 40 °C/min, 1.05 min isothermal at 100 °C, cool down to 45 °C at 50 °C/min; total analysis time 8.70 min.

A set of gas mixtures purchased from Messer Schweiz AG was used for calibration. The performance of the GC was always checked before sample analysis by measurement of a calibration gas.

3.4.5. ICP-OES (Inductively Coupled Plasma Optical Emission Spectrometry)

Quantitative analysis of K, Na, S and P contained in aqueous samples was carried out using an ICP-OES device (SPECTRO Ciros Vision SOP). The analyzer was calibrated with different dilutions of multi-element standard solutions (purchased either from Kraft or from Merck). To gain concentrations within the calibrated range, the samples were diluted by a factor of 100 with deionized water. Argon was used as a carrier gas. Each sample was measured multiple times until the SD was low and the last three measurements were used for evaluation.

3.4.6. Analysis of sulfur adsorber and catalyst

As KONTI-C was used for further tests and an experimental campaign right after our work, the reactor was not discharged after the last experiment (Section 5.7). Therefore, no analysis with respect to ZnO and 5%-Ru/C could be conducted, which would have enabled a more detailed evaluation of the experiments with microalgae (Section 5). The ZnO that was used for the third (Section 5.4) and the fourth liquefaction test (Section 5.5) was not processed long enough for gaining reliable surface analysis results.

4. Results of the experiments with model solutions

4.1. General information

Three KONTI-C tests were performed with model solutions. The aim of these tests was to get familiar with the new pilot plant and its equipment and to assess the performance of the new salt separator prior to processing algal biomass. The model solutions were aqueous salt solutions of Na_2SO_4 (0.1 mol/kg) and K_2SO_4 (0.05 mol/kg), two of them additionally contained 10 wt% isopropanol. A detailed study on continuous hydrothermal salt separation of different water-salt mixtures had already been conducted by Schubert [59–62].

During the assessment of the salt separation performance, the reactor filled with activated carbon was not needed. For the third experiment the reactor was replaced by a bypass pipe. The temperature setpoints for the heating blocks of the salt separator were chosen in such a way so that two zones were generated inside – a lower subcritical and a higher supercritical water zone. As a result, the salts should stay in the lower part and leave the salt separator at the bottom (brine effluent) and salt-free water could exit the salt separator at the top (reactor effluent). This idea has already been described in Sections 2.1.6 and 3.1.

4.2. Results of the first salt separation test (Na_2SO_4-K_2SO_4-H_2O)

4.2.1. Basic and starting conditions

The basic and starting conditions of the first salt separation test are listed in Table 4.1. The aim of this experiment was to assess the efficiency of the salt separator being fed with a simple solution consisting only of water and two salts. Although the reactor was not wittingly heated, it was warmed by the hot stream coming from the salt separator to temperatures up to 365 °C at the bottom and 242 °C at the top. The actual mass flow rate was determined through dividing the weight difference of the feed tank by the feeding time of the model solution.

4.2.2. Progression of temperature, pressure, electrical conductivity and sulfur content

The important comments noted during the test are summarized in Table 4.2. The on-line measurements of temperature, pressure and conductivity are depicted in Figures 4.1, 4.2, 4.3 and 4.4.

The temperature measurements at the inner wall and the lance of the salt separator (Figures 4.1 and 4.2) illustrate that the temperature profile inside the salt separator was nearly constant when the model solution was fed (TOS: 1.22 to 4.02 h). This implies that fluid dynamics and heat transfer hardly changed. As mentioned in Table 4.2, the jump of the lance temperatures

(Figure 4.2) after 0.95 h occurred due to stuck measurements. When the data transfer cable between the lance and the PC was disconnected and after a few seconds reconnected again, the measurements updated. The reason why the temperatures rapidly increased by 10-20 °C after about 4 h was that air went inside the feed tank and was pumped into KONTI-C.

Table 4.1: Basic and starting conditions of the first salt separation test.

Parameter	Unit	Value
Desired time on stream	h	4.00
Na_2SO_4 in feed	mol/kg	0.10
K_2SO_4 in feed	mol/kg	0.05
Feed temperature	°C	23-24
Desired inner T-profile of salt separator	°C	240-430
Setpoint for pressure controller (PTRC 5-3)	barg	280.00
Setpoint for chiller	°C	18.00
Setpoint for HPLC pump	mL/min	18.00
Actual feed flow rate	g/min	18.22
Setpoint for Liquiflow	% (g/min)	100 (3.2)
Reactor/Bypass	-	Reactor
Reactor filling	-	Activated carbon

Table 4.2: Comments on the first salt separation test.

Time	Time on stream (in h)	Comment
07:45	-	Start with heating up
11:48	0.95	Temperature values of the lances were frozen
12:04	1.22	Switch to model solution
12:20	1.48	Start sampling, every 20 min (reactor: for 10 s, brine: for 4 min)
13:00	2.14	Pressure swings are becoming bigger
13:12	2.34	ECTR 3-1: peak jump, disconnected & reconnected
14:52	4.02	Switch back to water
15:00	4.14	Cooling down and rinsing overnight

The pressure measurements (Figure 4.3) show a different behavior. After about two hours PTR 2-2 and PTR 2-3 started to oscillate, which became more intense with time so that PTR 4-1, PTR 5-1 and PTRC 5-3 started to fluctuate, too. Since PTR 4-1 did not change at the beginning, plugging might have occurred at a position between the measurement point of PTR 2-3 in the middle of the salt separator and the measurement point of PTR 4-1 at the reactor top. It is known that type 2 salts, like Na_2SO_4 and K_2SO_4, tend to precipitate in the salt separator and stick to the hot walls [62, 111].

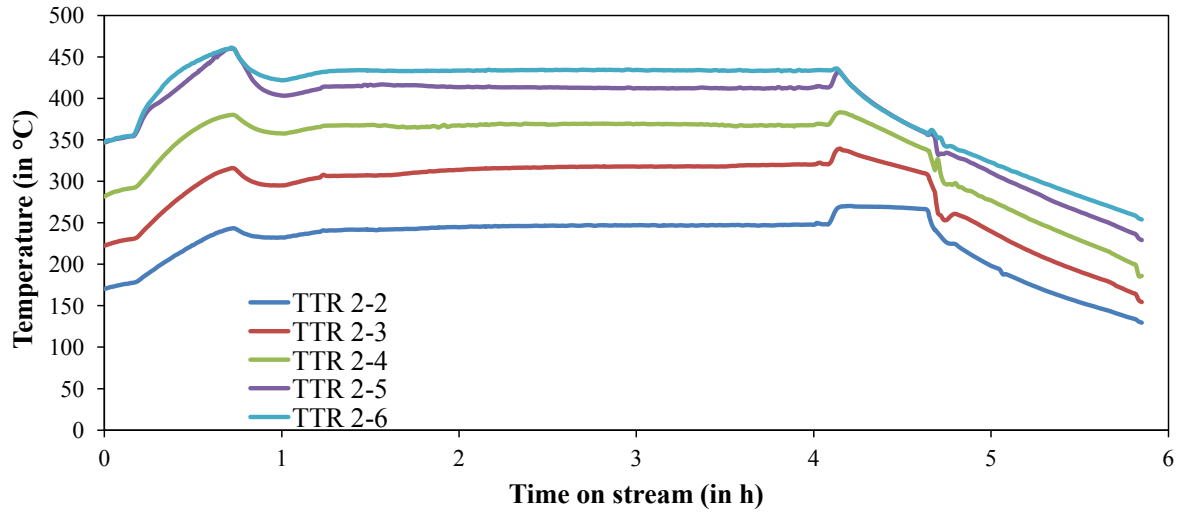

Figure 4.1: Evolution of the temperature at the inner wall of the salt separator (first salt separation test).

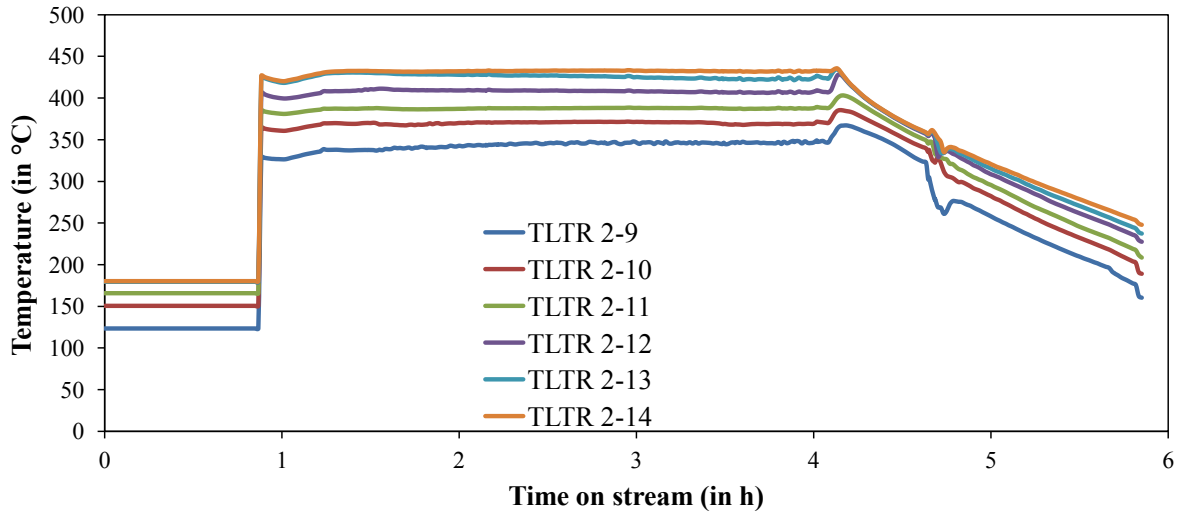

Figure 4.2: Evolution of the temperature at the lance of the salt separator (first salt separation test).

Since no change in heat transfer conditions can be seen either in Figure 4.1 or in Figure 4.2, salts might have precipitated at a place where no temperature sensors were present, which makes it difficult to identify the exact location. Interestingly, the measurements of PTR 2-3 were bigger than the ones of PTR 2-2 and the measurements of PTRC 5-3 were bigger than the ones of PTR 5-1. Theoretically, this is not possible but that might have been due to inaccuracies of the manometers. The pressure drop after four hours occurred because of air pumped into KONTI-C.

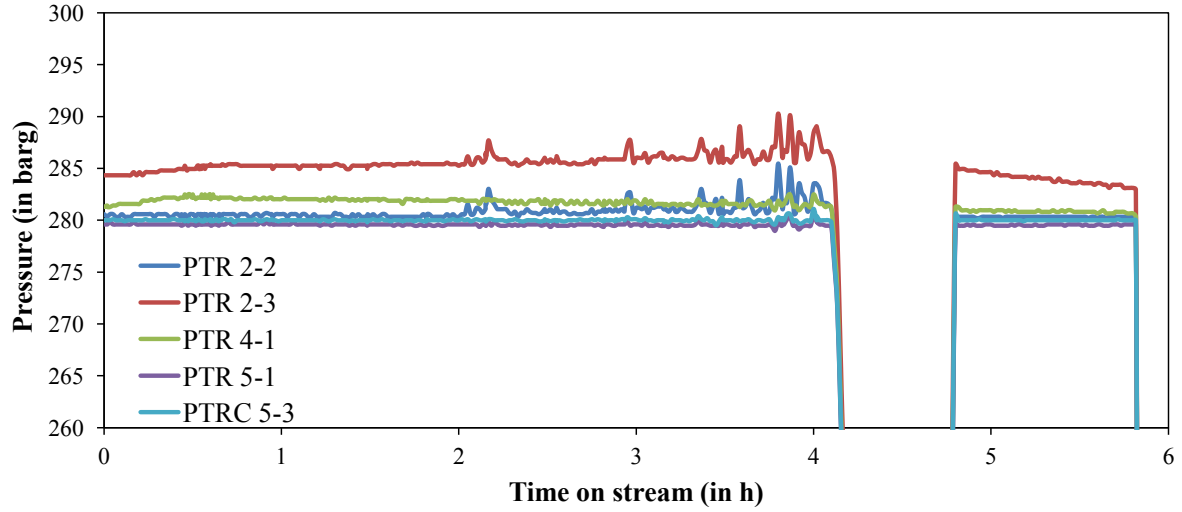

Figure 4.3: Evolution of the pressure (first salt separation test).

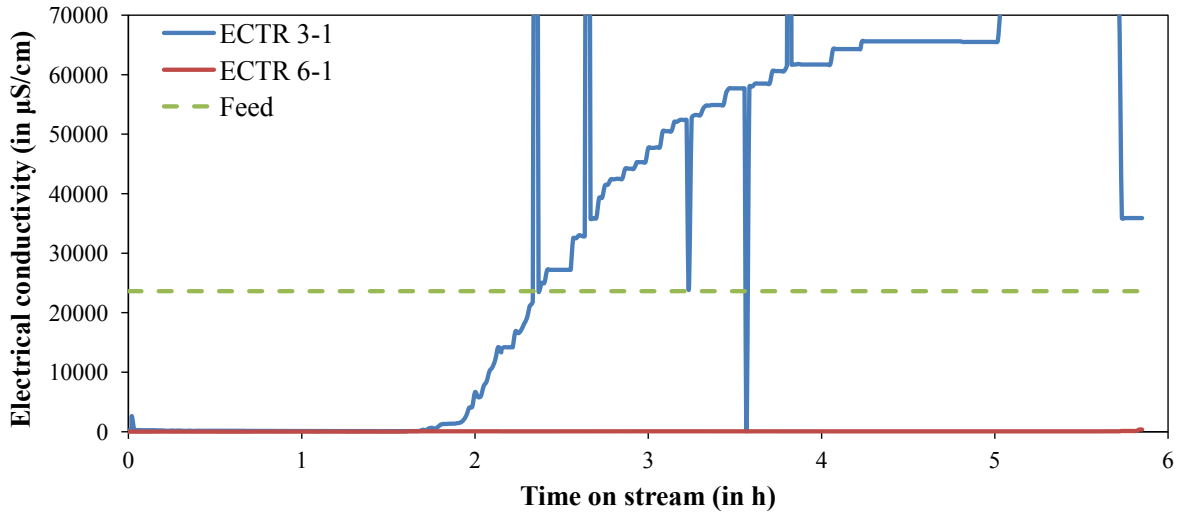

Figure 4.4: Evolution of the electrical conductivity (first salt separation test).

The conductivity measurements (Figure 4.4) suggest that the salt separation was successful. The electrical conductivity of the brine effluent (ECTR 3-1) started to increase rapidly after about two hours and reached a maximum value of about 65 000 µS/cm at the end of the experiment, which was nearly three times higher than the electrical conductivity of the feed. After 2.34 h the measurement of ECTR 3-1 suddenly jumped to a very high value. When the data transfer cable to the PC was removed from the conductivity meter, the measurement updated to its real value. Unfortunately, the value stuck again when the data transfer cable was plugged in again. Therefore, the cable had to be disconnected and reconnected every few minutes to get the real electrical conductivity of the brine effluent. This is why the curve of ECTR 3-1 looks steplike. This problem could not be solved during the campaign and would occur in every experiment

since no other conductivity meters were available. In the next sections, those peaks will be removed in the figures of the electrical conductivity measurements for overview purposes.

The electrical conductivity of the reactor effluent (ECTR 6-1) was below 70 µS/cm throughout the experiment. This indicates that hardly any ions were present in the reactor effluent. One might wonder if the activated carbon in the reactor could have retained parts of the salts. Schubert [62] carried out similar experiments with a reactor filled with a 2%-Ru/C catalyst and was able to have closed mass balances based on the concentrations of inlet and outlet streams. He conducted an experiment with a Na_2SO_4-K_2SO_4-H_2O solution, too. The main differences to our setup were: the configuration of the salt separator (a dip tube instead of a standpipe), the salt concentration (0.05 instead of 0.1 mol/kg Na_2SO_4), and the mass flow rate. Schubert ran his experiment at different temperature setpoints for the salt separator to find a temperature range where the best salt separation could be achieved. Whenever the electrical conductivity of the brine effluent reached steady-state, the experiment was carried out at a different temperature. He did not state anything about pressure problems or plugging during his experiment with Na_2SO_4 and K_2SO_4. This could have possibly been achieved by his lower Na_2SO_4 concentration and his higher brine effluent to feed flow ratio. However, in Schubert's experiment the electrical conductivity of the reactor effluent did not go below 5000 µS/cm, which emphasizes the positive result of our first KONTI-C salt separation test.

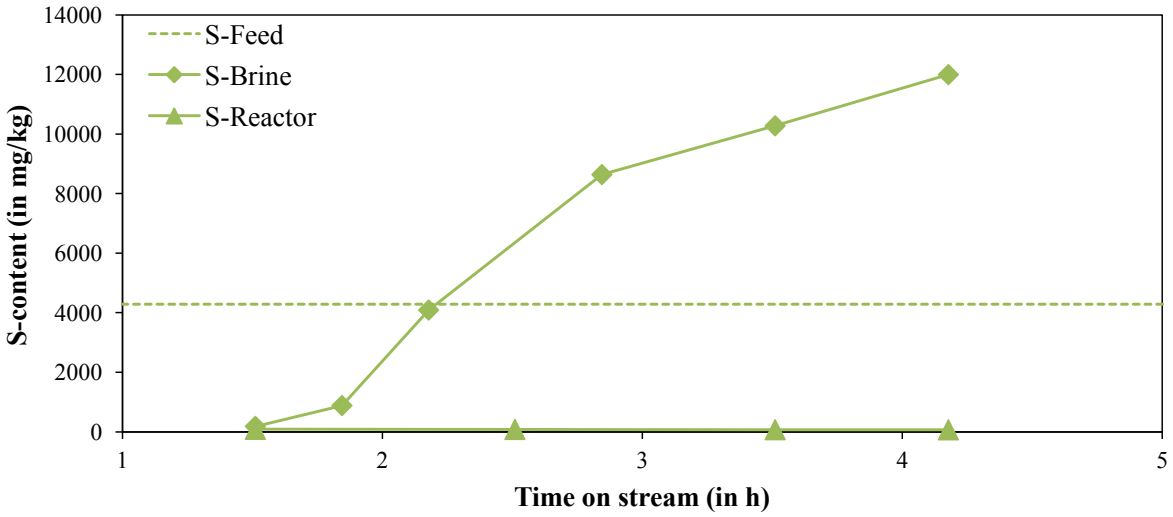

Figure 4.5: Evolution of the sulfur content in brine- and reactor effluent (first salt separation test).

To get an additional indicator for the efficiency of the salt separation, the sulfur concentration of feed, brine effluent and reactor effluent of samples taken during the run were measured off-line. As it can be seen in Figure 4.5, the sulfur content of the reactor effluent was below 100 mg/kg throughout the experiment. The progression of the sulfur in the brine effluent shows the same trend as the electrical conductivity confirming a successful salt separation (compare Figure 4.5 with Figure 4.4). As outlined in Table 4.3, a sulfur recovery in the brine effluent of less than 50%

could be calculated. Since the other 50% could not be found in the reactor effluent, the mass balance is not closed. This implies that steady-state had not been reached and/or some kind of salt deposition inside the salt separator had taken place. It is not believed that sulfur could have left KONTI-C in a gaseous form because Schubert [62] always had closed mass balances with respect to the liquid phases in all his experiments with sulfuric compounds.

Table 4.3: Sulfur recovery in the brine effluent (first salt separation test).

Parameter	Unit	Value
Mass flow rate of feed	g/min	18.22
Sulfur content in feed	mg/kg	4283
Mass flow rate of brine	g/min	3.20
Final sulfur content in brine	mg/kg	11994
Sulfur recovery in brine	%	49.18

4.3. Results of the second salt separation test (Na_2SO_4-K_2SO_4-IPA-H_2O)

4.3.1. Basic and starting conditions

The basic and starting conditions of the second salt separation test are listed in Table 4.4. The aim of this experiment was to determine the effect of an organic compound (isopropanol) on the performance of the salt separation.

Table 4.4: Basic and starting conditions of the second salt separation test.

Parameter	Unit	Value
Desired time on stream	h	4.00
Na_2SO_4 in feed	mol/kg	0.10
K_2SO_4 in feed	mol/kg	0.05
Isopropanol in feed	wt%	10.00
Feed temperature	°C	22-24
Desired inner T-profile of salt separator	°C	240-430
Setpoint for chiller	°C	18.00
Setpoint for pressure controller (PTRC 5-3)	barg	280.00
Setpoint for HPLC pump	mL/min	18.00
Actual feed flow rate	g/min	17.83
Setpoint for Liquiflow	% (g/min)	100 (3.2)
Reactor/Bypass	-	Reactor
Reactor filling	-	Activated carbon

Although the reactor was not heated by its heating blocks, it was warmed by the hot stream coming from the salt separator to temperatures up to 356 °C at the bottom and 245 °C at the top. The actual mass flow rate was determined through dividing the weight difference of the feed tank by the feeding time of the model solution.

4.3.2. Progression of temperature, pressure, electrical conductivity and sulfur content

The important comments noted during the test are summarized in Table 4.5. The on-line measurements of temperature, pressure and conductivity are depicted in Figures 4.6, 4.7, 4.8 and 4.9.

Table 4.5: Comments on the second salt separation test.

Time	Time on stream (in h)	Comment
07:45	0.01	Start with heating up
10:12	2.46	Salt separator: T-setpoint = 485 °C (both heating blocks)
10:29	2.74	Switch to model solution
10:50	3.10	Start sampling, every 20 min (reactor: for 6 s, brine: for 3 min)
12:29	4.73	Pressure swings are becoming bigger
13:39	5.90	Liquiflow decreased to 80% to get higher concentration
14:34	6.83	Switch back to water, Liquiflow increased to 100%
15:16	7.53	Pressure set to 250 bar, cooling down and rinsing overnight

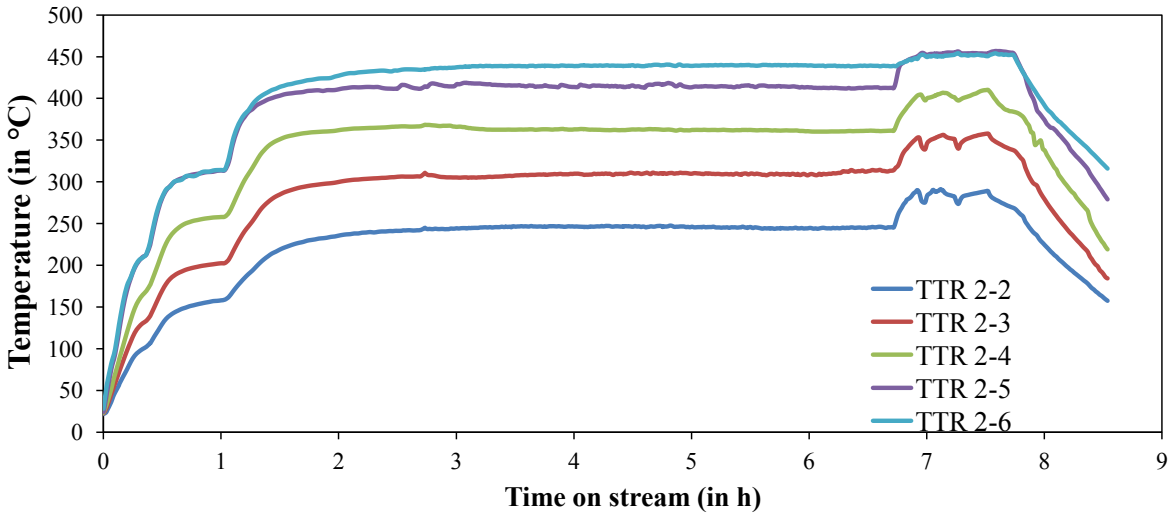

Figure 4.6: Evolution of the temperature at the inner wall of the salt separator (second salt separation test).

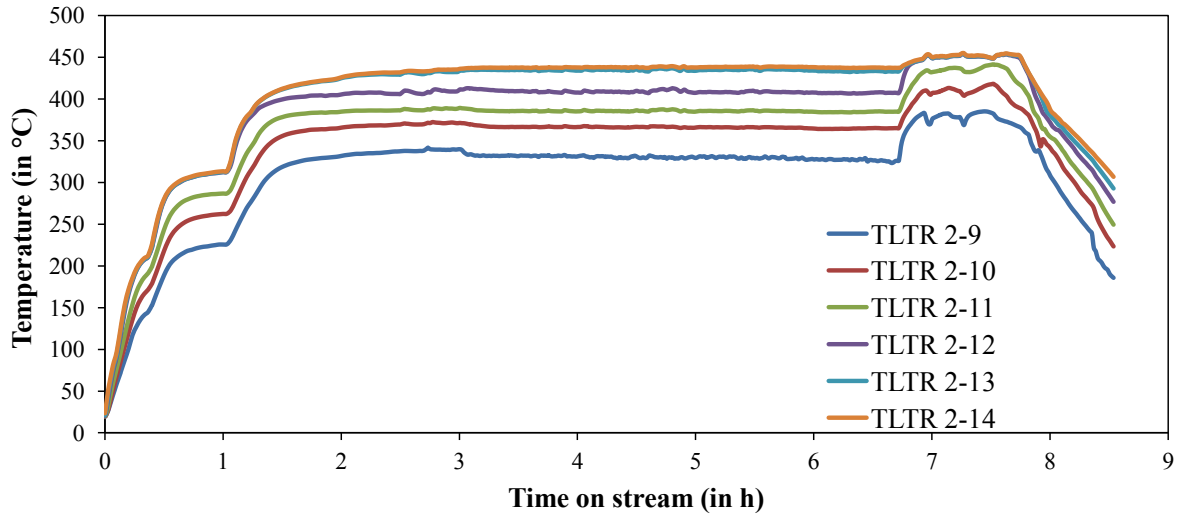

Figure 4.7: Evolution of the temperature at the lance of the salt separator (second salt separation test).

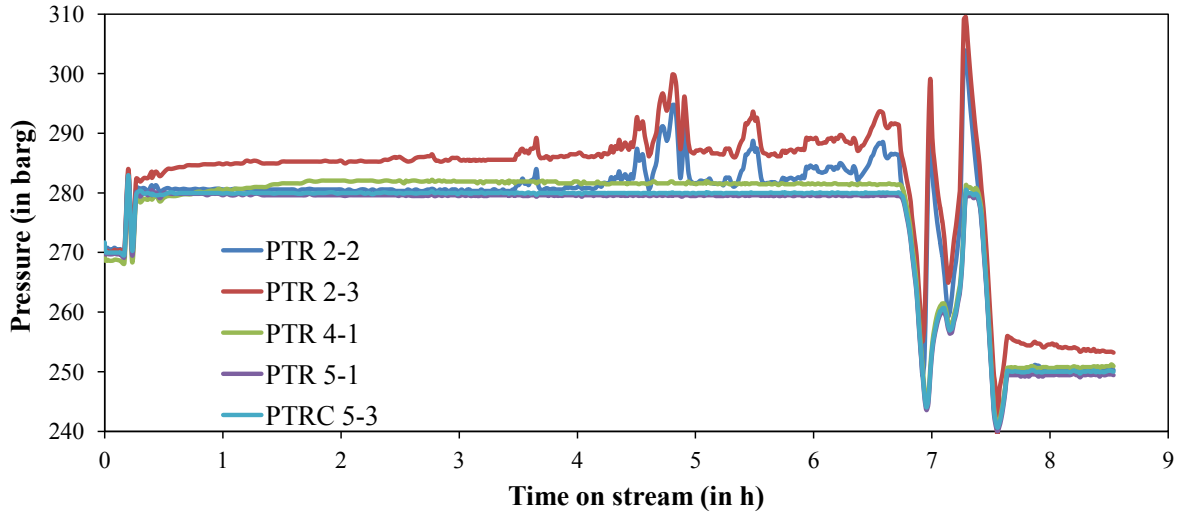

Figure 4.8: Evolution of the pressure (second salt separation test).

The temperature measurements at the inner wall and the lance of the salt separator (Figures 4.6 and 4.7) illustrate that the temperature profile hardly changed when the model solution was fed (TOS: 2.74 to 6.83 h). This implies that fluid dynamics and heat transfer did not change. The reason why the temperatures increased by 10-50 °C after 6.8 h was again that air went inside the feed tank and was pumped into KONTI-C.

The pressure measurements (Figure 4.8) look similar to the ones of the first salt separation test. PTR 2-2 and PTR 2-3 started to oscillate after 3.75 h, which became more intense with time. Since PTR 4-1 did not change, plugging might have occurred at a position between the measurement point of PTR 2-3 in the middle of the salt separator and the measurement point

of PTR 4-1 at the reactor top. The pressure fluctuations could have been related to the buildup and subsequent breakdown of precipitated salts. Again, a change of heat transfer conditions can be seen neither in Figure 4.6 nor in Figure 4.7. Therefore, the exact location of the plugging could not have been identified. After 6.8 h all the pressure measurements fluctuated a lot due to air inside KONTI-C.

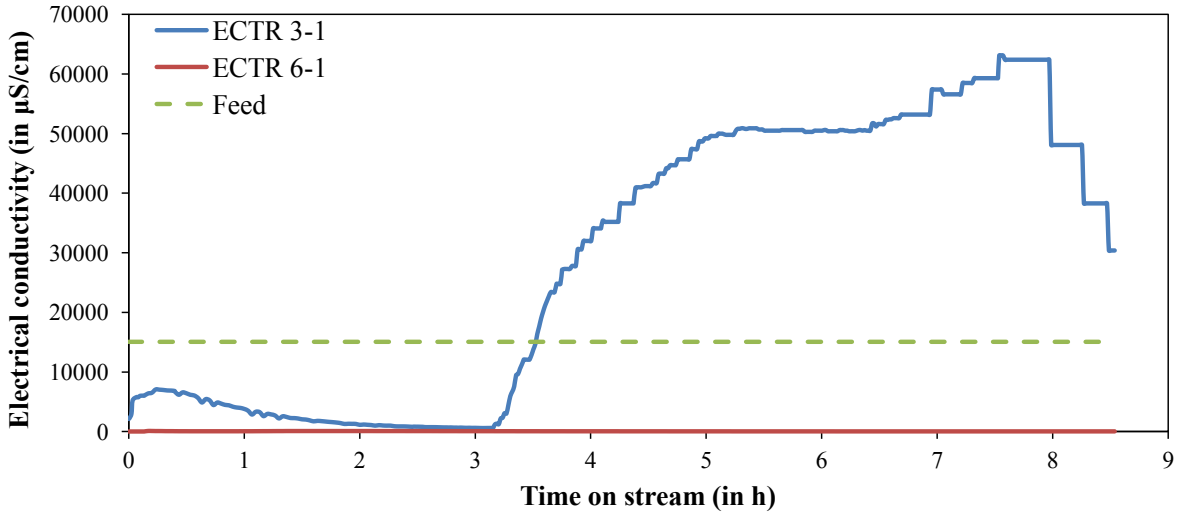

Figure 4.9: Evolution of the electrical conductivity (second salt separation test).

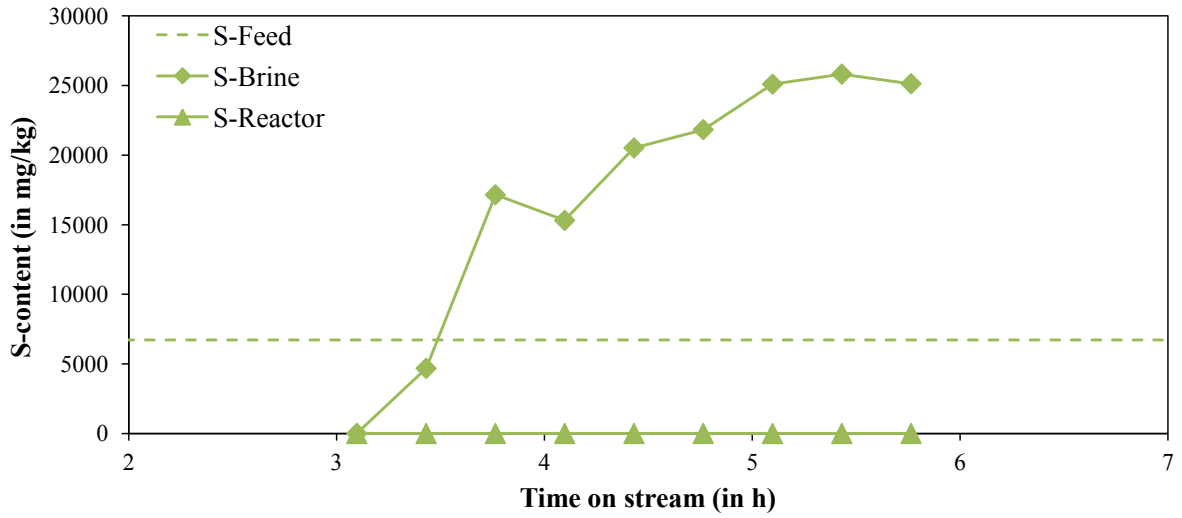

Figure 4.10: Evolution of the sulfur content in brine- and reactor effluent (second salt separation test).

The conductivity measurements (Figure 4.9) suggest that the salt separation was successful. The electrical conductivity of the brine effluent (ECTR 3-1) started to increase rapidly after about 3 h and reached a first constant value of around 50 000 µS/cm after about 5 h, which was more than three times higher than the electrical conductivity of the feed. Later on the conductivity of the

brine grew even further to values higher than 60 000 µS/cm. On the one hand, this could have been the consequence of the Liquiflow reduction after 5.9 h (see Table 4.5). On the other hand, this could have correlated with the strong pressure fluctuations after 6.8 h, which may have unfixed the precipitated salts from the walls or have washed them out from dead zones. To be mentioned at this point, a delayed change in conductivity was always observed during this campaign whenever the pressure of KONTI-C changed abruptly. The electrical conductivity of the reactor effluent (ECTR 6-1) was below 100 µS/cm throughout the experiment. This indicates that hardly any ions were in the reactor effluent and that the efficiency of the salt separation was not influenced by isopropanol.

The sulfur content of feed, brine effluent and reactor effluent are shown in Figure 4.10. The sulfur content of the reactor effluent stayed below the detection limit throughout the experiment. The progression of the sulfur in the brine effluent shows the same trend as the electrical conductivity confirming a successful salt separation (compare Figure 4.10 with Figure 4.9). The sulfur concentration started to increase rapidly after 3 h and reached a constant value of around 25 100 mg/kg after about 5.5 h. As outlined in Table 4.6, a sulfur recovery in the brine effluent of less than 70% can be calculated. Since the other 30% could not be found in the reactor effluent, the mass balance is not closed. Again, this implies that steady-state had not been reached and/or some kind of salt deposition inside the salt separator had taken place. The fact that the electrical conductivity further increased after the strong pressure fluctuations may be a hint for the deposition of salts inside the salt separator.

Table 4.6: Sulfur recovery in the brine effluent (second salt separation test).

Parameter	Unit	Value
Mass flow rate of feed	g/min	17.83
Sulfur content in feed	mg/kg	6720
Mass flow rate of brine	g/min	3.20
Final sulfur content in brine	mg/kg	25100
Sulfur recovery in brine	%	67.04

4.4. Results of the third salt separation test (Na_2SO_4-K_2SO_4-IPA-H_2O)

4.4.1. Basic and starting conditions

The basic and starting conditions of the third salt separation test are listed in Table 4.7. This was the first time that a bypass pipe for the reactor was used. The aim of this experiment was to repeat the second salt separation test with a different setpoint for the flow controller of the brine effluent (Liquiflow). It was set to 50% instead of 100% to see if the salt concentration could be further improved. The actual mass flow rate was determined through dividing the weight difference of the feed tank by the feeding time of the model solution.

Table 4.7: Basic and starting conditions of the third salt separation test.

Parameter	Unit	Value
Desired time on stream	h	4.00
Na_2SO_4 in feed	mol/kg	0.10
K_2SO_4 in feed	mol/kg	0.05
Isopropanol in feed	wt%	10.00
Feed temperature	°C	22-24
Desired inner T-profile of salt separator	°C	240-430
Setpoint for chiller	°C	18.00
Setpoint for pressure controller (PTRC 5-3)	barg	280.00
Setpoint for HPLC pump	mL/min	18.00
Actual feed flow rate	g/min	16.52
Setpoint for Liquiflow	% (g/min)	50 (1.6)
Reactor/Bypass	-	Bypass
Reactor filling	-	-

4.4.2. Progression of temperature, pressure, electrical conductivity and sulfur content

The important comments noted during the test are summarized in Table 4.8. The on-line measurements of temperature, pressure and conductivity are depicted in Figures 4.11, 4.12, 4.13 and 4.14.

The temperature measurements at the inner wall and the lance of the salt separator (Figures 4.11 and 4.12) illustrate that the temperature profile changed significantly twice when the model solution was fed (TOS: 1.88 to 4.99 h). The reason for this was that air was unwittingly pumped into KONTI-C. For the rest of the feeding time the temperature trend inside the salt separator was more or less constant but not as smooth as during the first two experiments. This was likely related to the lower setpoint for the Liquiflow.

The pressure trends (Figure 4.13) are more chaotic than the ones of the two previous salt separation tests. As in the first two experiments, PTR 2-2 and PTR 2-3 started to oscillate but this time 50 min after switching to the model solution already. The oscillations became more intense with time so that PTR 5-1 and PTRC 5-3 started to fluctuate, too. Since PTR 5-1 did not change at the beginning, plugging might have occurred at a position between the measurement point of PTR 2-3 in the middle of the salt separator and the measurement point of PTR 5-1 before the filter of the reactor effluent.

Table 4.8: Comments on the third salt separation test.

Time	Time on stream (in h)	Comment
07:45	-	Start with heating up
10:17	1.88	Switch to model solution
10:20	1.92	Start sampling, every 20 min (reactor: 15 s, brine: 8 min)
11:38	3.23	Liquiflow set to 100% due to pressure problem
11:40	3.27	Liquiflow: 70%
11:42	3.29	Liquiflow: 100%
11:51	3.45	ECTR 6-1 causes problems again
11:52	3.47	Liquiflow: 75%
11:54	3.50	ECTR 6-1 causes problems again
12:27	4.05	Air was in the HPLC pump
12:30	4.10	Liquiflow: 50%
13:24	4.99	Switch back to water, Liquiflow: 100%
13:27	5.04	Cooling down and rinsing overnight

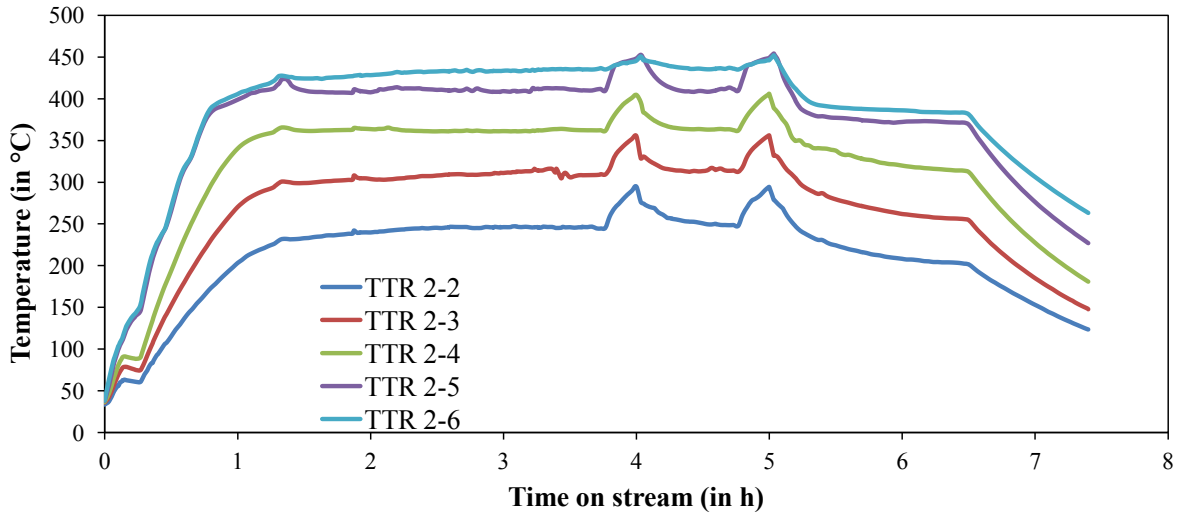

Figure 4.11: Evolution of the temperature at the inner wall of the salt separator (third salt separation test).

The pressure fluctuations could have been related to the buildup and subsequent breakdown of precipitated salts. In contrast to the two previous salt tests, the oscillations were much stronger. The reason was probably the lower brine effluent flow leading to longer retention of the salts inside the salt separator. When the pressure reached nearly 300 bar, the Liquiflow was set to 100% (see Table 4.8). After the system had settled down, the Liquiflow was reduced again. The pressure drops after four and five hours arose because of air pumped into KONTI-C.

The conductivity measurements (Figure 4.14) show that the salt separation was successful again. The electrical conductivity of the brine effluent (ECTR 3-1) started to increase rapidly

after 3 h and reached a maximum value of about 73 000 µS/cm 25 min after the feed had been switched back to water. This was nearly five times higher than the electrical conductivity of the feed. The start of the conductivity incline occurred half an hour later than during the previous experiments, which could be explained by the lower brine effluent flow. The electrical conductivity of the reactor effluent (ECTR 6-1) was very low for the first 5.5 h. This indicates that hardly any ions were in the reactor effluent and proves the high efficiency of the salt separator for such a solution. The subsequent conductivity gain (up to 6700 µS/cm) could have been caused by the strong pressure fluctuations leading to "slopping over" at the top of the salt separator.

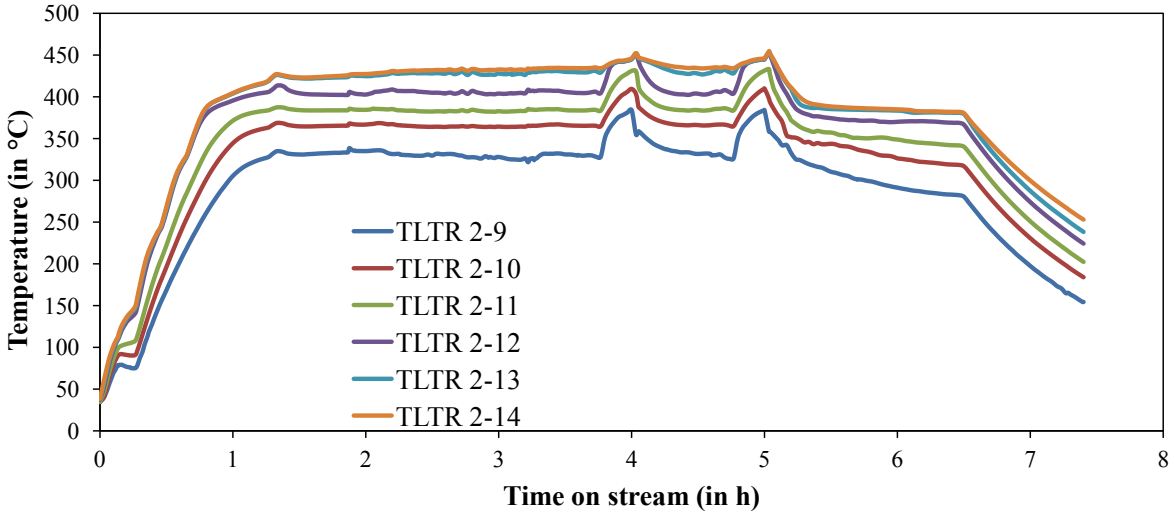

Figure 4.12: Evolution of the temperature at the lance of the salt separator (third salt separation test).

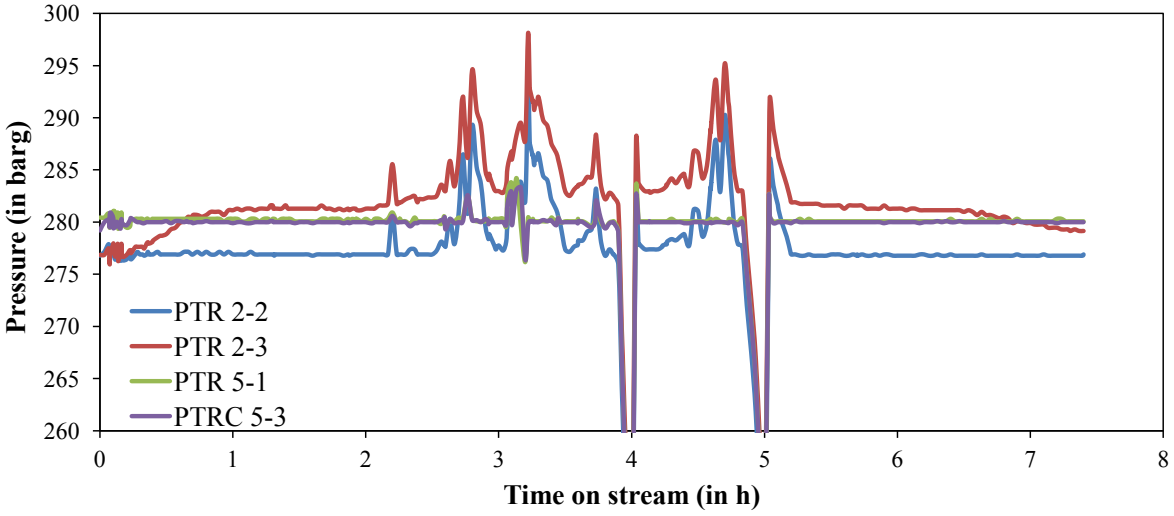

Figure 4.13: Evolution of the pressure (third salt separation test).

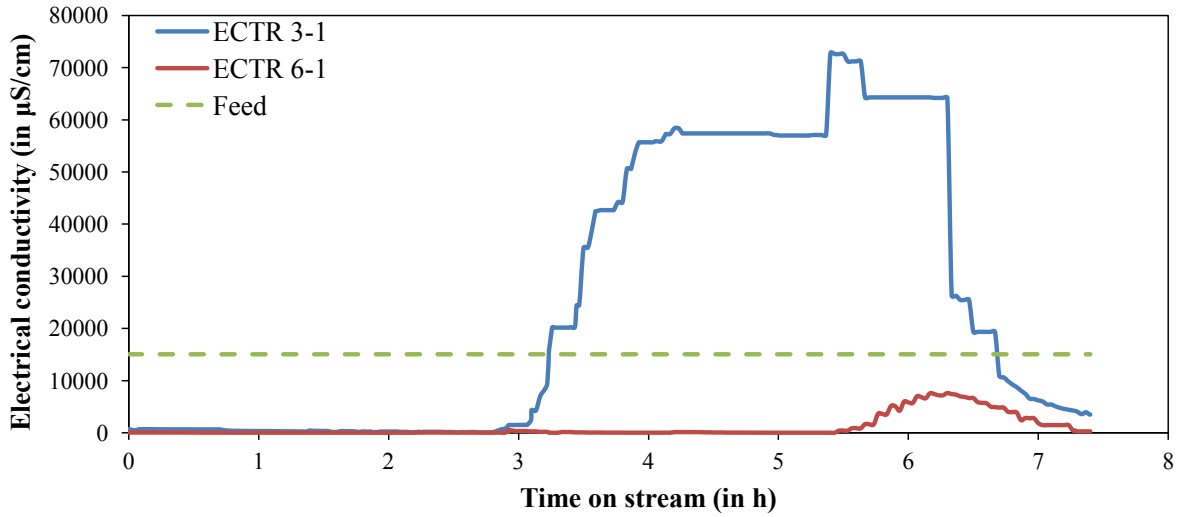

Figure 4.14: Evolution of the electrical conductivity (third salt separation test).

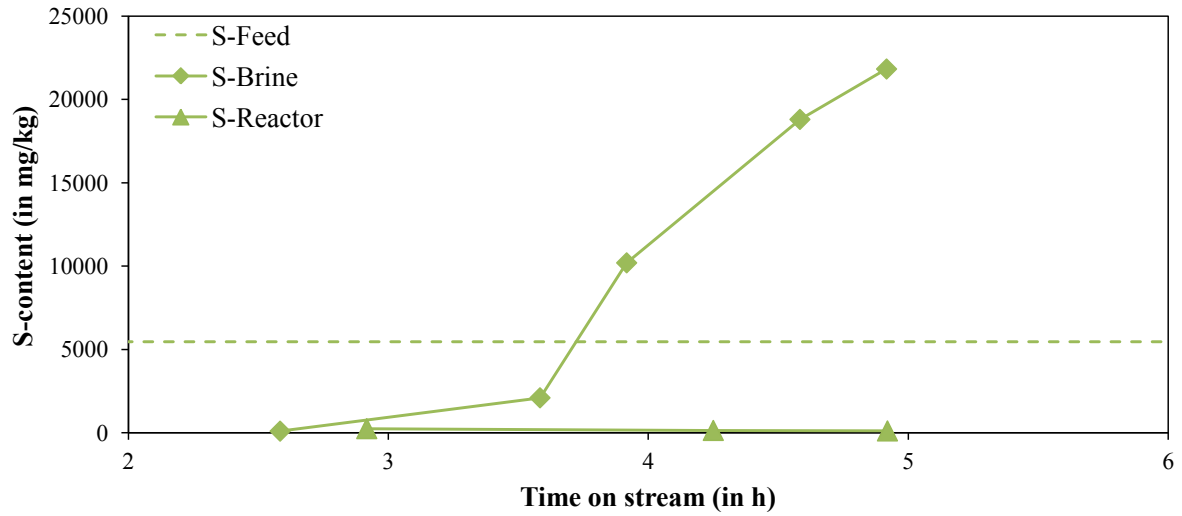

Figure 4.15: Evolution of the sulfur content in brine- and reactor effluent (third salt separation test).

The sulfur content of feed, brine effluent and reactor effluent are shown in Figure 4.15. The sulfur content of the reactor effluent stayed below 200 mg/kg throughout the run. The progression of the sulfur in the brine effluent shows the same trend as the electrical conductivity confirming a successful salt separation (compare Figure 4.15 with Figure 4.14). As outlined in Table 4.9, a sulfur recovery in the brine effluent of less than 40% can be calculated. However, the absence of the other 60% in the reactor effluent and the shape of the temporal course of the sulfur content suggest that steady-state had not been reached or that salts had been deposited inside the plant.

Table 4.9: Sulfur recovery in the brine effluent (third salt separation test).

Parameter	Unit	Value
Mass flow rate of feed	g/min	16.52
Sulfur content in feed	mg/kg	5468
Mass flow rate of brine	g/min	1.60
Final sulfur content in brine	mg/kg	21825
Sulfur recovery in brine	%	38.66

4.5. Summary of the experiments with model solutions

- Three experiments with aqueous solutions containing 0.1 mol/kg Na_2SO_4 and 0.05 mol/kg K_2SO_4 were conducted. Two of them contained 10 wt% isopropanol as well. The aim was to get familiar with PSI's new continuous plant (KONTI-C) and to test the efficiency of the salt separator.
- In terms of electrical conductivity and sulfur analysis, salt separation was very efficient. In contrast to Schubert's experiment [62], the electrical conductivity of the reactor effluent stayed very low throughout the tests when working with a Na_2SO_4-K_2SO_4-H_2O solution.
- The mass balance of sulfur could not be closed (< 70%) indicating that steady-state had not been reached or that some kind of salt deposition had taken place.
- The addition of an organic compound (isopropanol) did not have a significant effect regarding salt separation efficiency.

5. Results of the experiments with microalgae

5.1. General information

After having tested salt separation with model solutions, it was time to start working with algal biomass. Firstly, the performance of the salt separator should be assessed, when working with microalgae. Parameters, such as the temperature, had to be optimized in order to achieve a stable liquefaction process. Additionally, the recovery of inorganic substances was of great interest. For those liquefaction tests the reactor bypass pipe was used.

Secondly, the performance of a ZnO adsorbent regarding continuous sulfur removal should be investigated. Besides sulfur adsorption, its catalytic performance should be assessed, too. The aim was to find out if sulfur adsorption took place and in how far ZnO had a catalytic effect on the gasification reactions.

Finally, the catalytic performance of a 5%-Ru/C catalyst during catalytic supercritical water gasification of microalgae had to be examined. The aim was to determine the gasification performance of KONTI-C.

5.2. Results of the first liquefaction test

5.2.1. Basic and starting conditions

The basic and starting conditions of the first liquefaction test are listed in Table 5.1. Since separation of the inorganic compounds was very efficient during the previous tests with model solutions, it was decided to arrange a similar temperature distribution inside the salt separator. As already mentioned in Section 3.1, the flow of the Slurry Feeder could be controlled by defining its working frequency (0-50 Hz). Unfortunately, no data was available correlating the frequency with the flow and no flow meter was built in downstream of the Slurry Feeder. Due to experience and Zöhrer's work [98], it was known that a frequency of 21 Hz corresponded to a mass flow rate of about 1 kg/h. It was decided to start at 23 Hz to rather have a higher than a lower flow to reduce the possibility of plugging. For the actual mass flow rate (weight difference of the feed tank divided by the feeding time) only an approximate value could be stated because the working frequency of the Slurry Feeder was changed during the experiment (see next section). The setpoint for the Liquiflow was set to 100% to minimize the possibility of plugging inside the salt separator, too.

5.2.2. Progression of temperature, pressure, electrical conductivity and composition

The important comments noted during the test are summarized in Table 5.2. The on-line measurements of temperature, pressure and conductivity are depicted in Figures 5.1, 5.2, 5.3

and 5.4.

Table 5.1: Basic and starting conditions of the first liquefaction test.

Parameter	Unit	Value
Desired time on stream	h	4.00
Microalgae content (dry matter)[(a)]	wt%	13.16
Feed temperature	°C	22-24
Desired inner T-profile of salt separator	°C	240-430
Setpoint for chiller	°C	18.00
Setpoint for pressure controller (PTRC 5-3)	barg	280.00
Setpoint for Slurry Feeder	Hz	23.00
Actual feed flow rate	g/min	17.50
Setpoint for Liquiflow	% (g/min)	100 (3.2)
Reactor/Bypass	-	Bypass
Reactor filling	-	-

[(a)]Based on the C-content of the feed (gained from CNS analysis) compared to the C-content of Ph. tricornutum from [14].

Table 5.2: Comments on the first liquefaction test.

Time	Time on stream (in h)	Comment
07:50	0.00	Start with heating up
10:00	2.18	Slurry Feeder valve opened, air inside!!
10:41	2.84	Switch to feed (cylinder 1)
11:11	3.36	Tar can be seen in reactor effluent
11:12	3.37	Color of reactor effluent changed from greenish to brownish
11:22	3.54	Color of brine became orange-brown
11:24	3.57	Gas in the reactor effluent, foam in the brine effluent
12:05	4.24	Problems with conductivity meters again
12:32	4.69	Pressure problem at PTR 2-2, Pmax set to 320 bar
12:56	5.10	Pressure problem at Flowserve (probably due to tar)
13:38	5.80	Pressure swings because of Flowserve fluctuations
14:04	6.23	Pressure problem at PTR 2-2 again
14:15	6.43	Temperature settings reduced to 450 °C
14:21	6.53	Trying to flush standpipe with water (HPLC)
14:42	6.87	Trying to feed microalgae again at 20 Hz
14:43	6.88	Temperature of SS set to 470 °C
14:47	6.95	Plugging in standpipe
14:47	6.96	Cooling down and rinsing overnight

A first qualitative look at the temperature measurements at the inner wall and the lance of

the salt separator (Figures 5.1 and 5.2) illustrates already that the temperature profile inside the salt separator was not constant at all when the algal slurry was fed (TOS: 2.84 to 6.95 h). This implies that fluid dynamics and heat transfer changed throughout the experiment. As mentioned in Table 5.2, the temperature hump after 2.18 h was related to the opening of the valve downstream of the Slurry Feeder (V-2-1). In the pipe between the Slurry Feeder and the valve there was air, which got compressed due to the high pressure difference. As a result, hot water from the salt separator was pulled backwards into the standpipe leading to a too strong temperature increase of TTR 2-1 (feed filter) and activation of the alarm. When the temperature went below its allowed maximum again, heating up of KONTI-C could be continued.

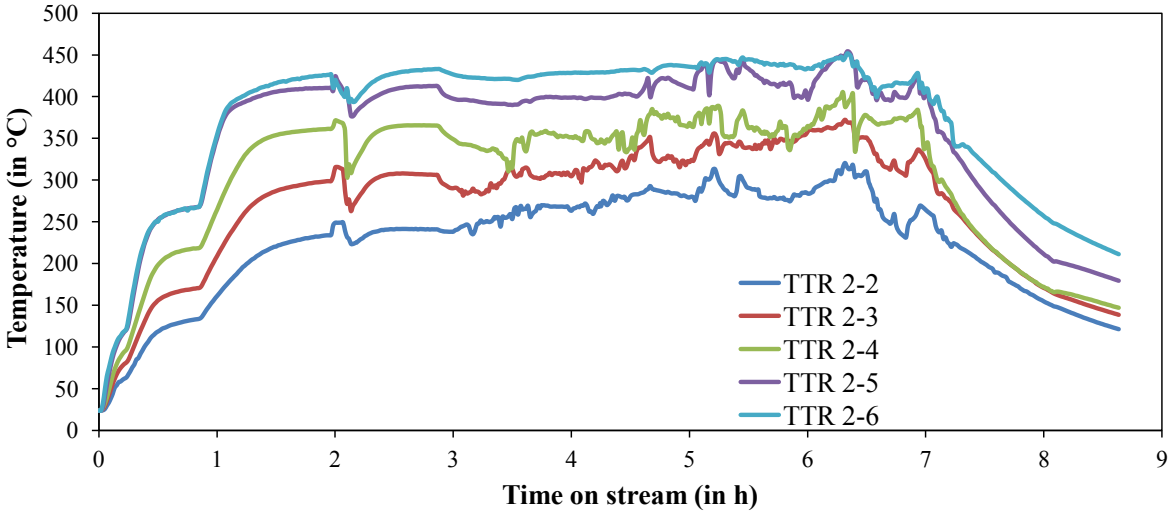

Figure 5.1: Evolution of the temperature at the inner wall of the salt separator (first liquefaction test).

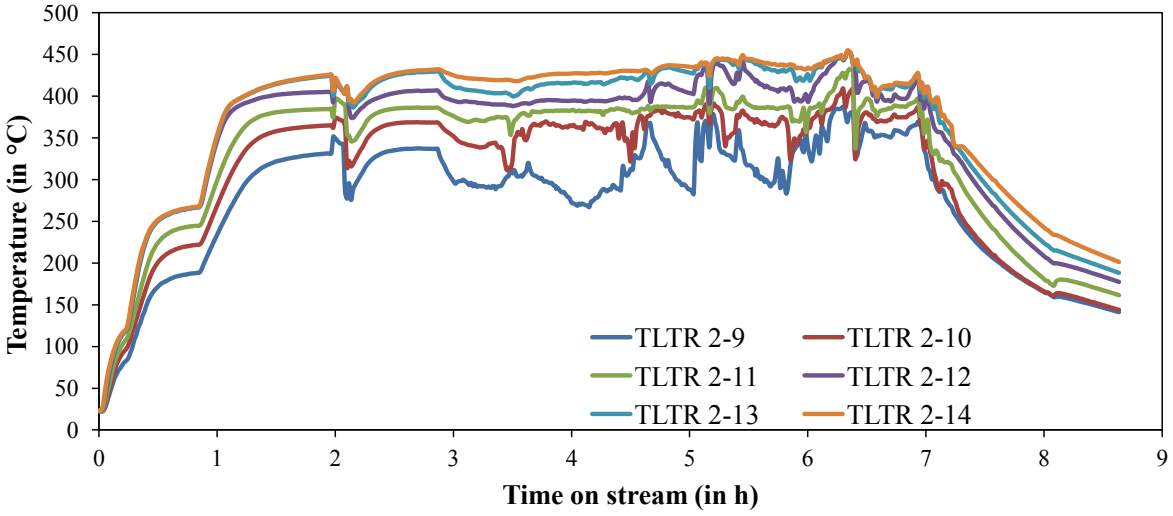

Figure 5.2: Evolution of the temperature at the lance of the salt separator (first liquefaction test).

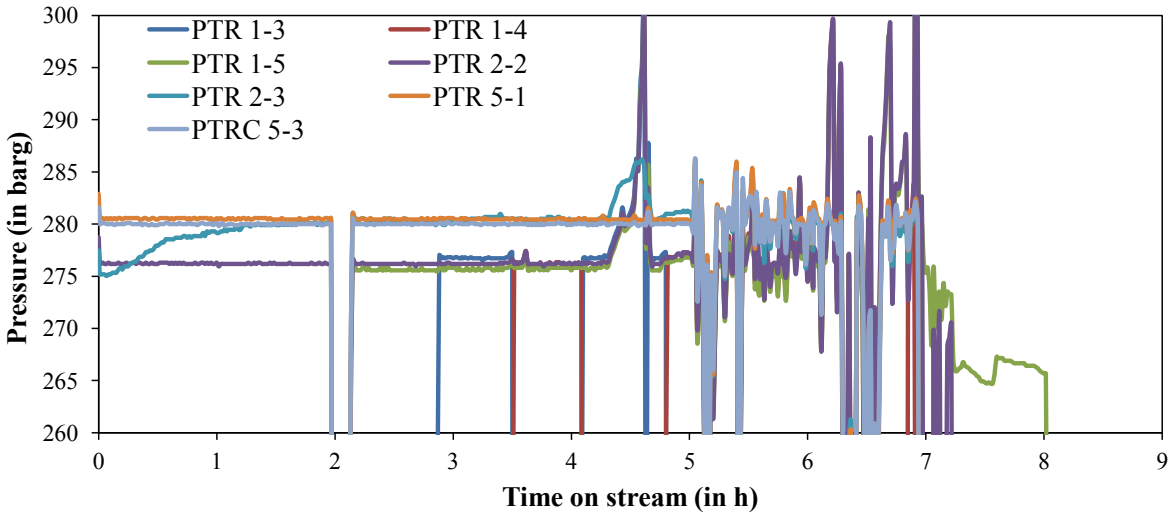

Figure 5.3: Evolution of the pressure (first liquefaction test).

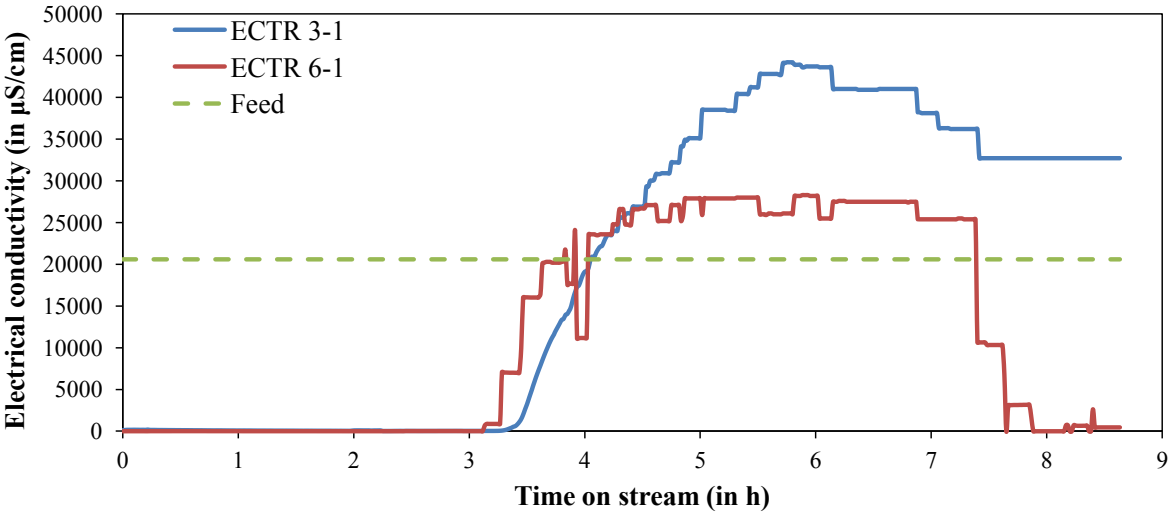

Figure 5.4: Evolution of the electrical conductivity (first liquefaction test).

The pressure (Figure 5.3) was quite stable for the first four hours. Then the pressure inside the salt separator (PTR 2-3) increased by about 6 bar and the pressure inside the standpipe (PTR 2-2) went up to even more than 300 bar. It seems that some kind of plugging inside the standpipe took place. Possible reasons could have been that particles in the feed were not withheld by the filter, that coke was formed or that salts precipitated at the nozzle of the standpipe caused by a too high temperature. After that huge pressure peak of PTR 2-2 it seemed that KONTI-C would calm down again, but then problems at the Flowserve (PTRC 5-3) arose. The tars, which had already been seen for 1.5 h (see Table 5.2), may have made it difficult for the Flowserve to work properly. In parallel, pressure problems inside the standpipe occurred again. After about 6.5 h it was decided to stop the Slurry Feeder for a few minutes and to flush the standpipe with

water by the use of the HPLC pump. 20 min later the Slurry Feeder was activated again at a lower mass flow rate (20 Hz), but plugging inside the standpipe led to the termination of the experiment.

The conductivity measurements (Figure 5.4) show a completely different trend than the ones of the tests with the salt solutions. The electrical conductivity of the reactor effluent did not stay very low when the algal slurry was processed. Interestingly, it started to grow earlier and steeper than the electrical conductivity of the brine effluent. This could be explained by the fact that the reactor and the brine effluent had a filter of the same volume, but the flow of the reactor effluent was 4-5 times higher than the one of the brine effluent. The conductivity of the reactor effluent reached a steady-state value of 27000-28 000 µS/cm after about 5 h. The fact that the electrical conductivity of the reactor effluent reached very high values suggests that salt separation was much less efficient compared to the tests with model solutions. However, compounds having an electrical conductivity, like organic acids and ammonia [54, 112], could have been formed during liquefaction in the salt separator, too. The conductivity of the brine effluent reached a maximum of more than 44 000 µS/cm after nearly 6 h, went back to about 41 000 µS/cm and stayed there until the end of the experiment.

Carbon-, nitrogen- and sulfur concentration of feed and brine effluent of the samples taken during the run were measured off-line. The results are shown in Figure 5.5. It can be seen that the C-, N- and S-concentration of the brine effluent had a similar progression as the electrical conductivity. They started to increase after about 3 h and reached a steady level two hours later.

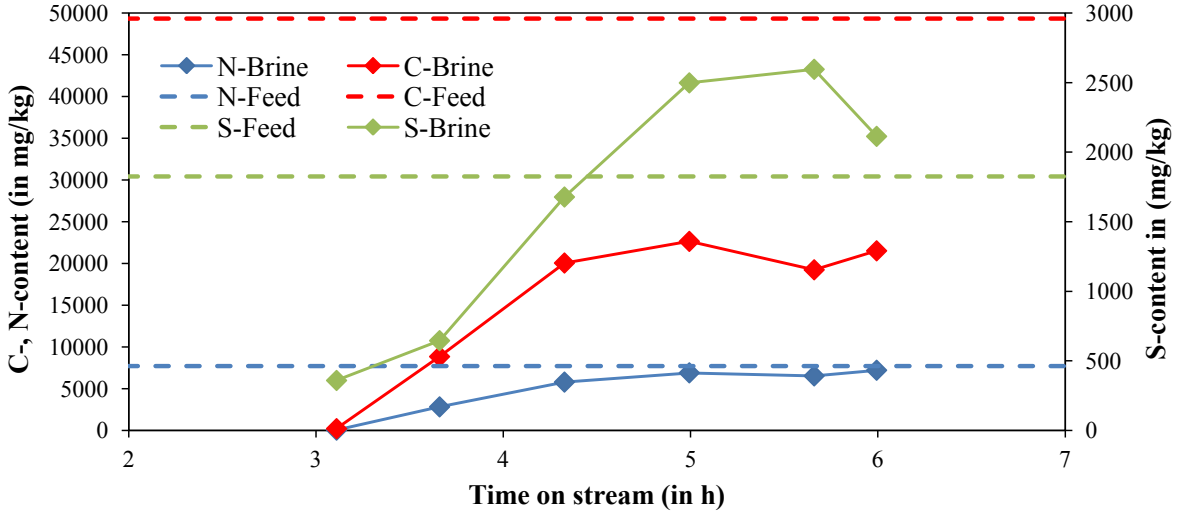

Figure 5.5: Evolution of carbon-, nitrogen- and sulfur content in the brine effluent (first liquefaction test).

Additionally, CNS analysis was conducted with respect to the samples of the reactor effluent taken during the run. Although the samples contained an aqueous and a (sticky) tarry phase,

only the aqueous phase was analyzed for a later comparison with the experiments where ZnO would be used. The progressions of the carbon-, nitrogen- and sulfur concentration are depicted in Figure 5.6. They started to increase after about 3.1 h and reached a steady level one hour later.

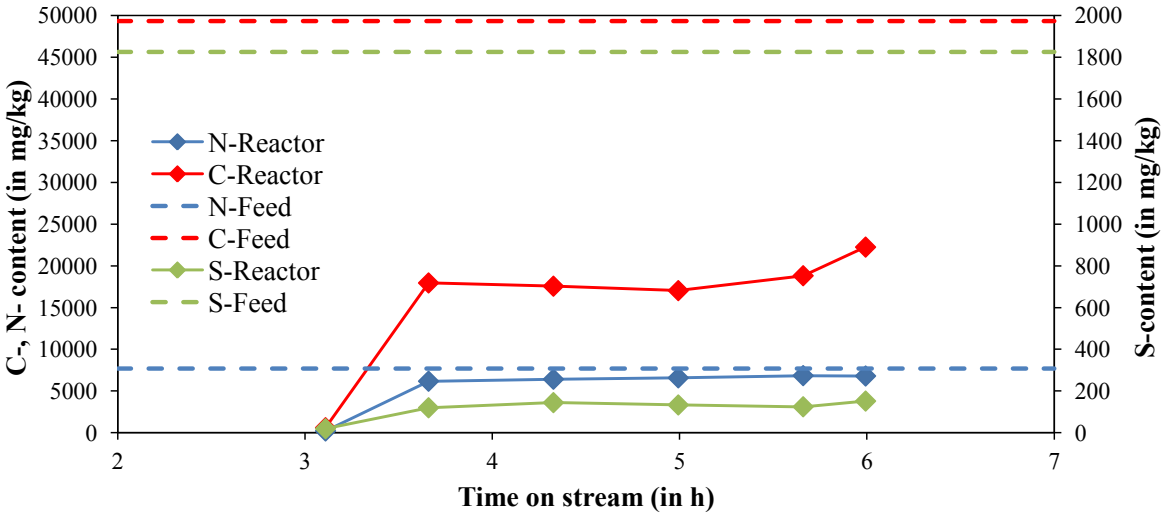

Figure 5.6: Evolution of carbon-, nitrogen- and sulfur content in the aqueous phase of the reactor effluent (first liquefaction test).

The maximum concentrations of carbon, nitrogen and sulfur in the brine effluent and the aqueous phase of the reactor effluent are compared with the corresponding concentrations in the feed in Table 5.3. It can be seen that most of the carbon left the salt separator at the top and should be found in high amounts in the tarry phase of the reactor effluent. Nitrogen was not separated in the salt separator and could be equally found in the brine effluent and the aqueous phase of the reactor effluent. The sulfur content in the brine effluent was much higher than the one of the aqueous phase of the reactor effluent (factor 17.1) suggesting good performance of the salt separator with respect to sulfur removal.

Table 5.3: Comparison of carbon-, nitrogen- and sulfur content of feed, brine effluent and reactor effluent (first liquefaction test).

	Feed	Brine effluent	Reactor effluent (aqueous phase)
Maximum C-content (in mg/kg)	49333	22643	22243
Maximum N-content (in mg/kg)	7700	7206	6842
Maximum S-content (in mg/kg)	1825	2595	152

As mentioned in Table 5.2, the brine effluent had a clear orange-brown color and the reactor effluent contained an aqueous and a tarry phase (see Figure 5.7). Moreover, some gas could be

seen in both the reactor and the brine effluent. Unfortunately, no tools were available by that time for gas sampling. For the next experiment a gas bag would be used.

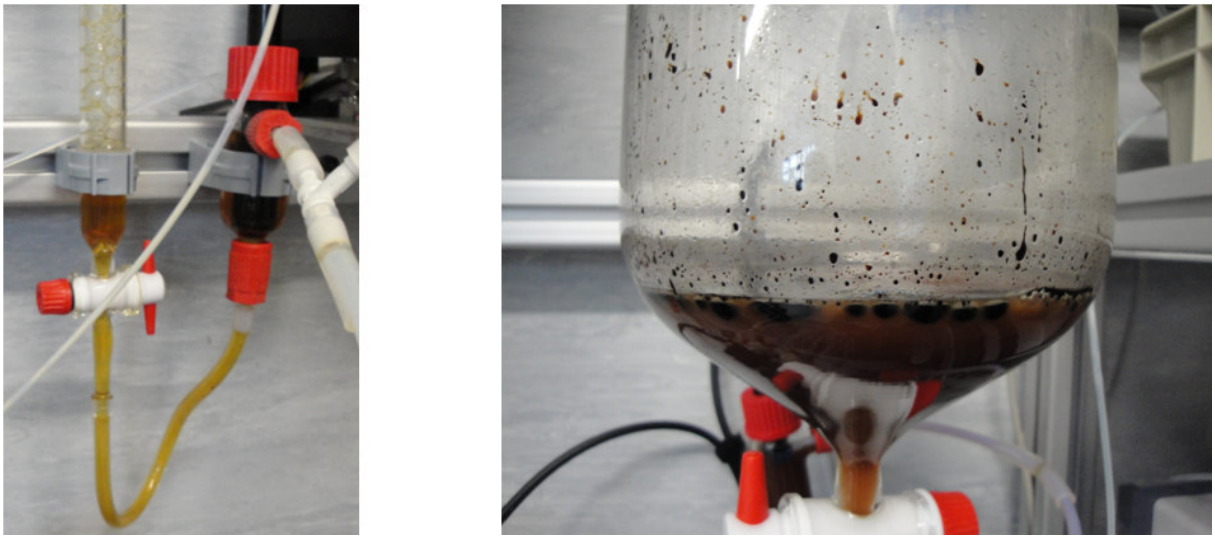

Figure 5.7: Left: Phase separator of the brine effluent (TOS: 5.05 h). Right: Phase separator of the reactor effluent (TOS: 5.88 h).

5.2.3. Post-experimental observation of KONTI-C

After rinsing overnight with water by the use of the HPLC pump, the filters of feed, brine effluent and reactor effluent were removed, inspected and cleaned. Moreover, the salt separator was opened to take a look inside since this was the first KONTI-C test with real biomass.

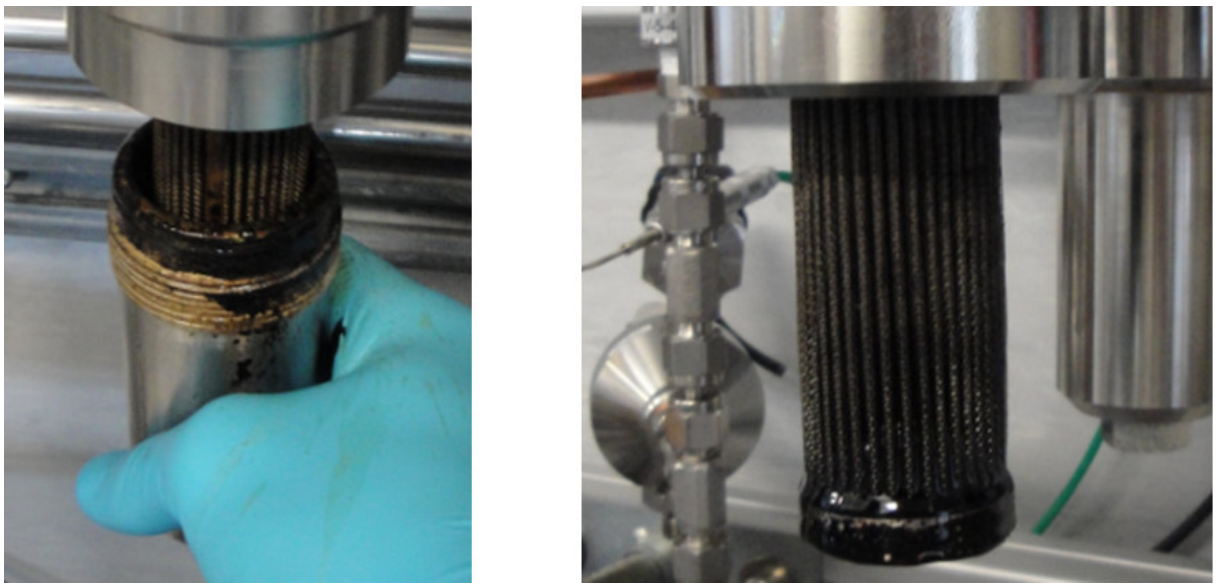

Figure 5.8: Left: Brine effluent filter after the experiment. Right: Reactor effluent filter after the experiment.

The feed filter was dirty with algae slurry, but hardly any particles could be found on it. Figure 5.8 shows that the filters of brine- and reactor effluent were covered with tar. Regarding filter 5-1 this was not a surprise because tar could have been seen in the reactor effluent during the experiment. But the brine effluent did not contain any tar (see Figure 5.7). Zöhrer [98] also reported the filters being covered with tar after liquifying fermentation residues with PSI's old continuous test rig. She supposed that the tar formation had already been taken place in a preheating unit upstream of the salt separator. Since KONTI-C did not have such a unit, the tar formation of our experiment must have occurred under different circumstances. In Sections 2.1.6 and 2.2.8 it was explained why tar is expected to be formed rather under subthan under supercritical conditions. Müller [104] observed that tar was most likely generated in the higher subcritical regime between 350 and 370 °C. Therefore, the tar in the reactor effluent might have been formed in the reactor bypass pipe between the salt separator and the chiller crossing the subcritical area. The tar in the brine effluent could have been created from the non-supercritically-dissolved organic matter in the lower part of the salt separator.

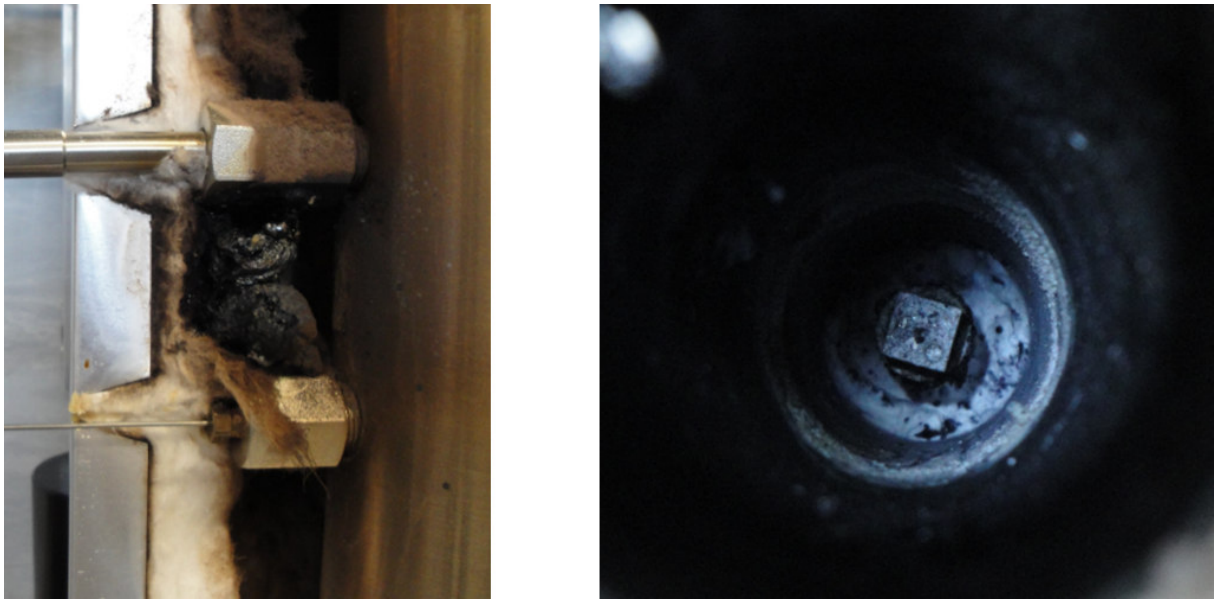

Figure 5.9: Left: Leakage at PTR 2-3. Right: Look into Salt separator after rinsing overnight.

Prior to opening the salt separator for inspection, the insulation had to be removed. Unfortunately, a leakage due to lack of tightness was localized at the pressure sensor PTR 2-3 and tar could be seen (Figure 5.9 left). The tar had either exited the salt separator through the leakage or had been converted from the leaked matter. Later on the parts of the pressure sensor were welded to prevent further leakages. When the salt separator was opened, some interesting things could be observed (see Fig 5.9 right). Although KONTI-C was rinsed overnight with water, there was a layer of precipitated salts at the bottom of the salt separator. Having taken a look at the on-line measurements from overnight, it was figured out that the setpoint of the Liquiflow had been unwittingly set to 0%. As a result, the separated and precipitated inorganic substances had not been able to leave the salt separator during rinsing. Moreover, the lower

part of the inner wall of the salt separator (subcritical zone) was covered by precipitated salts too, whereas the higher part (supercritical zone) was salt-free. This observation gave a visual evidence of the two zones and their different interactions with salts. Additionally, it could explain why the sulfur mass balance of the experiments with model solutions could not be closed.

5.3. Results of the second liquefaction test

5.3.1. Basic and starting conditions

The basic and starting conditions of the second liquefaction test are listed in Table 5.4. The aim of this experiment was to repeat the first liquefaction test by varying some parameters in order to minimize plugging and tar formation in the brine effluent. A higher flow rate should counteract plugging and a milder temperature in the lower part of the salt separator should reduce the possibility of tar formation. The actual mass flow rate was determined through dividing the weight difference of the feed tank by the feeding time. The setpoint for the Liquiflow was also set to 100% for minimizing plugging.

Table 5.4: Basic and starting conditions of the second liquefaction test.

Parameter	Unit	Value
Desired time on stream	h	4.00
Microalgae content (dry matter)[(a)]	wt%	7.85
Feed temperature	°C	24-30
Desired inner T-profile of salt separator	°C	200-400
Setpoint for chiller	°C	24.00
Setpoint for pressure controller (PTRC 5-3)	barg	280.00
Setpoint for Slurry Feeder	Hz	25.00
Actual feed flow rate	g/min	19.73
Setpoint for Liquiflow	% (g/min)	100 (3.2)
Reactor/Bypass	-	Bypass
Reactor filling	-	-

[(a)]Based on the C-content of the feed (gained from CNS analysis) compared to the C-content of Ph. tricornutum from [14].

5.3.2. Progression of temperature, pressure, electrical conductivity and composition

The important comments noted during the test are summarized in Table 5.5. The on-line measurements of temperature, pressure and conductivity are depicted in Figures 5.10, 5.11,

5.12 and 5.13.

Table 5.5: Comments on the second liquefaction test.

Time	Time on stream (in h)	Comment
10:42	0.11	Switch to feed (25 Hz)
10:59	0.39	Start sampling
11:08	0.55	Tar can be seen in the phase separator of the reactor effluent
11:30	0.90	Gas in the reactor effluent, foam in the brine effluent
11:38	1.03	Gas sample: reactor effluent for 19 min, brine effluent for 28 min
12:09	1.56	Brine effluent green, temperature setpoints for SS increased
12:29	1.89	Liquiflow has problems, brine effluent flow too high
13:04	2.47	Stop of the experiment due to Liquiflow problem
13:06	2.50	Cooling down and rinsing overnight

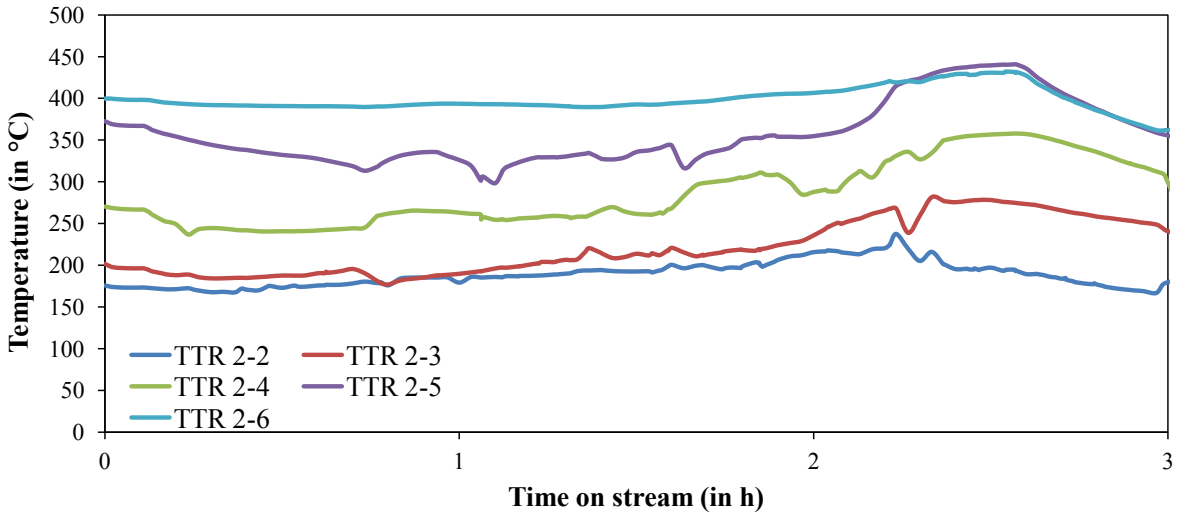

Figure 5.10: Evolution of the temperature at the inner wall of the salt separator (second liquefaction test).

When the algal slurry was fed (TOS: 0.11 to 2.47 h), the temperature profile inside the salt separator was not constant (Figures 5.10 and 5.11). For the first 1.56 h the temperature setpoints of the salt separator were not varied implying that changes of fluid dynamics and heat transfer caused the temperature fluctuations. Then the temperature of the lower heating blocks of the salt separator was increased because non-liquefied feed could be seen in the brine effluent (see Table 5.5).

The pressure (Figure 5.12) was more or less constant for the first 1.5 h. Then the pressure inside the standpipe (PTR 2-2) increased by about 5 bar but normalized again. After around 2 h PTR 2-2 strongly increased again up to a maximum value of about 285 bar. Again, it seems that some kind of plugging inside the standpipe took place. Then the pressure of KONTI-C suddenly

collapsed. At first, a possible leakage was believed to be the reason for that. But then it was figured out that a malfunction of the Liquiflow, which had started after 1.89 h (see Table 5.5), was the cause. For some reason the Liquiflow could not control the flow anymore leading to a very high flow rate of the brine effluent. As a consequence, the pressure regulator (PTRC 5-3) could not maintain the pressure any longer.

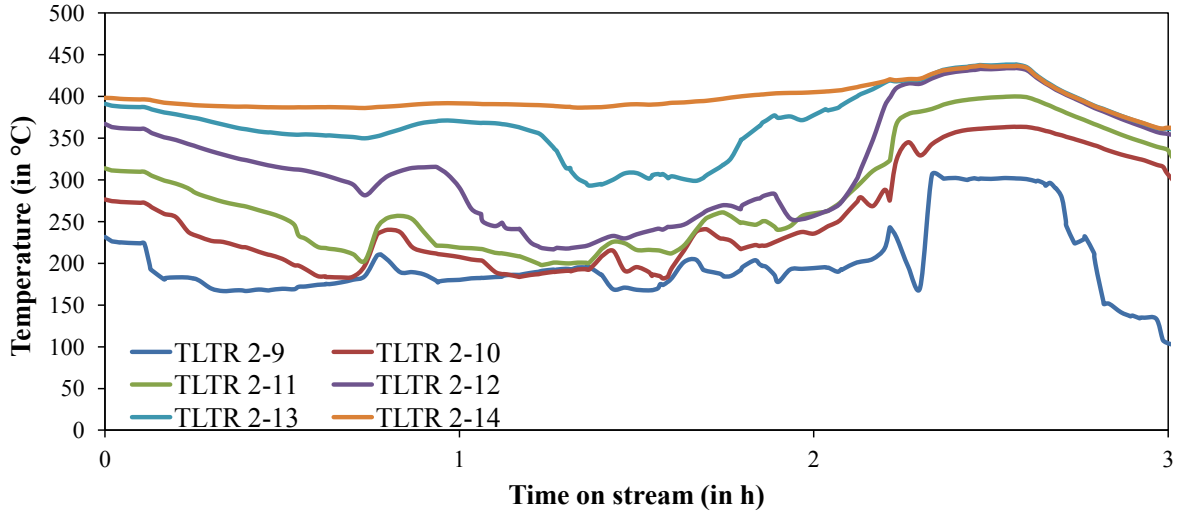

Figure 5.11: Evolution of the temperature at the lance of the salt separator (second liquefaction test).

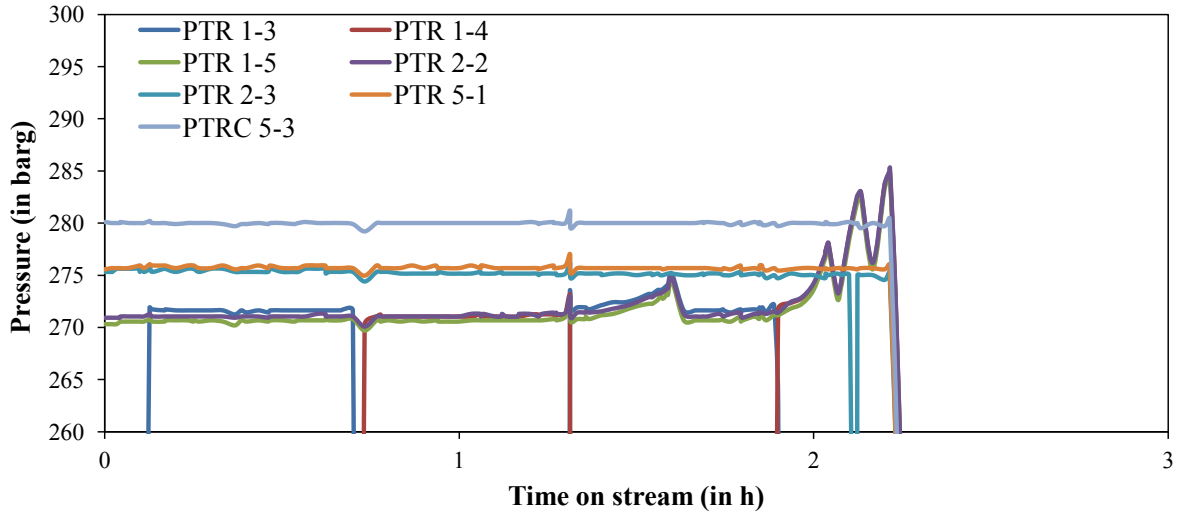

Figure 5.12: Evolution of the pressure (second liquefaction test).

As in the first liquefaction test, the electrical conductivity of the reactor effluent started to grow earlier and steeper than the one of the brine effluent (Figure 5.13). After about one hour it reached a first steady-state value of about 18 000 µS/cm. Later it increased further to about 19 000 µS/cm before it decreased to about 16 000 µS/cm, where it stayed for the rest of the feeding

time. The conductivity of the brine effluent reached a first steady value of about 11 000 µS/cm, after 1.9 h it gained its maximum of about 11 400 µS/cm and decreased drastically when the flow of the brine effluent broke through due to the malfunction of the Liquiflow. Compared to the first liquefaction test, the electrical conductivity of the brine effluent was much lower than the one of the reactor effluent. This means that liquefaction and mineral separation were much less efficient than before, which had already been expected by the green color of the brine effluent.

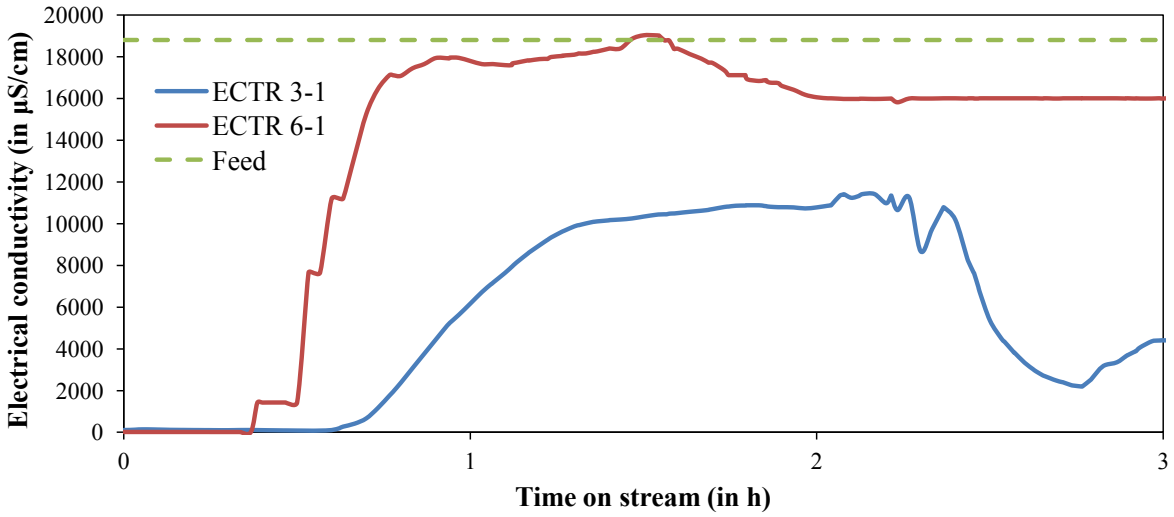

Figure 5.13: Evolution of the electrical conductivity (second liquefaction test).

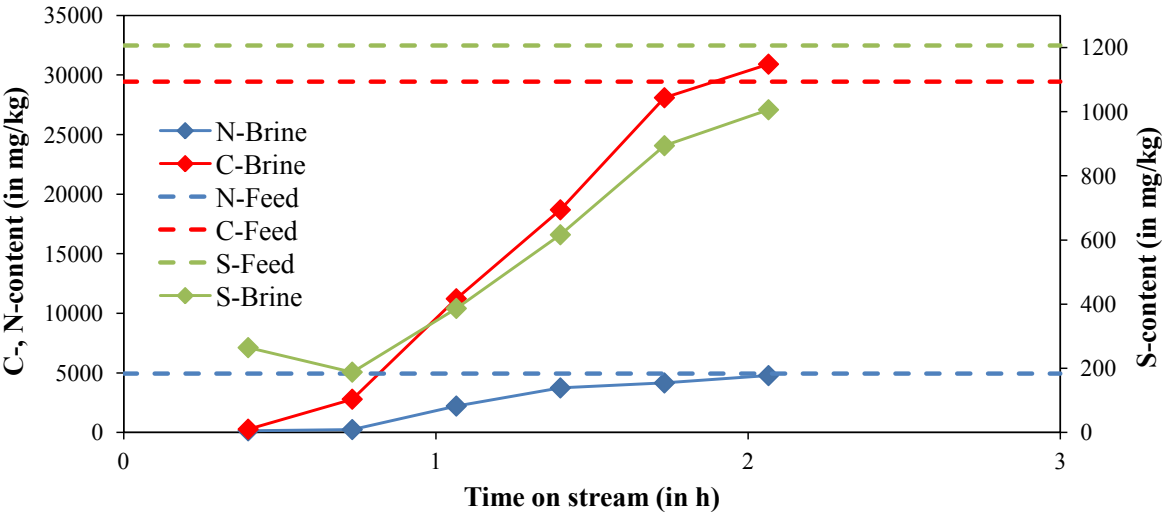

Figure 5.14: Evolution of carbon-, nitrogen- and sulfur content in the brine effluent (second liquefaction test).

Carbon-, nitrogen- and sulfur concentration of feed and brine effluent of the samples taken during the run were measured off-line. The results are shown in Figure 5.14. It can be seen that

the C-, N- and S-concentration of the brine effluent had a similar progression as the electrical conductivity. They started to increase after 40 min and reached their maximum values after about two hours. The fact that the carbon content of the brine reached the one of the feed and that the sulfur content of the brine stayed below the one of the feed point out incomplete liquefaction and poor separation, which had already been suspected during the test by the green color of the brine and the monitored electrical conductivity. Compared to the first liquefaction test, the concentrations of carbon, nitrogen and sulfur in the feed were much lower. A discussion about this circumstance can be found in Appendix J.

Like in the first liquefaction test, gas could be seen in the reactor and partially in the brine effluent (see Table 5.5). A sample of the reactor effluent and a sample of the brine effluent were collected in sampling bags for 19 min and 28 min. Since no gas accumulated in the bag of the brine effluent, its production was negligible and no GC analysis could be performed. Table 5.6 shows that the gas sample of the reactor effluent consisted mostly of CO_2. The concentrations of CH_4 and CO were very low, whereas no H_2 could be detected. The high amount of CO_2 is consistent with previous publications regarding hydrothermal liquefaction of microalgae in batch- [14,113–117] and continuous mode [118,119]. Brown *et al.* [113] obtained a gas containing 91.5-56.2 mol% CO_2, Duan *et al.* [114] a gas containing more than 80 mol% CO_2 and Valdez *et al.* [115] a gas containing 74 mol% CO_2 after treatment of Nannochloropsis sp. at 300-400 °C, at 350 °C and 350 °C, respectively. Christensen *et al.* [14] reported the gas containing 100-87.5 vol% CO_2 after hydrothermal liquefaction of Ph. tricornutum at 300-400 °C. Jazrawi *et al.* [119] obtained a gas that contained 99-95 mol% CO_2 at 300-350 °C during their continuous tests with Chlorella and Spirulina. Interestingly, Elliott *et al.* [118] also found high amounts of ammonia in the gas phase of their continuous tests. However, they claimed a possible overestimation of up to 50% and their method of depressurization having an influence on the analytical results.

Table 5.6: Off-line GC analysis of the gas sample of the reactor effluent (dry, TOS: 1.03-1.35 h).

Parameter	Unit	Value
Flow rate	mL/min	58.95
CO_2	vol%	92.32
H_2	vol%	0.00
CH_4	vol%	4.79
CO	vol%	2.89

As described in Table 5.5, the temperature inside the salt separator was too mild for complete algae liquefaction. The different look of the brine effluent compared to the previous test can be seen in Figure 5.15.

5.3.3. Post-experimental observation of KONTI-C

After rinsing overnight with water by the use of the HPLC pump, the filters of feed, brine effluent and reactor effluent were removed, inspected and cleaned. The feed filter was covered by only a few particles. The filters of both the reactor- and the brine effluent were covered with tar again. At the filter of the brine effluent some non-liquefied feed could be seen, too. Therefore, lowering the temperature at the bottom of the salt separator and increasing the mass flow rate of the feed did not prevent tar formation, but rather worsened the liquefaction efficiency.

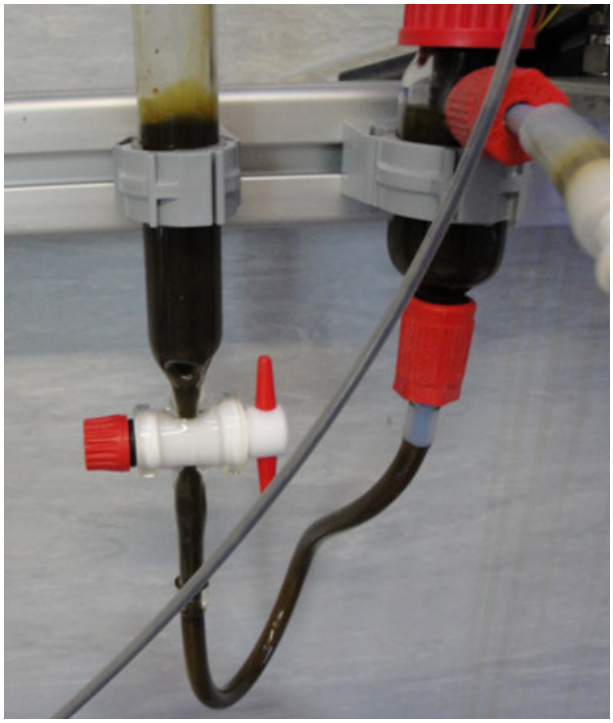

Figure 5.15: Phase separator of the brine effluent (TOS: 1.36 h).

5.4. Results of the third liquefaction test

5.4.1. Basic and starting conditions

Although the conditions in the salt separator could not have been optimized yet, the experimental schedule (see Section 3.2) had to proceed by testing the S-adsorber (ZnO). The basic and starting conditions of this third liquefaction test are listed in Table 5.7. For the first time the top outlet stream of the salt separator went through the reactor, which was filled with ZnO. The aim of this experiment was to investigate the performance of the S-adsorber and to determine the catalytic activity of ZnO regarding gasification of liquefied biomass. In parallel, the conditions in the salt separator should be improved. On the one hand, the second salt separation test

showed that too mild thermal conditions inside the salt separator led to incomplete liquefaction. On the other hand, the reason for the plugging during the first liquefaction test was still not clear. Therefore, the temperature at the bottom of the salt separator was increased and the mass flow rate of the feed was decreased a little bit compared to the second liquefaction test. The heater for the transfer pipe between the salt separator and the reactor was adjusted in a way just to keep the liquefied fluid above the critical point of water. The actual mass flow rate was determined through dividing the weight difference of the feed tank by the feeding time. The Liquiflow, which had caused the termination of the second liquefaction test, was exchanged and its operating point was set to 90% (compared to 100% in the previous test). The idea was that the possibility for a malfunction could be reduced if the setpoint of the Liquiflow was not at its boundary value.

5.4.2. Progression of temperature, pressure, electrical conductivity and composition

The important comments noted during the test are summarized in Table 5.8. The on-line measurements of temperature, pressure and conductivity are depicted in Figures 5.16, 5.17, 5.18, 5.19 and 5.20.

Table 5.7: Basic and starting conditions of the third liquefaction test.

Parameter	Unit	Value
Desired time on stream	h	4.00
Microalgae content (dry matter)[(a)]	wt%	8.61
Feed temperature	°C	23-26
Desired inner T-profile of salt separator	°C	230-410
Desired temperature inside reactor	°C	400.00
Setpoint for chiller	°C	25.00
Setpoint for pressure controller (PTRC 5-3)	barg	280.00
Setpoint for Slurry Feeder	Hz	23.70
Actual feed flow rate	g/min	18.86
Setpoint for Liquiflow	% (g/min)	90 (2.88)
Reactor/Bypass	-	Reactor
Reactor filling	-	Katalco (ZnO)
Reactor filling - amount	g	1944

[(a)]Based on the C-content of the feed (gained from CNS analysis) compared to the C-content of Ph. tricornutum from [14].

Figure 5.16 and 5.17 show that the temperature inside the salt separator was very stable until the feed was changed from water to algal slurry after 4.38 h. Then the temperature measurements

fluctuated a lot like in the previous tests. After 6.32 h the setpoint for the lower heating block of the salt separator was reduced by 10 °C because TTR 2-2 was rising slowly. Temperature regulation problems of the reactor occurred at the beginning of the test, which were caused by two interchanged thermocouple connections (compare Table 5.8). After the connections had been corrected, the temperature inside the reactor stabilized.

Table 5.8: Comments on the third liquefaction test.

Time	Time on stream (in h)	Comment
09:21	0.14	Start heating up with water
12:06	2.90	Alarm: temperature at reactor top
12:37	3.41	Problems with temperature regulation of reactor
12:44	3.53	Switch thermocouples TLTR 4-5 and TTRC 4-2
13:26	4.23	Gas cooler activated, but no pumping
13:35	4.38	Switch to feed (23.7 Hz)
14:11	4.98	Set flow to 24.7 Hz due to pressure issues
14:25	5.22	Tar can be seen in reactor effluent, foam in the brine effluent
14:27	5.24	Brine has still clear orange-brown color
14:49	5.62	Foam in brine disappeared
14:50	5.63	Reactor effl. more liquid-like compared to experiments w/o ZnO
14:59	5.77	Brine color becomes more brownish
15:03	5.84	Liquiflow reduced to 70%
15:14	6.02	Gas sample of reactor effluent: 15:07-15:10 (leakage!!)
15:31	6.32	TTRC 2-7 reduced by 10 °C, temperature was increasing slowly
15:36	6.38	Liquiflow set to 100% due to pressure problem
15:54	6.70	Very quick plugging in standpipe
15:54	6.70	Switch back to water, cooling down and rinsing overnight

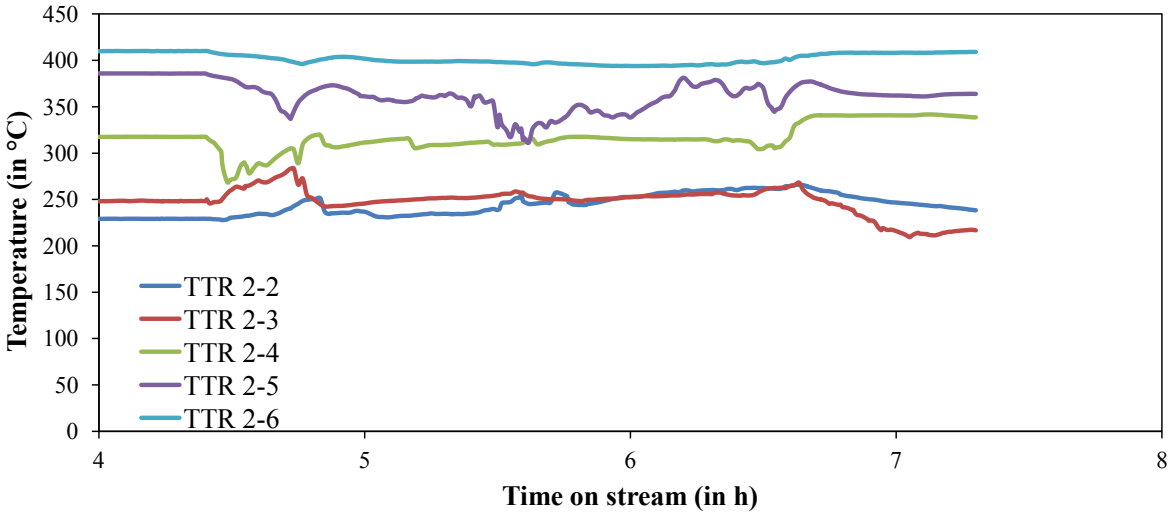

Figure 5.16: Evolution of the temperature at the inner wall of the salt separator (third liquefaction test).

The temperature at the bottom (TLTR 4-5) and close to the top (TLTR 4-19) stayed at around 380 to 390 °C, whereas the temperature in the middle part (TLTR 4-9) reached values up to 405 °C. Between TLTR 4-19 and TLTR 4-20, which is at the very top of the reactor already outside of the insulated zone, a transition from super- to subcritical state occurred. This can be seen by the temperature difference and the unstable measurements of TLTR 4-20. TLTR 4-5 was used as an indicator to make sure that the fluid in the transfer pipe stayed in supercritical state.

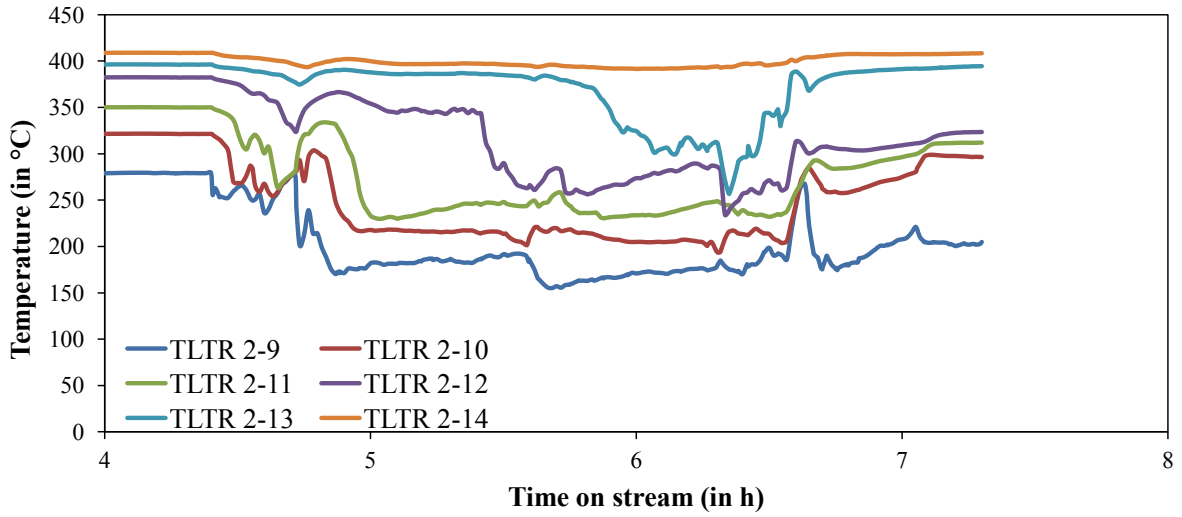

Figure 5.17: Evolution of the temperature at the lance of the salt separator (third liquefaction test).

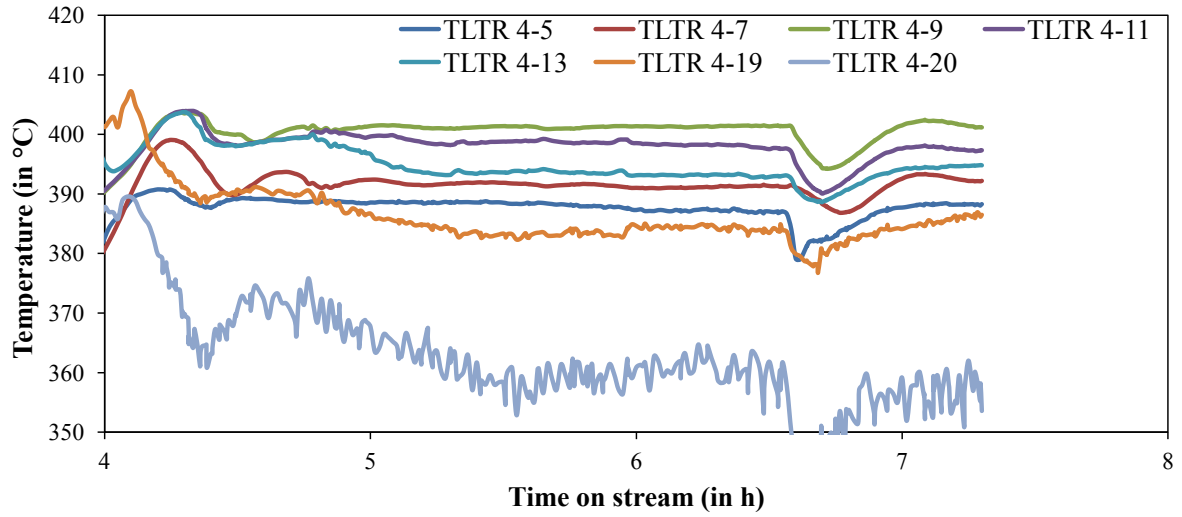

Figure 5.18: Evolution of the temperature at the lance of the reactor (third liquefaction test).

The pressure (Figure 5.19) was very stable as long as water was fed into the system. When the feed was changed to slurry after 4.38 h, the pressure inside the standpipe (PTR 2-2) increased very fast and went up and down for the following two hours. It seems that some kind of

build-up and breakthrough was taking place. After about 6.7 h PTR 2-2 went up to 295 bar very quickly indicating plugging and the experiment had to be stopped.

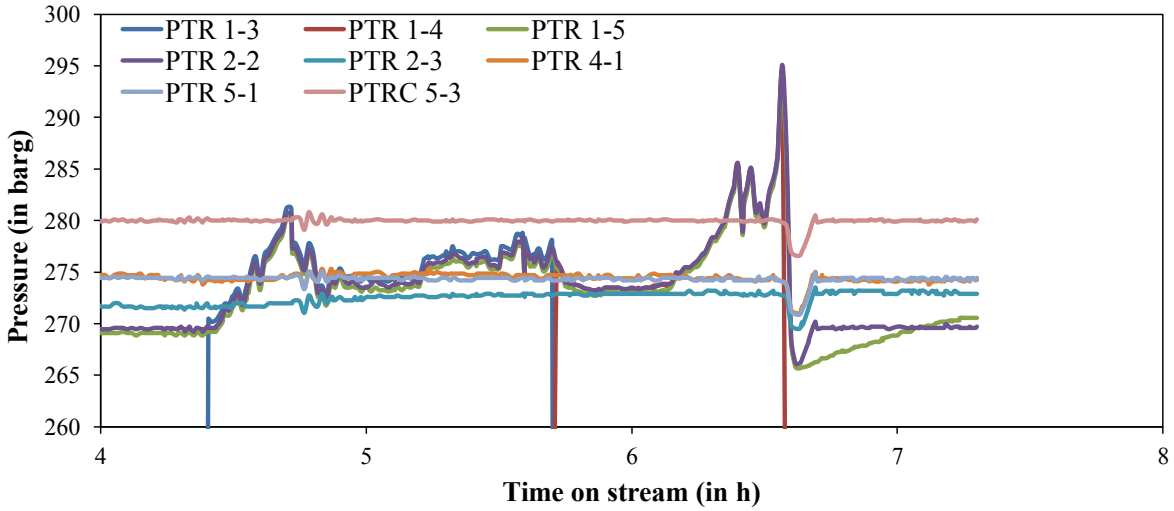

Figure 5.19: Evolution of the pressure (third liquefaction test).

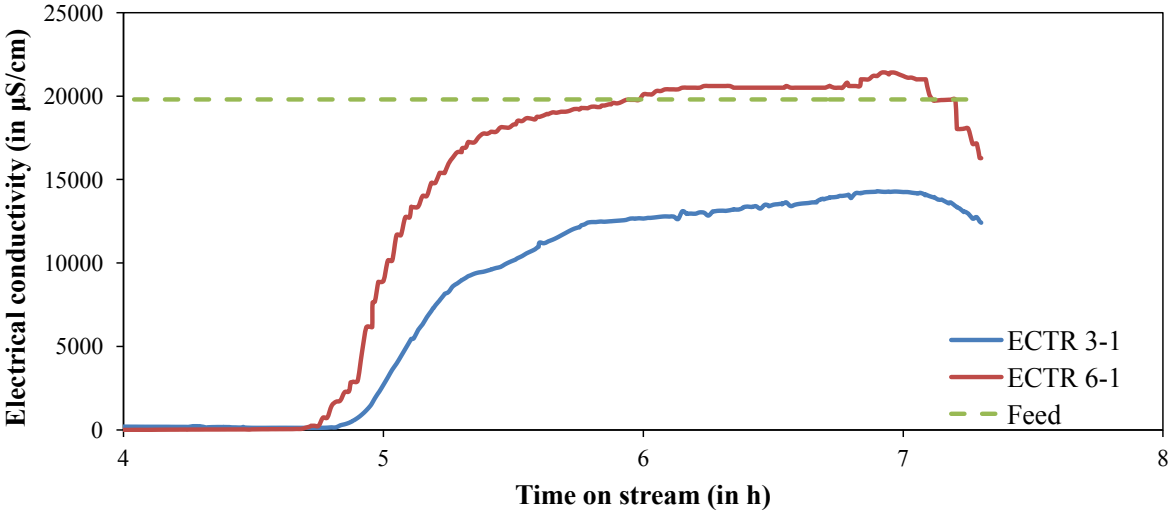

Figure 5.20: Evolution of the electrical conductivity (third liquefaction test).

The conductivity measurements (Figure 5.20) look similar to the ones of the previous experiment. The electrical conductivity of the reactor effluent started to grow earlier and steeper than the one of the brine effluent and reached a steady value of about 20 500 µS/cm after about 6.5 h. The electrical conductivity of the brine effluent slowly increased until the end of the experiment, where it reached a value of about 14 300 µS/cm.

Carbon-, nitrogen- and sulfur concentration of feed and brine effluent of the samples taken during the run were measured off-line. The results are shown in Figure 5.21. It can be seen that

the C-, N- and S-concentration of the brine effluent had a similar progression as the electrical conductivity. They started to increase after 4.75 h and reached their maximum values towards the end of the test. Carbon-, nitrogen- and sulfur content of the brine effluent went up to about 50%, 88% and 69% of the corresponding content in the feed. This suggests that most of the carbon either left the salt separator at the top or stayed inside due to coke formation, whereas nitrogen and sulfur could not be separated.

As in the previous two liquefaction tests, gas could be seen in the reactor effluent and foam in the brine effluent (see Table 5.8). From the brine sample taken during the second liquefaction test it was known that the amount of gas in the brine effluent was negligible. Therefore, only a reactor effluent sample was taken. Unfortunately, the bag had a leakage so that no representative sample could be collected.

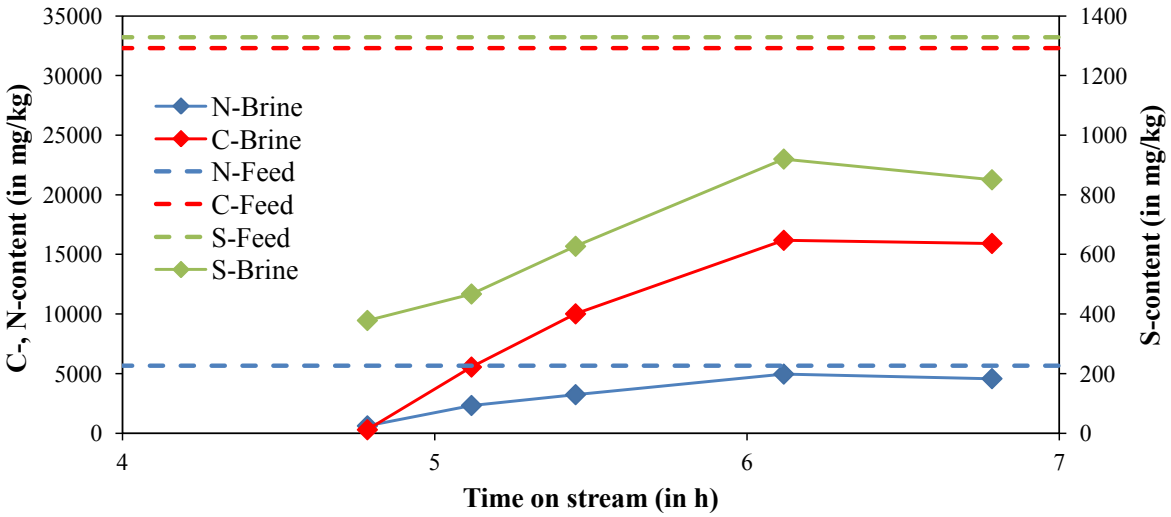

Figure 5.21: Evolution of carbon-, nitrogen- and sulfur content in the brine effluent (third liquefaction test).

5.4.3. Post-experimental observation of KONTI-C

After rinsing overnight with water by the use of the HPLC pump, the filters of feed, brine effluent and reactor effluent were removed, inspected and cleaned. The feed filter was dirty because of the algae slurry, but hardly any particles could be found on it. The filters of both the reactor- and the brine effluent were covered with tar. At the filter of the brine effluent some non-liquefied feed could be seen too, which means that the thermal conditions at the salt separator bottom were still too mild for complete liquefaction (Figure 5.22 left). Interestingly, the filter of the reactor effluent showed less tar than after the previous two liquefaction experiments, but was also coated by some solid particles that looked like coke (Figure 5.22 right).

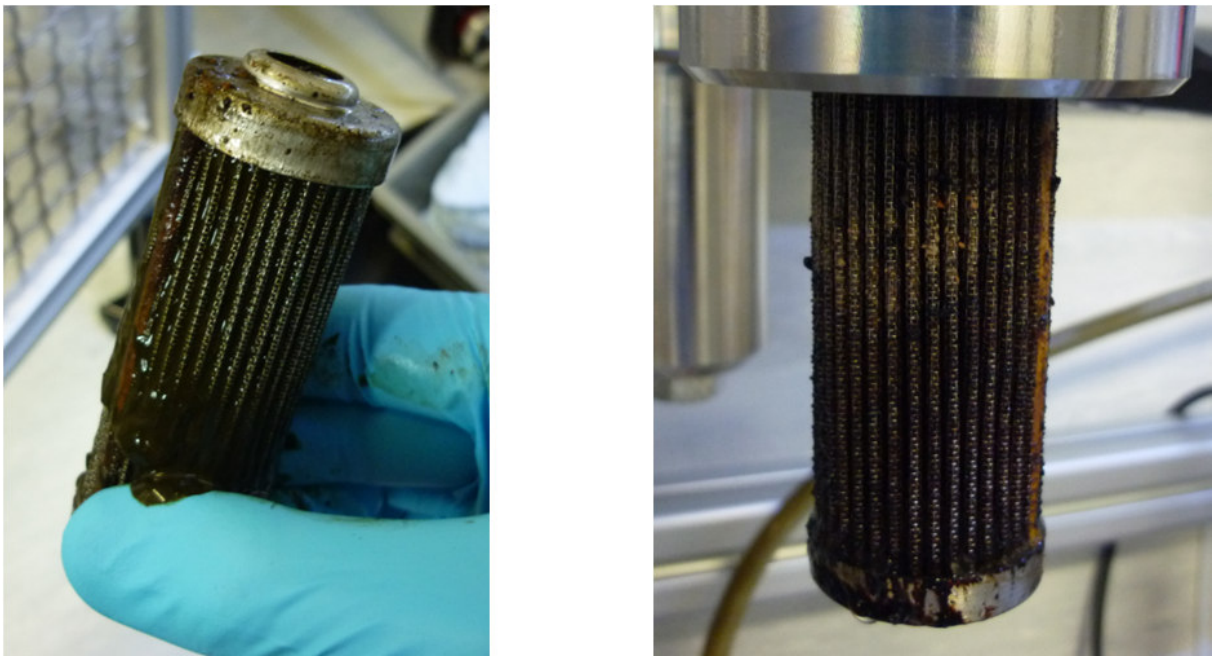

Figure 5.22: Left: Brine effluent filter after the experiment. Right: Reactor effluent filter after the experiment.

Before rinsing KONTI-C with ethanol (as described in Section 3.3.2), the transfer pipe between the salt separator and the reactor was uncoupled so that only the salt separator and its two outlets were flushed. It was decided not to rinse the reactor yet so that the ZnO stayed untreated.

5.5. Results of the fourth liquefaction test

5.5.1. Basic and starting conditions

Since the previous test was terminated by fast plugging inside the standpipe, it was strongly believed that the pore size of the feed filter was too big (250 µm). Therefore, the filter was exchanged by one as it was used for the brine- and the reactor effluent with a pore size of 25 µm. The basic and starting conditions of this fourth liquefaction test are listed in Table 5.9. The aim of this experiment was again to investigate the performance of the S-adsorber and to determine in how far ZnO has a catalytic effect regarding gasification of liquefied biomass. During the previous run it was found out that a temperature of 230 °C at the bottom of the salt separator was still too mild for complete liquefaction. Therefore, a temperature of 250-410 °C inside the salt separator was aimed at. The heater for the transfer pipe between the salt separator and the reactor was adjusted in a way just to keep the liquefied fluid above the critical point of water. The actual mass flow rate was determined through dividing the weight difference of the feed tank by the feeding time. Surprisingly, the flow was very high this time although the Slurry Feeder was set only to 23 Hz. A calculation of the flow based on the masses collected in the brine effluent- and the reactor effluent tank gave a similar result. So the question regarding this

high flow rate could not be answered at that point. As it will be mentioned in the next section, there were problems with the Liquiflow. It was not able to control the mass flow rate of the brine effluent at its setpoint. Therefore, the setpoint of the Liquiflow was varied throughout the experiment in the way so that the visually monitored mass flow rate of the brine effluent was similar to the ones in the tests before.

Table 5.9: Basic and starting conditions of the fourth liquefaction test.

Parameter	Unit	Value
Desired time on stream	h	4.00
Microalgae content (dry matter)[(a)]	wt%	6.49
Feed temperature	°C	18-21
Desired inner T-profile of salt separator	°C	250-410
Desired temperature inside reactor	°C	400.00
Setpoint for chiller	°C	19.00
Setpoint for pressure controller (PTRC 5-3)	barg	280.00
Setpoint for Slurry Feeder	Hz	23.00
Actual feed flow rate	g/min	23.00
Setpoint for Liquiflow	% (g/min)	80 (2.50)
Reactor/Bypass	-	Reactor
Reactor filling	-	Katalco (ZnO)
Reactor filling - amount	g	1944

[(a)]Based on the C-content of the feed (gained from CNS analysis) compared to the C-content of Ph. tricornutum from [14].

5.5.2. Progression of temperature, pressure, electrical conductivity and composition

The important comments noted during the test are summarized in Table 5.10. The on-line measurements of temperature, pressure and conductivity are depicted in Figures 5.23, 5.24, 5.25, 5.26 and 5.27.

Figure 5.23 and 5.24 show that the temperature inside the salt separator was quite stable until the feed was changed from water to algal slurry after 3.3 h. Then the temperature measurements dropped a little bit and became chaotic showing again the dynamic behavior of the processes inside the salt separator. After 3.93 h the setpoint for the lower heating block of the salt separator was increased by 10 °C, since the brine effluent contained non-liquefied feed (see Table 5.10). The sudden temperature change after 6.41 h could have had something to do with the change of Liquiflow settings (compare Table 5.10).

Table 5.10: Comments on the fourth liquefaction test.

Time	Time on stream (in h)	Comment
08:51	0.00	Start heating up with water
08:52	0.03	Plugging at flowserve during rinsing overnight
11:15	2.42	Air conditioner active
11:45	2.91	Problem with Liquiflow, it is not able to control constantly
12:08	3.30	Switch to feed (23 Hz), Liquiflow at 30% (not correct!!)
12:10	3.32	Start sampling
12:16	3.43	Liquiflow set to 25%
12:47	3.93	Brine greenish; TTRC 2-7 set to 460 °C
13:23	4.53	Further adjustment of TTRC 2-7 to keep temperature
14:12	5.36	Brine looks better now (brown-orange)
14:16	5.43	Despite Liquiflow problem, trying to keep running
15:15	6.41	Liquiflow seems to work again, set to 60%
15:37	6.78	Particle trap's valve opened!! (by mistake)
15:57	7.11	Brine color darker again
16:03	7.21	Switch back to water, cooling down and rinsing overnight

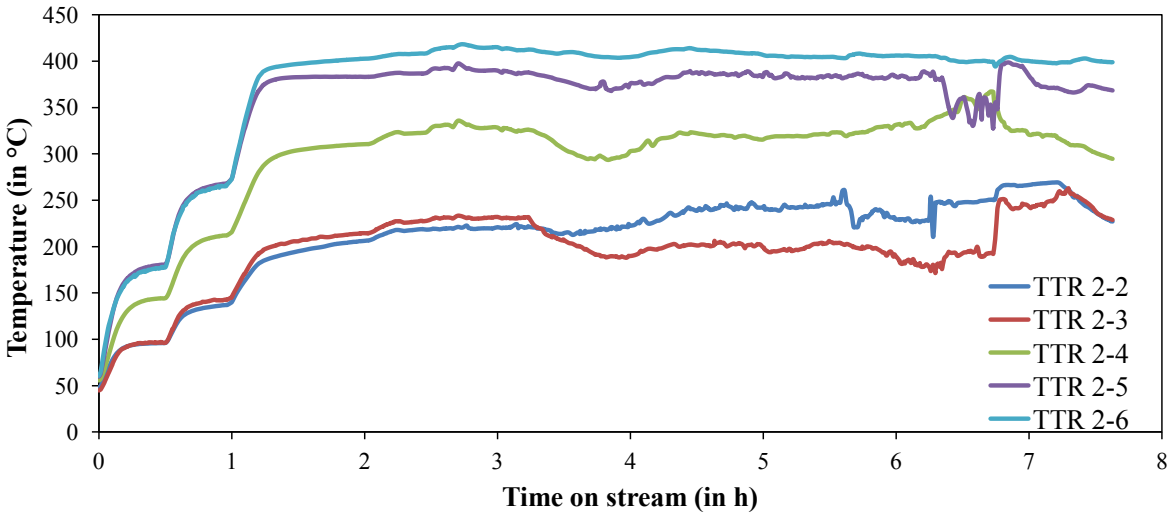

Figure 5.23: Evolution of the temperature at the inner wall of the salt separator (fourth liquefaction test).

In Figure 5.25 it can be seen that the temperature inside the reactor was very stable in the range of 380 to 410 °C up to the measuring point of TLTR 4-19. Between TLTR 4-19 and TLTR 4-20 a transition from super- to subcritical state occurred, which again can be seen by the temperature difference and the fluctuations of TLTR 4-20. The sudden and short temperature drop after 6.73 h was caused by the unwittingly opening of a valve (see Table 5.10). TLTR 4-5 was used as an indicator to make sure that the fluid in the transfer pipe stayed in supercritical state.

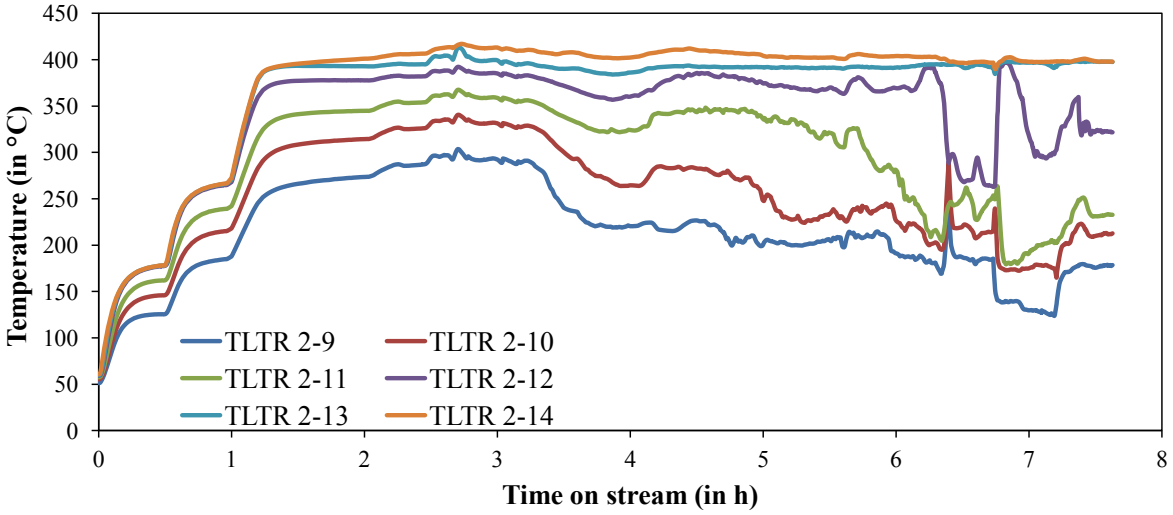

Figure 5.24: Evolution of the temperature at the lance of the salt separator (fourth liquefaction test).

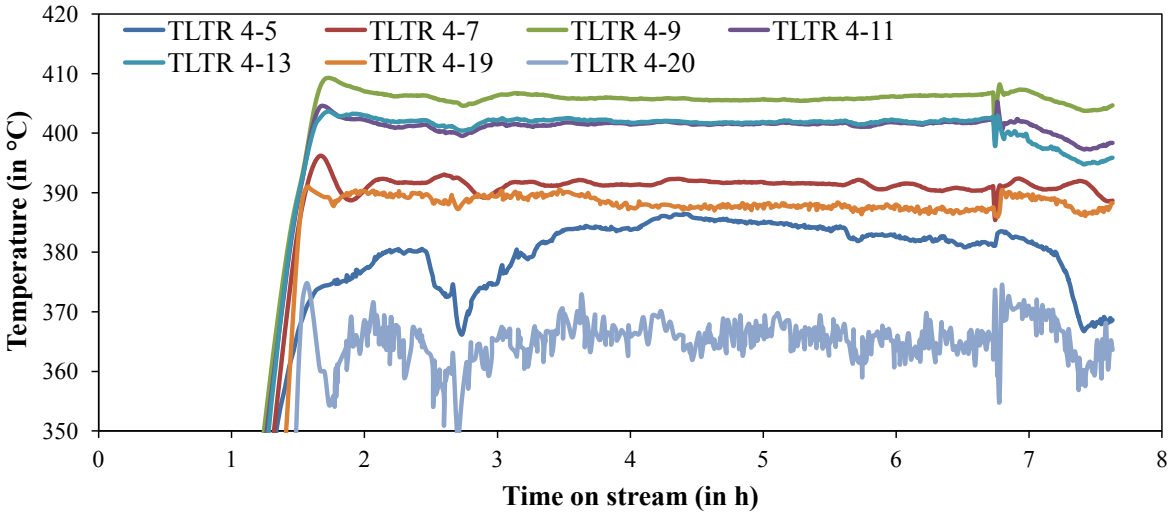

Figure 5.25: Evolution of the temperature at the lance of the reactor (fourth liquefaction test).

The pressure (Figure 5.26) was very stable as long as water was fed into the system. When the feed was changed to slurry after 3.3 h, the pressure inside the standpipe (PTR 2-2) started to fluctuate again but not as intensively as in the previous tests with algal feed. It reached only values of up to 280 bar, which indicates an improvement by having switched to a feed filter with a smaller pore size. The sudden and short pressure drop after 6.73 h was also caused by the unwittingly opening of a valve. After that the pressure inside the standpipe (PTR 2-2) relaxed.

The conductivity measurements (Figure 5.27) demonstrate similar trends as in the previous tests. The electrical conductivity of the reactor effluent started to grow earlier and steeper

than the one of the brine effluent and reached a value of about 13 500 µS/cm after six hours. Then it suddenly rose up to 16 400 µS/cm, which should have been related to the unwittingly opening of a valve as described before. The electrical conductivity of the brine effluent slowly increased until the end of the experiment, where it reached a value of about 14 700 µS/cm. In contrast to the two previous tests, where the temperature at the bottom was lower, the electrical conductivity of the brine effluent exceeded the one of the reactor effluent eventually.

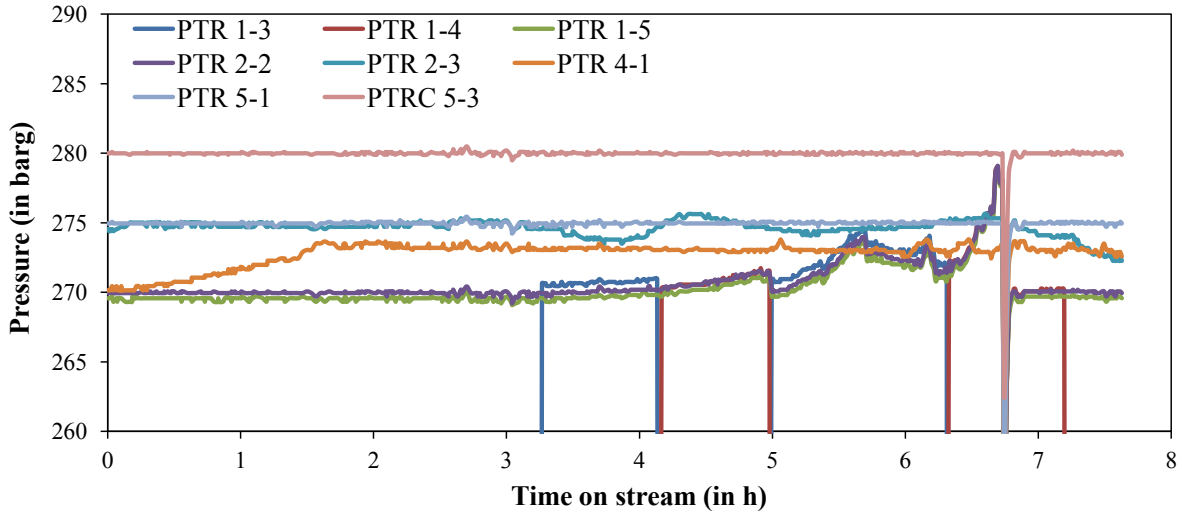

Figure 5.26: Evolution of the pressure (fourth liquefaction test).

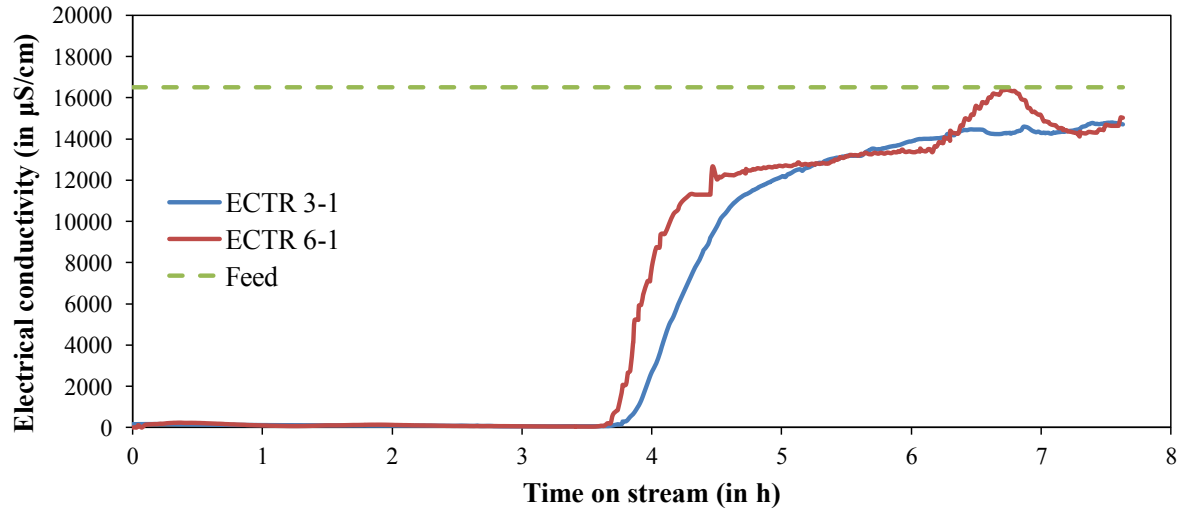

Figure 5.27: Evolution of the electrical conductivity (fourth liquefaction test).

Carbon-, nitrogen- and sulfur concentration of feed and brine effluent of the samples taken during the run were measured off-line. The results are depicted in Figure 5.28. As in the previous algal tests, the C-, the N- and the S-concentration of the brine effluent show a similar trend as the electrical conductivity. They started to increase after about 3.8 h and reached their

maximum values towards the end of the test. Additionally, CNS analysis was conducted with respect to the samples of the reactor effluent taken during the run. Although the samples contained an aqueous and a (sticky) tarry phase, only the aqueous phase was analyzed for comparison with the corresponding analysis from the first liquefaction test. The progressions of the carbon-, nitrogen- and sulfur concentration are depicted in Figure 5.29. They started to increase after about 3.3 h and reached a steady level two hours later.

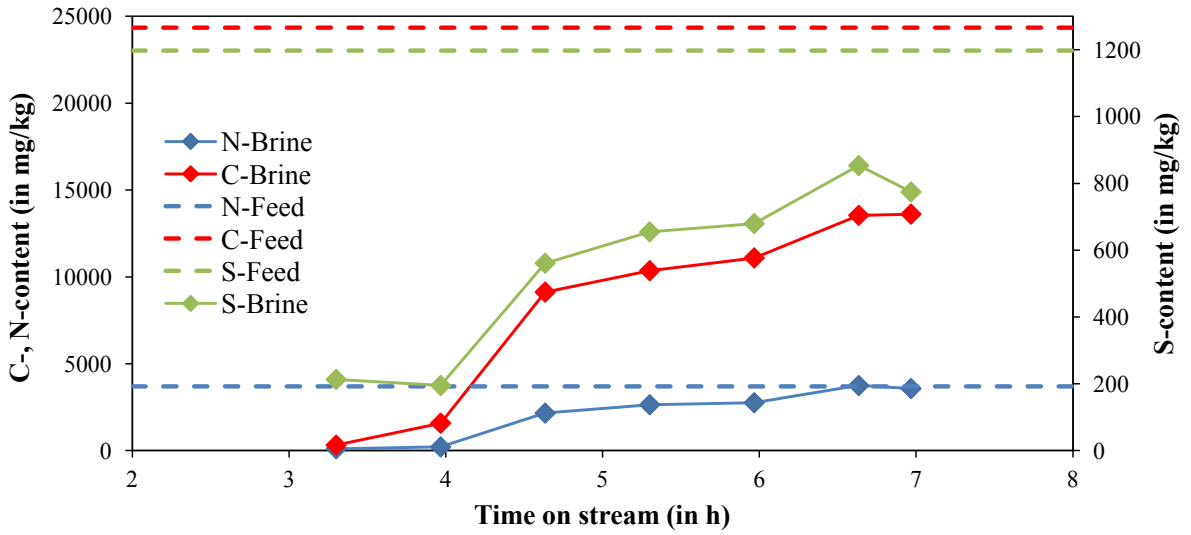

Figure 5.28: Evolution of carbon-, nitrogen- and sulfur content in the brine effluent (fourth liquefaction test).

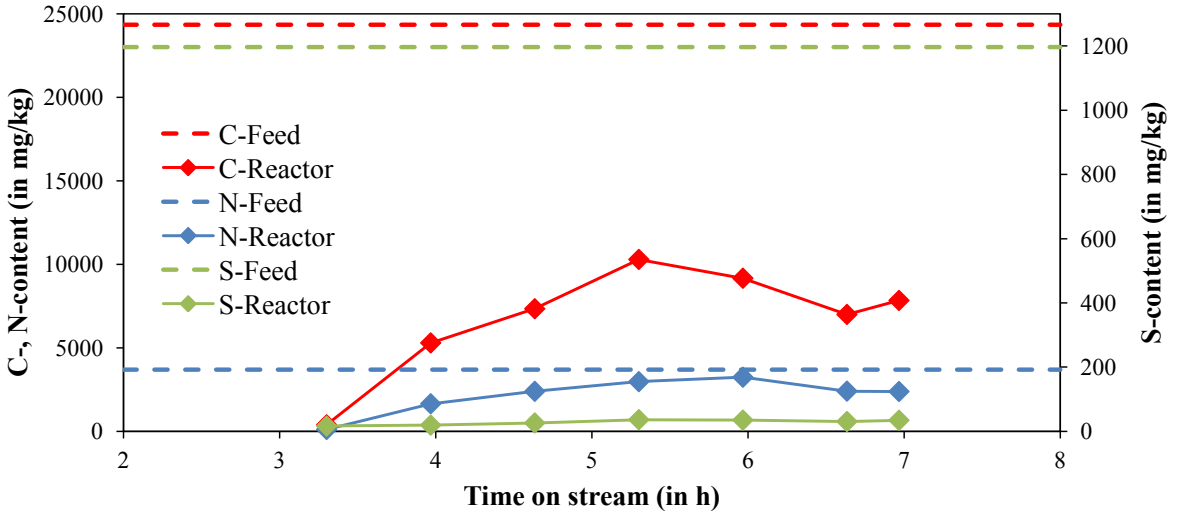

Figure 5.29: Evolution of carbon-, nitrogen- and sulfur content in the aqueous phase of the reactor effluent (fourth liquefaction test).

The maximum concentrations of carbon, nitrogen and sulfur in the brine effluent and the aqueous phase of the reactor effluent are compared with the corresponding concentrations in

the feed in Table 5.11. It can be seen that most of the carbon left the salt separator at the top and is expected to be found in high amounts in the tarry phase of the reactor effluent. Nitrogen was not separated in the salt separator and could be equally found in the brine effluent and the aqueous phase of the reactor effluent. The sulfur content in the brine effluent was much higher than the one of the aqueous phase of the reactor effluent (factor 23.6) suggesting good performance of the salt separator with respect to sulfur removal. Compared to the first liquefaction test, the ratio of the sulfur concentration in the brine- and the reactor effluent was higher (23.6 vs. 17.1) indicating that the use of ZnO made an additional contribution to the removal of sulfur. A discussion about the circumstance that the concentrations of carbon, nitrogen and sulfur of the feed were much lower compared to the first liquefaction test can be found in Appendix J.

Table 5.11: Comparison of carbon-, nitrogen- and sulfur content of feed, brine effluent and reactor effluent (fourth liquefaction test).

	Feed	Brine effluent	Reactor effluent (aqueous phase)
Maximum C-content (in mg/kg)	24350	13613	10294
Maximum N-content (in mg/kg)	3700	3748	3239
Maximum S-content (in mg/kg)	1197	853	36

As in the previous liquefaction tests, gas could be seen in the reactor effluent and foam in the brine effluent. Two samples of the gaseous product of the reactor effluent were collected; their results are summarized in Table 5.12. Interestingly, the gas samples contained mostly hydrogen and carbon dioxide. It seems that the adsorbens (ZnO) had a catalytic effect concerning hydrothermal gasification of microalgae by favoring the steam reforming and the WGS reactions rather than the methanation reactions (see Section 2.2). Sinag *et al.* [120] tested hydrothermal conversion of cellulose (10 wt%) over ZnO in an autoclave at 300, 400, 500 and 600 °C with a reaction time of 1 h. At 300 °C the gaseous product consisted mainly of CO_2 and H_2, whereas the amount of CH_4 exceeded the one of H_2 at 400, 500 and 600 °C. For catalytic processes under atmospheric pressure with the use of ZnO a lot of articles have been published. Especially for steam reforming of (bio-)alcohols, like methanol [121], ethanol [122] and butanol [123], ZnO has proven itself to be a suitable catalyst support.

Table 5.12: Off-line GC analysis of the gas samples of the reactor effluent (dry).

Parameter	Unit	TOS: 4.37-4.57 h	TOS: 5.40-5.55 h
Flow rate	mL/min	53.33	111.11
CO_2	vol%	41.92	49.76
H_2	vol%	56.46	49.05
CH_4	vol%	1.61	1.19
CO	vol%	0.00	0.00

In Table 5.13 the calculation of the gasification efficiency based on the carbon content in the feed and the second gas sample, which is expected to be close to steady-state with respect to the reactor effluent, is summarized. Although a hydrogen-rich gas could be produced, only a small portion of the feed was gasified.

Table 5.13: Calculation of the carbon gasification efficiency using the second gas sample of the reactor effluent (TOS: 5.40-5.55 h).

Parameter	Unit	Value
Mass flow rate of feed	g/min	23.00
Carbon content in feed	mg/kg	24350
Molar mass of carbon	g/mol	12.01
Gas flow rate	mL/min	111.11
CO_2 in gas	vol%	49.76
CH_4 in gas	vol%	1.19
Molar volume (ideal gas)	mL/mol	22414
Gasification efficiency	%	5.42

5.5.3. Post-experimental observation of KONTI-C

After rinsing overnight with water by the use of the HPLC pump, the filters of feed, brine effluent and reactor effluent were removed, inspected and cleaned. Only a few particles could be found on the feed filter. The filters of both the reactor- and the brine effluent were covered with tar. Again, the filter of the brine effluent showed some non-liquefied feed, too, which means that the thermal conditions at the salt separator bottom were still too mild for complete liquefaction. Also the filter of the reactor effluent was mounted with some solid particles again.

Before rinsing KONTI-C with ethanol, the transfer pipe between the salt separator and the reactor was uncoupled so that only the salt separator and its two outlets got flushed. It was decided not to rinse the reactor yet so that the ZnO stayed untreated.

5.6. Results of the first gasification test

5.6.1. Basic and starting conditions

After having performed liquefaction experiments with/without ZnO, as the next step, gasification of microalgae was carried out. The reactor that was only filled with ZnO was exchanged by another reactor, which was loaded with ZnO in the lower section and catalyst in the higher section. Therefore, the liquefied algae would pass first the adsorbens, where the sulfur would be withheld, and then the catalyst, where the bio-molecules were supposed to be gasified.

The basic and starting conditions of the first gasification experiment are listed in Table 5.14. From the last liquefaction test it was known that a temperature of about 250 °C at the bottom of the salt separator was still too cold for complete liquefaction of the microalgae. Therefore, a temperature profile inside the salt separator similar to the one obtained during the first liquefaction test was established. The heater for the transfer pipe between the salt separator and the reactor was adjusted in a way just to keep the liquefied fluid above the critical point of water. The actual mass flow rate was determined through dividing the weight difference of the feed tank by the feeding time. This time the mass flow rate was again in the expected range for a Slurry Feeder setpoint frequency of 23 Hz. As it will be mentioned in the next section, there were again problems with the Liquiflow. Fortunately, the malfunction was not as bad as in the previous test.

Table 5.14: Basic and starting conditions of the first gasification test.

Parameter	Unit	Value
Desired time on stream	h	4.00
Microalgae content (dry matter)[(a)]	wt%	10.55
Feed temperature	°C	23-24
Desired inner T-profile of salt separator	°C	300-430
Desired temperature inside reactor	°C	400.00
Setpoint for chiller	°C	20.00
Setpoint for pressure controller (PTRC 5-3)	barg	280.00
Setpoint for Slurry Feeder	Hz	23.00
Actual feed flow rate	g/min	16.94
Setpoint for Liquiflow	% (g/min)	90 (2.90)
Reactor/Bypass	-	Reactor
Reactor filling	-	Katalco (ZnO), Ru/C
Reactor filling - amount	g	528.5 (Katalco), 443.5 (Ru/C)
WHSV[(b)]	g_{Org}/g_{Cat}-h	< 0.24[(c)]

[(a)]Based on the C-content of the feed (gained from CNS analysis) compared to the C-content of Ph. tricornutum from [14].

[(b)]WHSV = weight hourly space velocity used in units of hourly rate of algae (dry matter) processed over the grams of catalyst.

[(c)]0.24, if the entire organic material from the feed left the salt separator at the top and passed the catalyst.

5.6.2. Progression of temperature, pressure, electrical conductivity and composition

The important comments noted during the test are summarized in Table 5.15. The on-line measurements of temperature, pressure and conductivity are depicted in Figures 5.30, 5.31, 5.32, 5.33 and 5.34.

Table 5.15: Comments on the first gasification test.

Time	Time on stream (in h)	Comment
10:23	0.02	Rinsed overnight at 200 °C
10:24	0.03	From 07:45 until now heated up with HPLC pump (18 mL/min)
10:46	0.39	TOC started after calibration and flushing
11:05	0.71	Switch to feed
11:23	1.02	Alarm was due to high pressure in slurry feeder (??)
11:33	1.19	Although the Liquiflow is not working correctly, we stay at 90%
11:37	1.24	Liquiflow reduced to 50%
11:41	1.32	Temperature setpoints of salt separator are being adjusted
12:27	2.07	Plugging at the pressure regulation system
12:58	2.61	Plugging at the pressure regulation system, stop of experiment
13:00	2.62	Switch back to water, cooling down and rinsing overnight
13:30	3.12	Brine effl.'s color: orange-brown, reactor effl.'s color: clear
14:24	4.03	ECTR 3-1 and ECTR 6-1 should be correct again

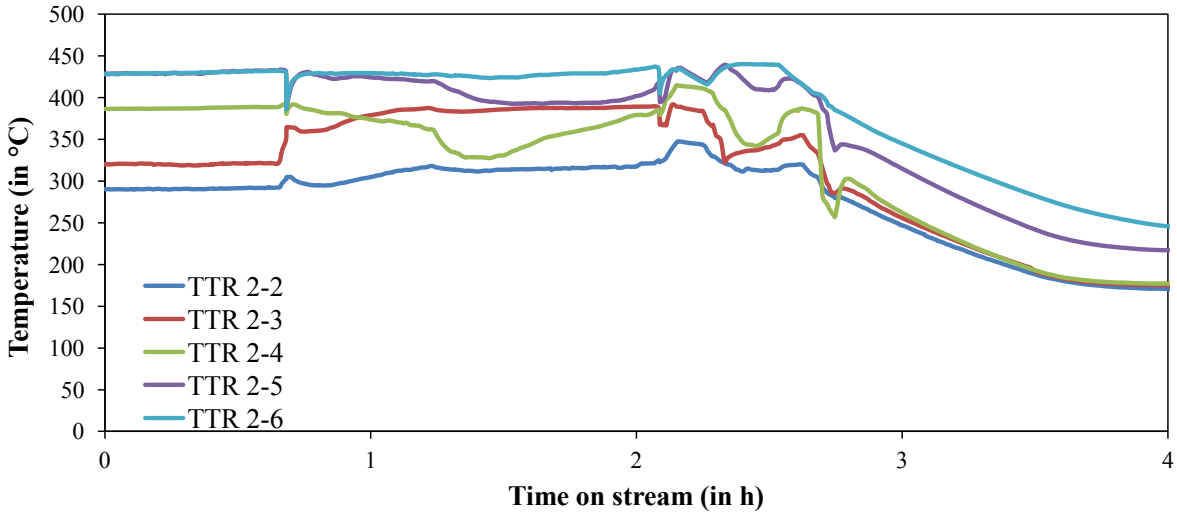

Figure 5.30: Evolution of the temperature at the inner wall of the salt separator (first gasification test).

Figure 5.30 and 5.31 show that the temperature inside the salt separator was very stable until the feed was changed from water to algal slurry after 0.71 h. Then the temperature measurements in the middle part of the salt separator (TTR 2-4, TTR 2-5, TLTR 2-9, TLTR 2-10) dropped a little

bit and became chaotic showing again the dynamic behavior of the processes inside the salt separator. After 1.32 h the setpoints for the heating blocks of the salt separator were adjusted to sustain the desired temperature profile. The horizontal lines in Figure 5.31 were caused by stuck measurements.

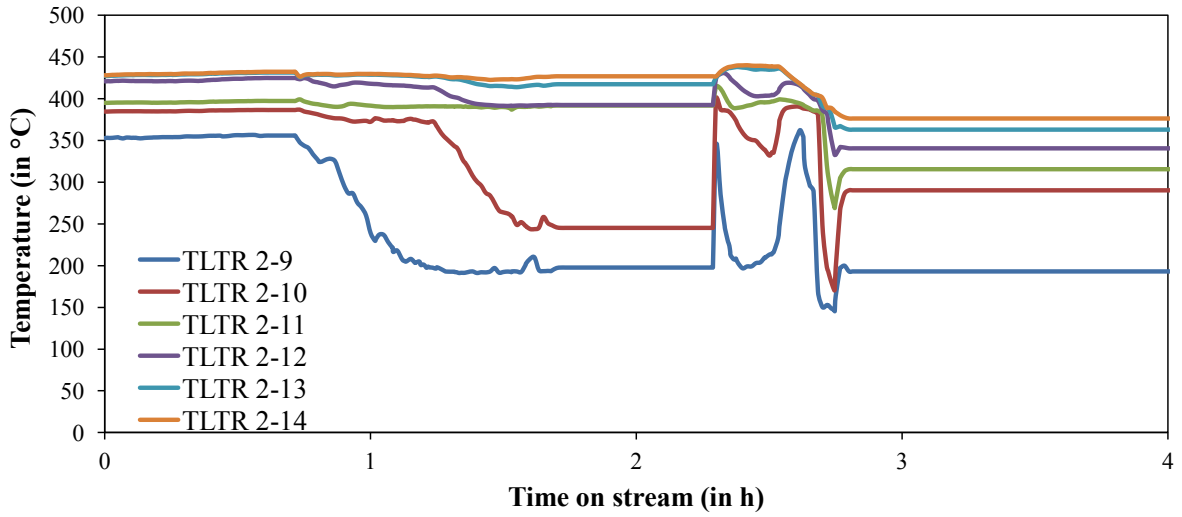

Figure 5.31: Evolution of the temperature at the lance of the salt separator (first gasification test).

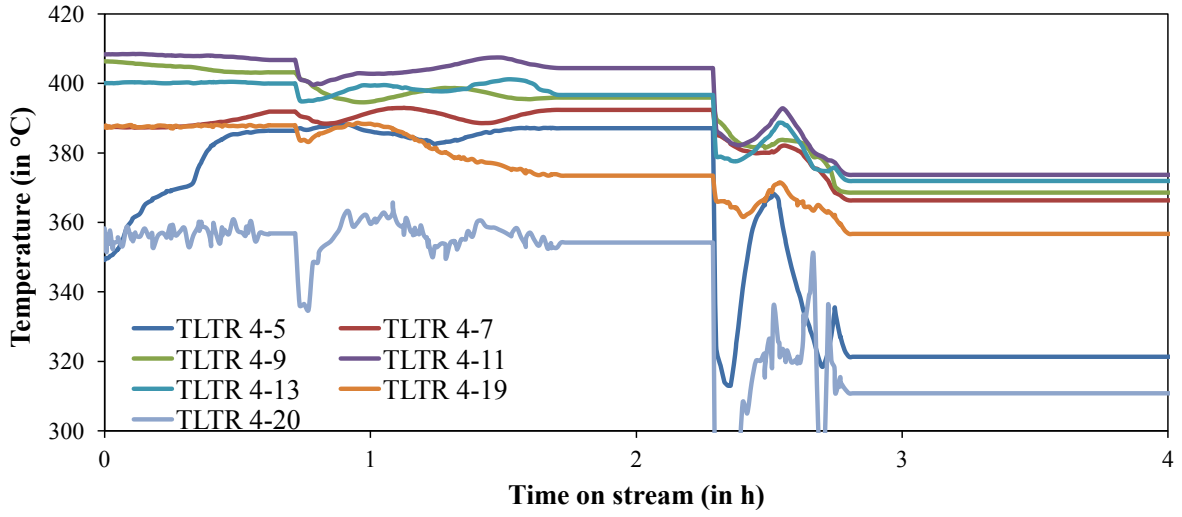

Figure 5.32: Evolution of the temperature at the lance of the reactor (first gasification test).

Figure 5.32 shows the measurements of the temperature lance of the reactor. Unfortunately, the measurements were stuck most of the time, which was overlooked during the run. When the feed was switched to algae, the temperature inside the reactor dropped by 5 to 7 °C and swung in the range of 375 to 410 °C from TLTR 4-5 to TLTR 4-19. Between TLTR 4-19 and TLTR 4-20 a transition from super- to subcritical state occurred again, which can be seen by the temperature

difference and the fluctuations of TLTR 4-20. After 2.26 h the stuck measurements were noticed and the connection cables unplugged and plugged in again for updating the values.

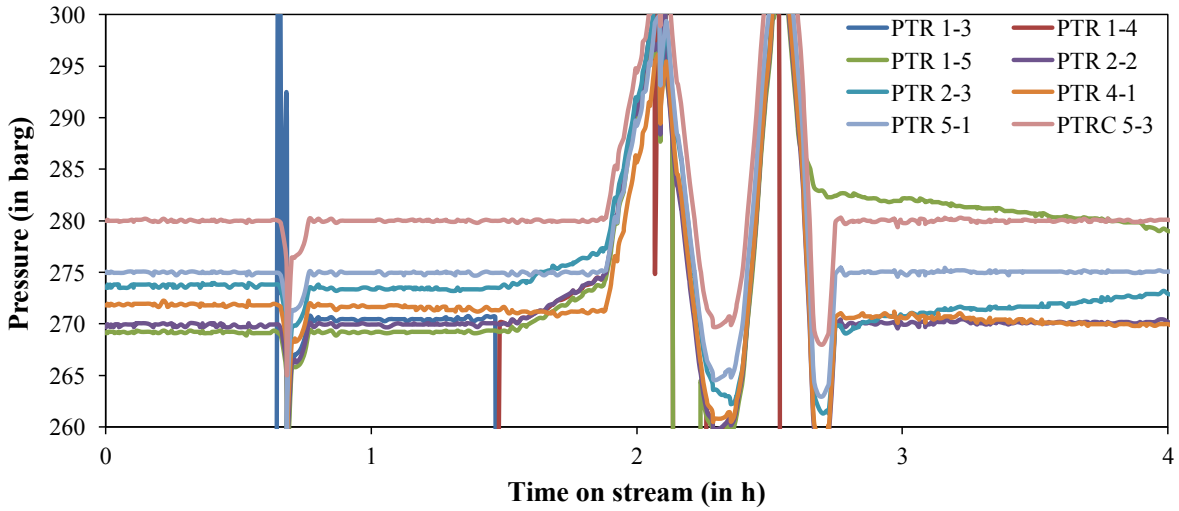

Figure 5.33: Evolution of the pressure (first gasification test).

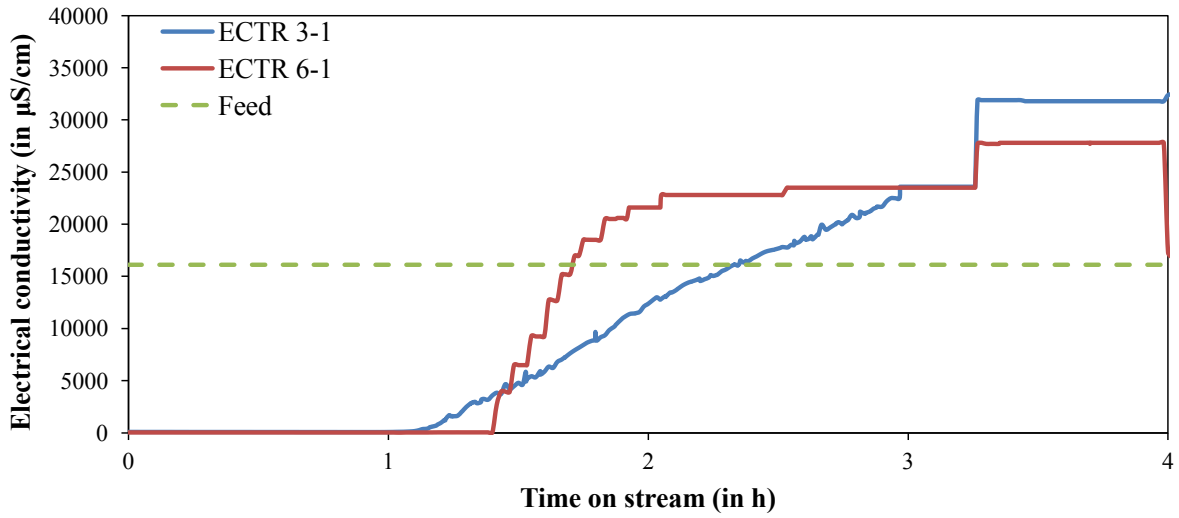

Figure 5.34: Evolution of the electrical conductivity (first gasification test).

Actually, the temperature was far below the desired temperature range. The reason for this was that an alarm caused by a pressure issue 20 min earlier (see Figure 5.33) shut down the heating blocks (part of KONTI-C safety system), which had not been recognized. Then the heating blocks were activated again and the temperature inside the reactor rose until the experiment had to be stopped after 2.61 h due to another pressure issue.

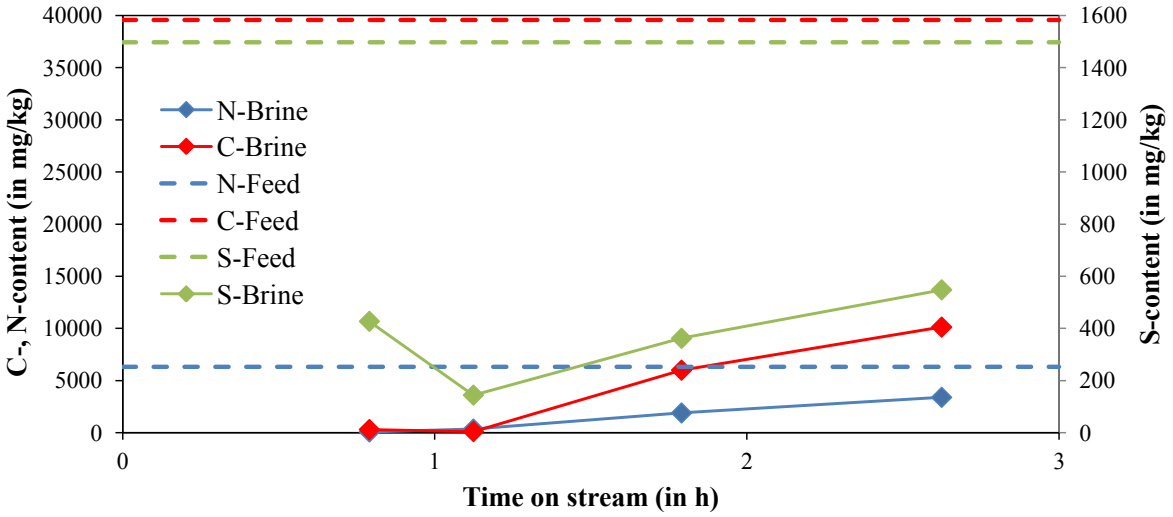

Figure 5.35: Evolution of carbon-, nitrogen- and sulfur content in the brine effluent (first gasification test).

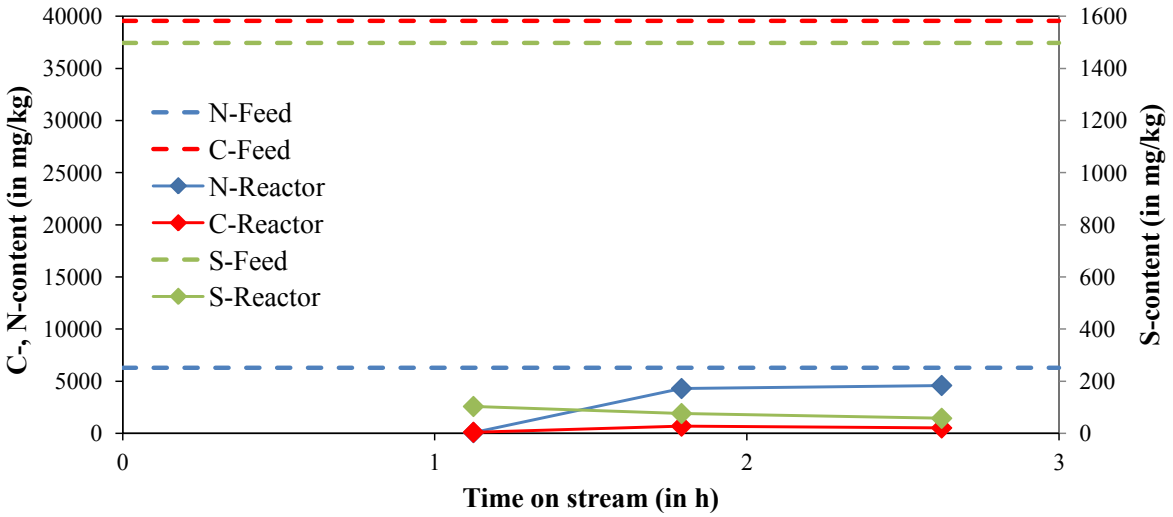

Figure 5.36: Evolution of carbon-, nitrogen- and sulfur content in the reactor effluent (first gasification test).

The pressure (Figure 5.33) was very stable when water was fed and also at the beginning when algal slurry was processed. The pressure peak after 0.67 h occurred due to high pressure inside the Slurry Feeder. This was the only time that this happened and no reason could be found. After 1.5 h the pressure inside the salt separator (PTR 2-3) started to increase slowly, but the overpressure-alarm after about two hours was caused by PTRC 5-3. Probably a particle plugged either the Flowserve or the pressure relief valve (V-5-8). The Slurry Feeder was stopped immediately and started again after the pressure had settled down. Unfortunately, the plugging had not been gone and the experiment had to be canceled.

The conductivity measurements (Figure 5.34) look a little bit different from the ones of the previous algae test. The conductivity of the brine effluent started to grow 15 min before the conductivity of the reactor effluent and reached a maximum value of 32 000 µS/cm after the test had been terminated. The conductivity of the reactor effluent went up to about 28 000 µS/cm. The jumps after 3.26 h corresponded to the malfunction of the conductivity meters as described before. The fact that the brine effluent had a "good" color (see Table 5.15) throughout the run and that the electrical conductivity of the brine effluent exceeded the one of reactor effluent suggest better liquefaction and salt separation than before.

Carbon-, nitrogen- and sulfur concentration of feed, brine effluent and reactor effluent of the samples taken during the run were measured off-line. The results are depicted in Figure 5.35 and Figure 5.36. As in the previous algal tests, the C-, the N- and the S-concentration of the brine effluent show a similar trend as the electrical conductivity. They started to increase after about 1.1 h and reached their maximum values towards the end of the test. The carbon- and the sulfur concentration in the reactor effluent stayed very low suggesting successful gasification and efficient sulfur removal by the salt separator and ZnO, whereas the nitrogen concentration went up close to the nitrogen concentration of the feed. The maximum concentrations of carbon, nitrogen and sulfur in the brine- and the reactor effluent are compared with the corresponding concentrations in the feed in Table 5.16. Since the test had to be already stopped after processing microalgae for less than two hours, samples for CNS analysis could not be taken long enough to gain more detailed information.

Table 5.16: Comparison of carbon-, nitrogen- and sulfur content of feed, brine effluent and reactor effluent (first gasification test).

	Feed	Brine effluent	Reactor effluent
Maximum C-content (in mg/kg)	39567	10123	690
Maximum N-content (in mg/kg)	6300	3386	4588
Maximum S-content (in mg/kg)	1498	548	103

Figure 5.37 shows the TOC- (total organic carbon) and the TIC content (total inorganic carbon) of the reactor effluent measured on-line. It can be seen that the TOC content stayed below 1000 mg/L and the TIC content below 500 mg/L during the whole test. On the one hand, the low TOC measurements suggest high catalytic activity. On the other hand, formation of N-heterocyclic compounds through the Maillard reaction could have been the reason why the TOC content did not reach even lower values. N-heterocyclic compounds are believed to be stable free radical cations acting as free radical scavengers during hydrothermal gasification [58, 69]. Indeed, a number of nitrogen-containing, like indoles, pyridins, pyrrolidins, pyrrols, pyrazines, piperidines and quinolines, could be identified in the oil- [72, 113–117, 124–126] and the aqueous product [127, 128] after hydrothermal liquefaction, as well as in the aqueous product after hydrothermal gasification of microalgae [2]. The TIC measurements should not be considered

too seriously because the analyzer had been calibrated for TIC only at very low concentrations. For the next test, a calibration for higher TIC concentrations would be carried out.

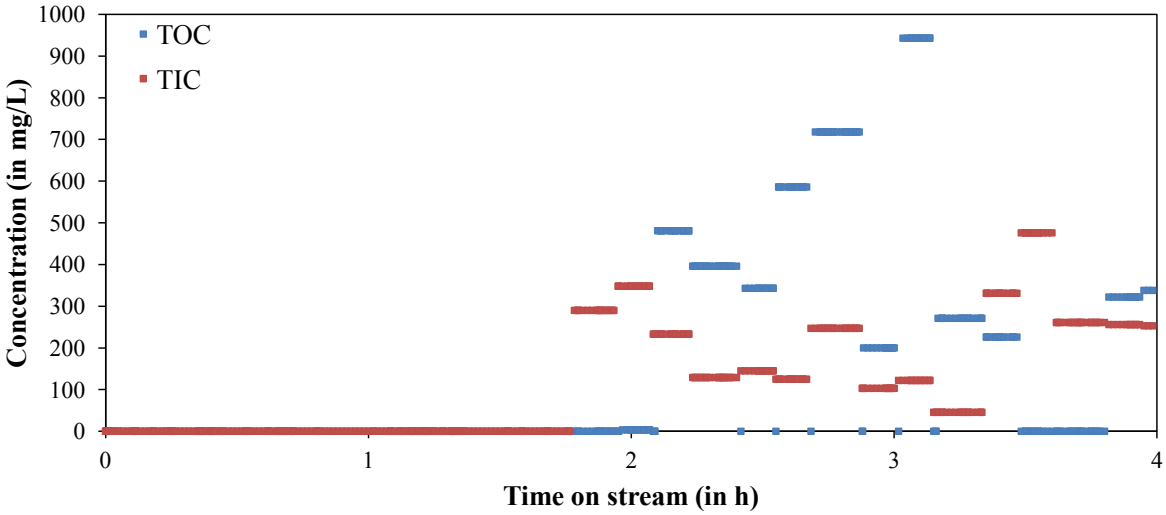

Figure 5.37: Evolution of TOC and TIC of the reactor effluent (first gasification test).

Unfortunately, the microGC section did not work properly and could not be fixed during the test. Therefore, no reasonable gas analysis of this first gasification test could be gained.

5.6.3. Post-experimental observation of KONTI-C

After rinsing overnight with water by the use of the HPLC pump, the filters of feed, brine effluent and reactor effluent were removed, inspected and cleaned. The feed filter was covered with algae slurry, but hardly any particles could be found on it. In contrast to the previous algae tests, only small amounts of tar could be seen on the filter of the brine effluent. The reasons for this were the short run time of the test (approx. 2 h) and possibly better algae liquefaction due to harsher salt separator conditions. The filter of the reactor effluent was very clean showing no tar, but contained a few coke particles.

Before rinsing KONTI-C with ethanol, the transfer pipe between the salt separator and the reactor was uncoupled so that only the salt separator and its two outlets got flushed. It was decided not to rinse the reactor yet so that the catalyst stayed untreated.

5.7. Results of the second gasification test

5.7.1. Basic and starting conditions

The reason for the plugging during the previous test could not have been determined yet. A second pressure relief valve (V-5-8) was installed parallel to the original one. The idea was

to switch from one to the other valve if plugging occurs again to identify the weak spot – the Flowserve or the pressure relief valve. Since the TIC measurements had exceeded the calibration range, the TOC analyzer was recalibrated for TIC concentration up to about 1130 mg/L.

The basic and starting conditions of the second gasification experiment are listed in Table 5.17. Since the first gasification test showed a good salt separator performance, hardly any parameters were varied. The Liquiflow was working properly again and set to only 60% to see if the brine could be concentrated more than before. The heater for the transfer pipe between the salt separator and the reactor was adjusted in a way just to keep the liquefied fluid above the critical point of water. The actual mass flow rate was determined through dividing the weight difference of the feed tank by the feeding time.

Table 5.17: Basic and starting conditions of the second gasification test.

Parameter	Unit	Value
Desired time on stream	h	4.00
Microalgae content (dry matter)[(a)]	wt%	9.02
Feed temperature	°C	20-24
Desired inner T-profile of salt separator	°C	300-430
Desired temperature inside reactor	°C	400.00
Setpoint for chiller	°C	25.00 (30.00)
Setpoint for pressure controller (PTRC 5-3)	barg	280.00
Setpoint for Slurry Feeder	Hz	23.00
Actual feed flow rate	g/min	17.01
Setpoint for Liquiflow	% (g/min)	60 (1.92)
Reactor/Bypass	-	Reactor
Reactor filling	-	Katalco (ZnO), Ru/C
Reactor filling - amount	g	528.5 (Katalco), 443.5 (Ru/C)
WHSV[(b)]	g_{Org}/g_{Cat}-h	< 0.21[(c)]

[(a)]Based on the C-content of the feed (gained from CNS analysis) compared to the C-content of Ph. tricornutum from [14].
[(b)]WHSV = weight hourly space velocity used in units of hourly rate of algae (dry matter) processed over the grams of catalyst.
[(c)]0.21, if the entire organic material from the feed left the salt separator at the top and passed the catalyst.

5.7.2. Progression of temperature, pressure, electrical conductivity and composition

The important comments noted during the test are summarized in Table 5.18. The on-line measurements of temperature, pressure and conductivity are depicted in Figures 5.38, 5.39,

5.40, 5.41 and 5.42.

Table 5.18: Comments on the second gasification test.

Time	Time on stream (in h)	Comment
09:12	0.01	PC restarted
10:51	1.66	Switch to Slurry Feeder
11:06	1.91	TTRC 2-7 and TTRC 2-8 continuously adjusted to keep 300-430 °C
12:00	2.81	Pressure problem at pressure regulation system
12:06	2.92	Opening and closing PTRC 5-3 to bring pressure down
12:13	3.03	Pressure still not constant, try to keep running as long as possible
12:14	3.04	ECTR 6-1 should be correct now
12:15	3.06	Switching to second pressure relief valve had no effect
12:25	3.24	New setpoint of the chiller: 30 °C
13:01	3.82	Conductivites should be correct again
13:49	4.63	Slurry feeder set to 20 Hz
13:51	4.66	Slurry feeder set to 27 Hz, then to 15 Hz
13:53	4.70	Slurry feeder set back to 23 Hz
16:01	6.84	Conductivity of brine seems to be correct
17:14	8.05	Switch back to water, cooling down and rinsing overnight

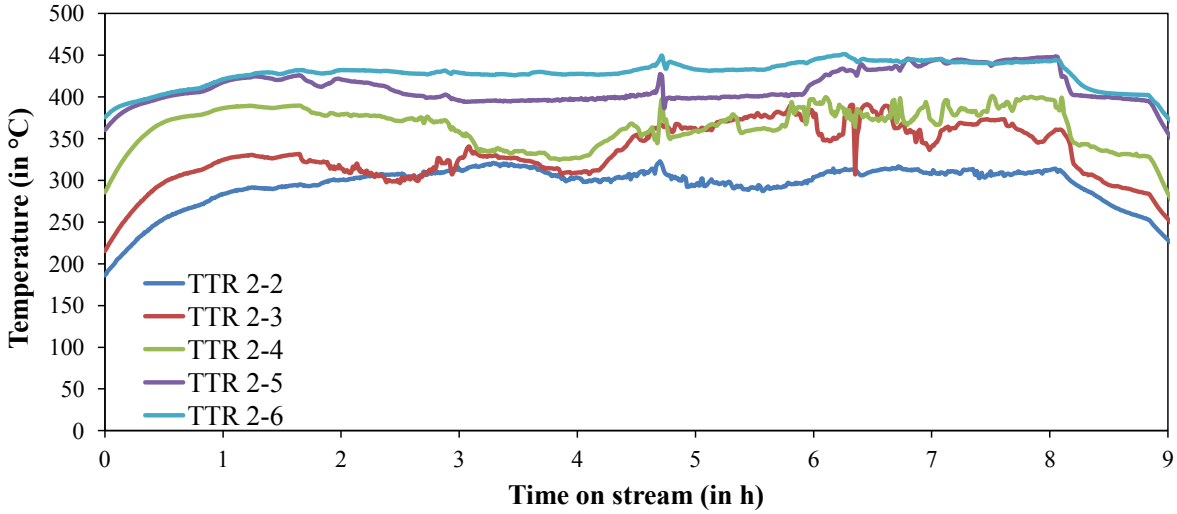

Figure 5.38: Evolution of the temperature at the inner wall of the salt separator (second gasification test).

Figure 5.38 and 5.39 show that the temperature inside the salt separator proceeded very smoothly until the feed was changed from water to algal slurry after 1.66 h. Then the measurements became more chaotic showing again the dynamic behavior of the processes inside the salt separator. Unfortunately, the measurements of the lance stuck quite often (horizontal lines in Figure 5.39), which was not detected immediately during this labor-intensive test.

Figure 5.40 illustrates the measurements of the temperature lance of the reactor. Although the measurements got stuck for long times, it can be seen that the temperature inside the reactor was in the range of 370 to 410 °C from TLTR 4-5 to TLTR 4-19. Again, between TLTR 4-19 and TLTR 4-20 a transition from super- to subcritical state occurred, which can be seen by the temperature difference and the fluctuations of TLTR 4-20.

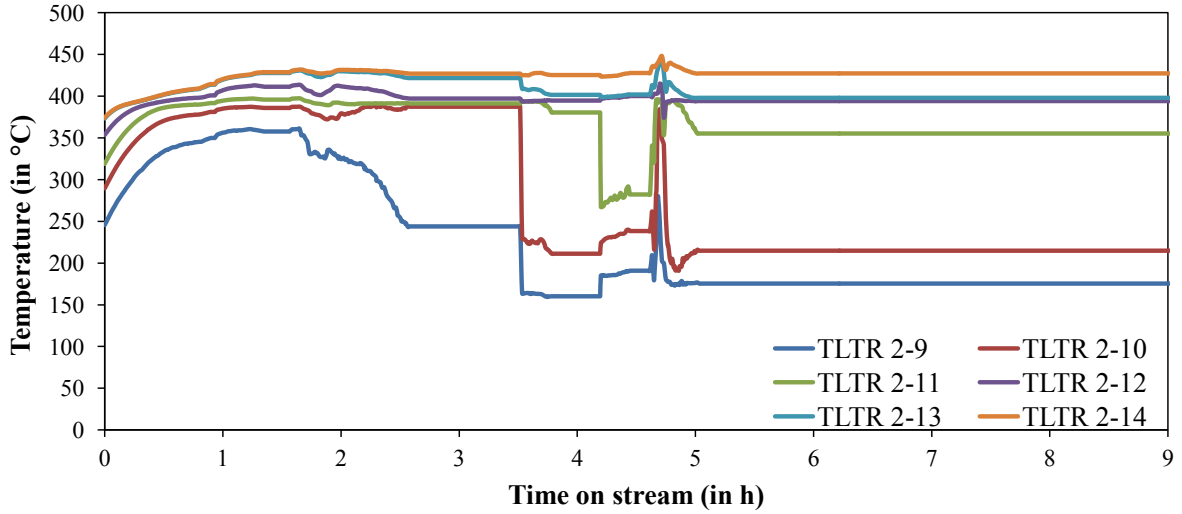

Figure 5.39: Evolution of the temperature at the lance of the salt separator (second gasification test).

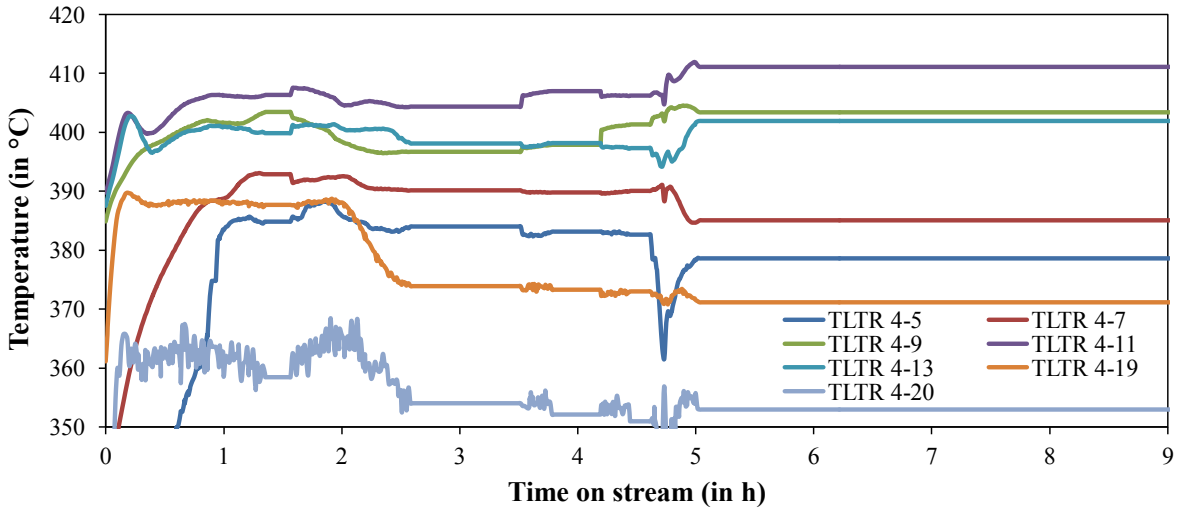

Figure 5.40: Evolution of the temperature at the lance of the reactor (second gasification test).

The pressure (Figure 5.41) was very stable when water was fed and also at the beginning when algal slurry was processed. After about 2.8 h PTRC 5-3 increased very quickly indicating plugging at the pressure regulation part. Neither moving up and down the regulation needle of the Flowserve manually nor switching to the second pressure relief valve improved the

situation (see Table 5.18). After 3.24 h it was decided to increase the setpoint temperature of the chiller from 25 °C to about 30 °C because the formation of methane hydrate was believed to be the reason. Indeed, the pressure went down. A look into literature revealed that the formation of methane hydrates at 28 MPa and 25 °C is possible [129]. Later on the pressure went up and down two more times caused by some kind of build-up and breakthrough inside the salt separator.

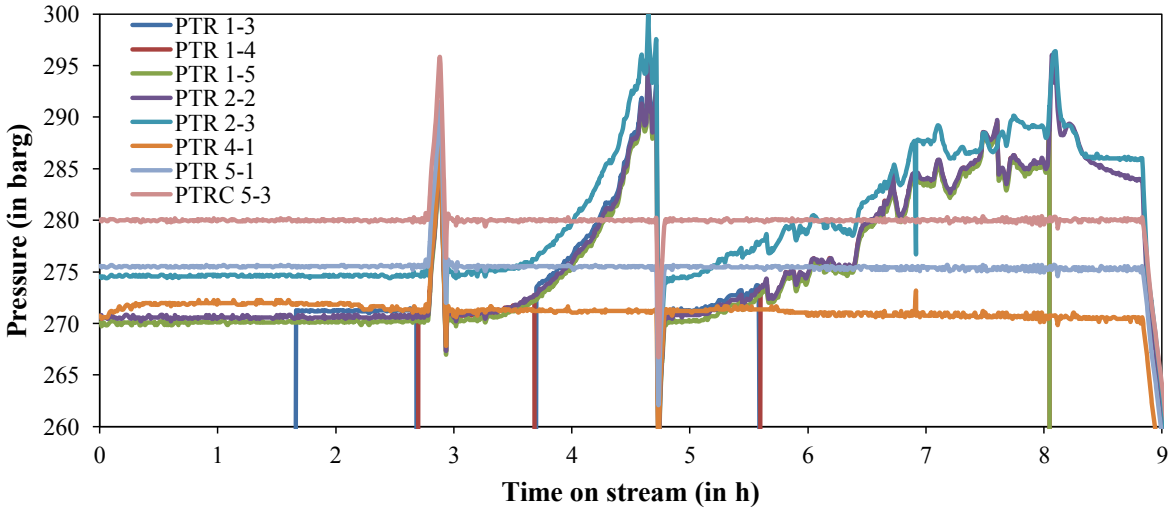

Figure 5.41: Evolution of the pressure (second gasification test).

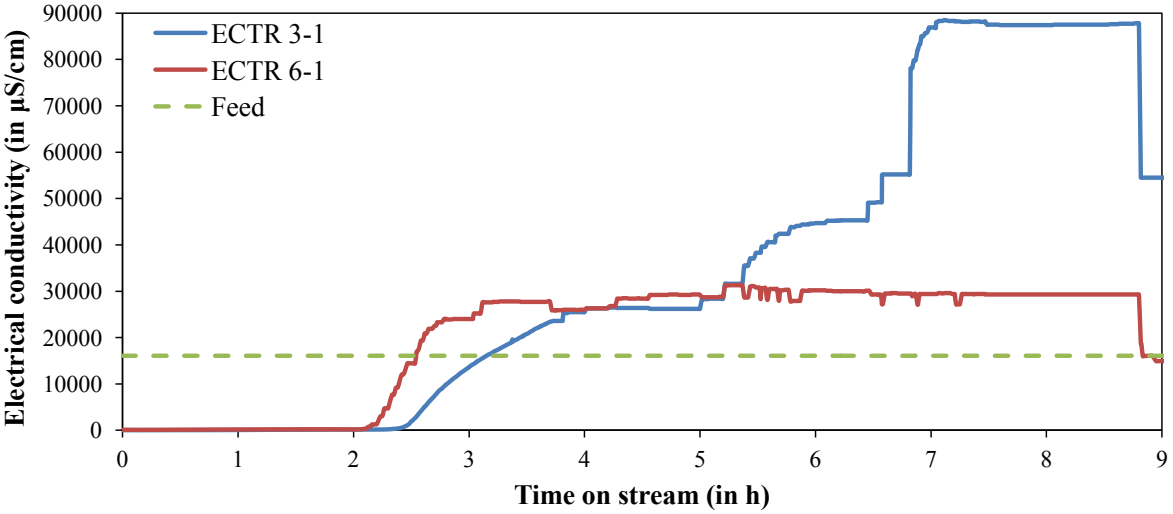

Figure 5.42: Evolution of the electrical conductivity (second gasification test).

The conductivity measurements of the second gasification test are depicted in Figure 5.42. As in the first four algae tests, the conductivity of the reactor effluent started to grow earlier and steeper than the one of the brine effluent. It reached a steady-state value of around 30 000 µS/cm after about 5 h. The electrical conductivity of the brine effluent exceeded the one

of the reactor effluent after 5.2 h. About 1.5 h later something happened that had not been observed in the previous algae tests. The conductivity of the brine increased rapidly again and reached a steady-state value of about 88 000 µS/cm. As described in Table 5.18, the conductivity meters were checked by disconnecting and reconnecting the cables. A possible explanation for this phenomenon could be that salts, especially type 2 salts (see Section 2.2.9), might have precipitated and stayed inside the salt separator, as it had been noticed after the first liquefaction test (see Section 5.2.3), or inside the filter vessel of the brine effluent until a certain point, where they broke through.

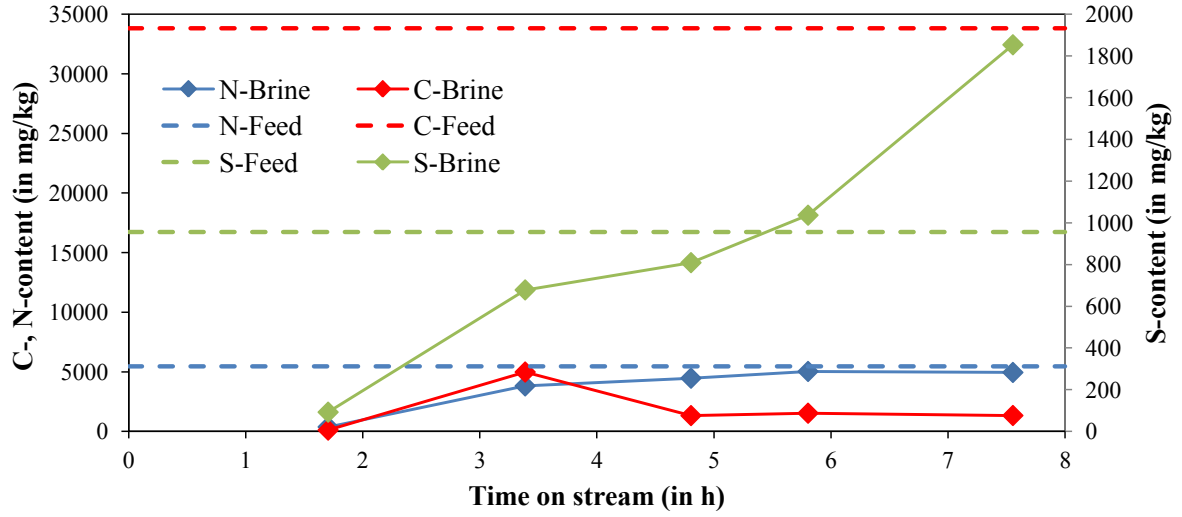

Figure 5.43: Evolution of carbon-, nitrogen- and sulfur content in the brine effluent (second gasification test).

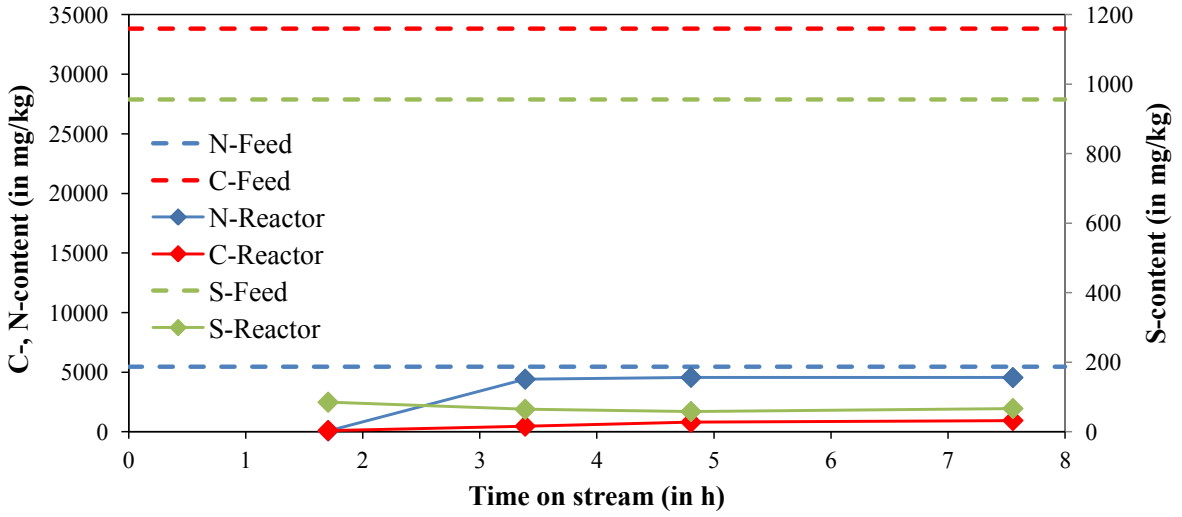

Figure 5.44: Evolution of carbon-, nitrogen- and sulfur content in the reactor effluent (second gasification test).

Carbon-, nitrogen- and sulfur concentration of feed, brine effluent and reactor effluent of the samples taken during the run were measured off-line. The results are shown in Figure 5.43 and Figure 5.44. The C-concentration in the brine effluent started to increase at the beginning of the test and flattened out towards the end. The N-concentration of the brine effluent reached values close to the N-concentration of the feed. The S-concentration in the brine effluent shows a trend similar to the electrical conductivity. It reached a first maximum after about 5 h and increased significantly towards the end of the experiment. This result is another hint for a possible breakthrough of precipitated salts during the last two hours of the test, since a couple of sulfates are classified as type 2 salts [110]. As it can be seen in Figure 5.44, the concentrations of carbon and sulfur stayed very low in the reactor effluent indicating high gasification- and sulfur removal efficiency. The N-concentration of the reactor effluent reached values similar to the N-concentration of the brine effluent. The final concentrations and calculations of the recoveries in the brine- and the reactor effluent with respect to carbon, nitrogen and sulfur are summarized in Table 5.19. It can be seen that less than 3% of the carbon from the feed could be found in the brine- and the reactor effluent, which means that more than 97% were gasified or deposited inside KONTI-C as tar or coke. In addition, nearly 74% of the nitrogen could be recovered in the brine- and the reactor effluent, whereas most of the sulfur (about 68%) was deposited inside the plant probably via salt precipitation, adsorption on ZnO or catalyst poisoning.

Table 5.19: Final concentrations and recoveries of carbon, nitrogen and sulfur in the brine- and the reactor effluent (second gasification test).

	Feed	Brine effluent	Reactor effluent
Mass flow rate (in g/min)[(a)]	17.01	2.37	12.50
Final C-content (in mg/kg)	33833	1333	945
C-recovery (in %)	-	0.55	2.05
Final N-content (in mg/kg)	5467	4946	4549
N-recovery (in %)	-	12.61	61.15
Final S-content (in mg/kg)	956	1854	67
S-recovery (in %)	-	27.02	5.15

[(a)]Based on the weights of the tanks before and after processing algal slurry.

The results of the ICP measurements with respect to K, Na, S and P are illustrated in Figure 5.45 and Figure 5.46. It can be seen that each of these elements could be concentrated in the brine effluent towards the end of the experiment, which explains the trend of the electrical conductivity (compare Figure 5.42). The concentration of those elements in the reactor effluent stayed very low and mostly below their detection limits. The final concentrations and calculations of the recoveries with respect to K, Na, S and P are summarized in Table 5.20. It seems that the

entire K and Na could be recovered in the brine effluent or partially stayed inside KONTI-C. The fact that their calculated recoveries have a value higher than 100% could have been related to the sudden breakthrough of the precipitated salts.

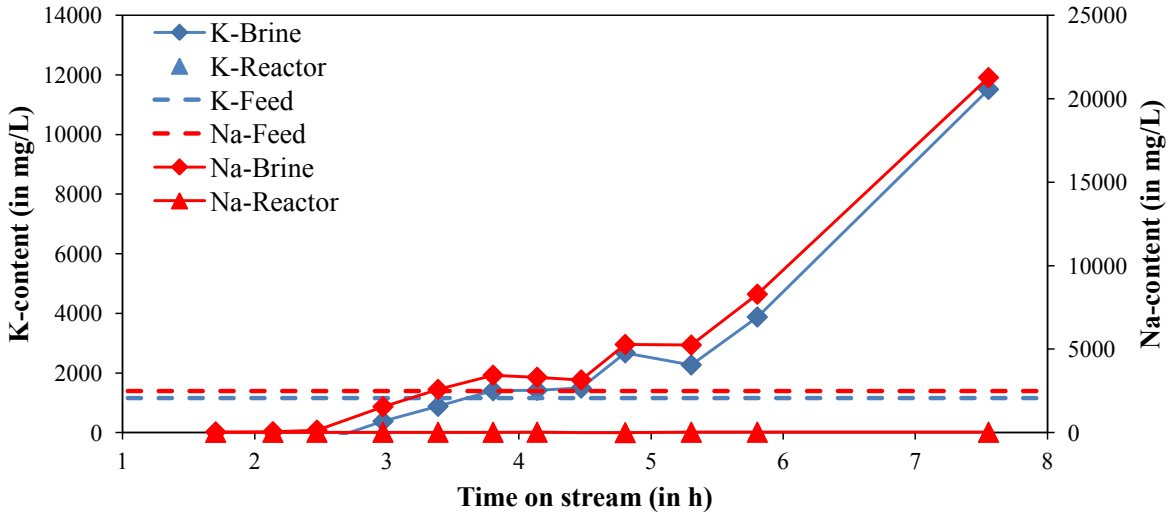

Figure 5.45: Evolution of potassium- and sodium content in the brine- and the reactor effluent (second gasification test).

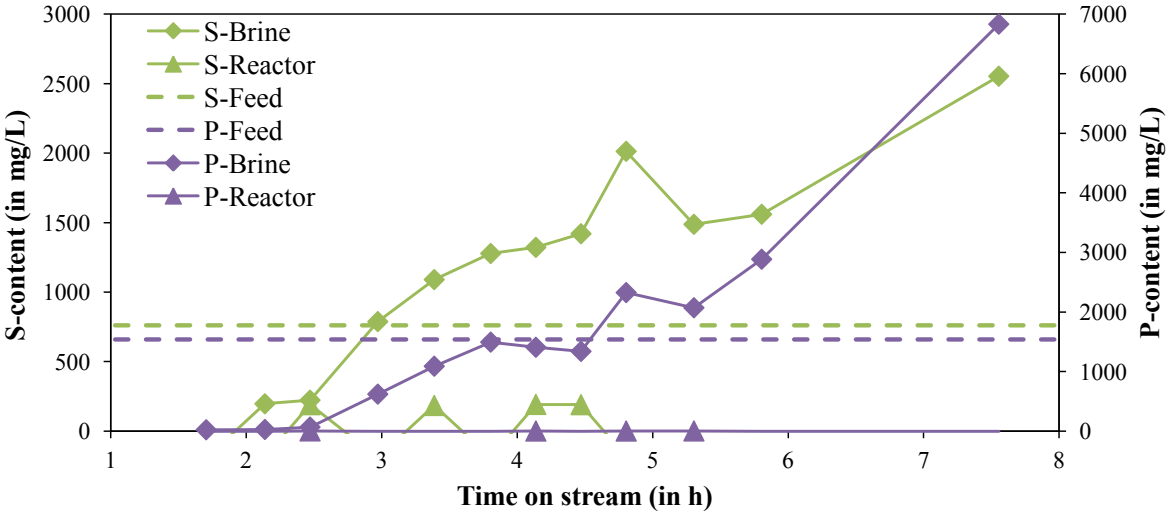

Figure 5.46: Evolution of sulfur- and phosphorus content in the brine- and the reactor effluent (second gasification test).

P and S could not be recovered in the brine effluent as successfully as K and Na. Since their concentrations in the reactor effluent stayed below the detection limit, it can be expected that high amounts were kept inside the plant through precipitation, adsorption on ZnO or catalyst poisoning. The different results of the CNS- and the ICP-analyzer with respect to sulfur may be attributed to the different measurement techniques. The results of the ICP measurements

suggest an elemental separation efficiency for the salt separator in the following order: K > Na > P > S. Although Elliott *et al.* [1] used a different method for the separation of inorganic substances as described in Section 2.3.1, they gained comparable results regarding the behavior of K, Na, P and S. As they conducted a fair bit of experiments with different algal species under different conditions with different results, a quantitative comparison is not possible.

Table 5.20: Final concentrations and recoveries of potassium, sodium, phosphorus and sulfur in the brine- and the reactor effluent (second gasification test).

	Feed	Brine effluent	Reactor effluent
Final K-content (in mg/L)	1161	11514	ND
K-recovery (in %)	-	138.18	ND
Final Na-content (in mg/L)	2492	21267	22
Na-recovery (in %)	-	118.91	0.65
Final P-content (in mg/L)	1537	6831	ND
P-recovery (in %)	-	61.92	ND
Final S-content (in mg/L)	760	2553	ND
S-recovery (in %)	-	46.80	ND

[(a)]Based on the weights of the tanks before and after processing algal slurry.

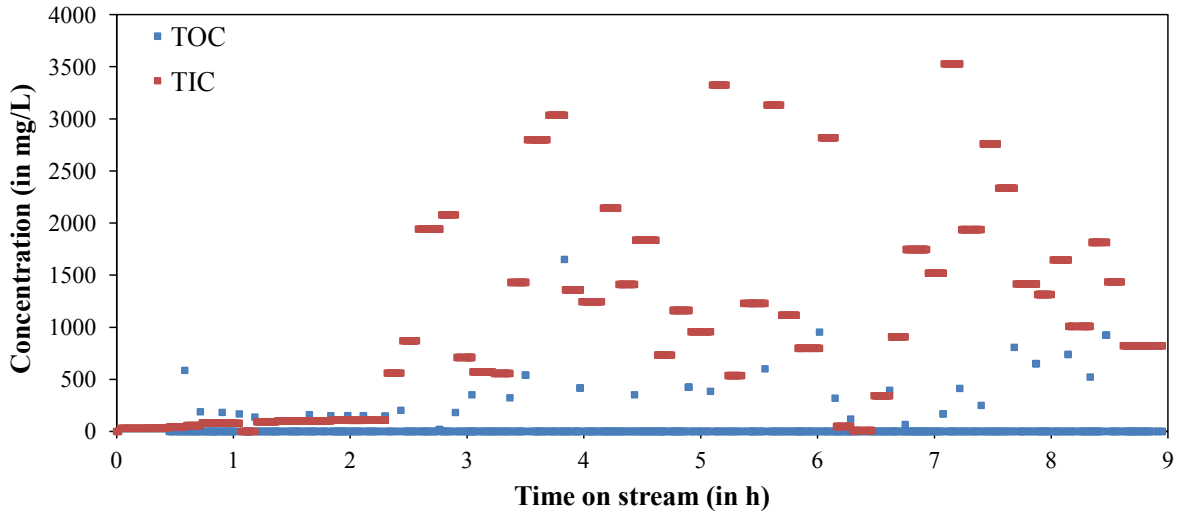

Figure 5.47: Evolution of TOC and TIC of the reactor effluent (second gasification test).

Figure 5.47 shows the TOC- and the TIC content of the reactor effluent measured on-line. It can be seen that most of the TOC measurements stayed below 1000 mg/L suggesting high catalytic activity and gasification efficiency. As described before, a possible reason for the TOC content not having reached even lower values is the formation of stable N-heterocyclic compounds

through the Maillard reaction. Interestingly, the TIC values scattered up to about 3500 mg/L, which was again higher than the calibration limit. Since CNS analysis with respect to carbon was in the range of the TOC values, those high TIC values could have been caused by dissolved CO_2 (It is believed that the dissolved CO_2 had degassed before the off-line CNS measurements were carried out.). It is difficult to compare the TIC measurements with data from literature regarding the solubility of CO_2 in water, because the time between relaxation (with respect to pressure) and TOC/TIC measurement was in the range of seconds/minutes.

The results of CNS-, ICP- and TOC/TIC analysis described above could not answer the question: Why did the electrical conductivity of the reactor effluent reach values up to 30 000 µS/cm? The only element that could be identified in significant amounts was nitrogen. Thus, ammonia was believed to be a possible reason. However, a prepared aqueous NH_4OH-solution containing about 4500 mg/kg nitrogen (similar to the N-content of the reactor effluent) had an electrical conductivity of only 473 µS/cm. Furthermore, compounds containing elements that were not detected could have been the reason for the high electrical conductivity of the reactor effluent. Ph. tricornutum contains significant amounts of Cl, Ca and Mg, too [14], which might not have been separated in the salt separator and could not be analyzed by the ICP instrument. Nevertheless, the exact reason for the high electrical conductivity of the reactor effluent could not be identified.

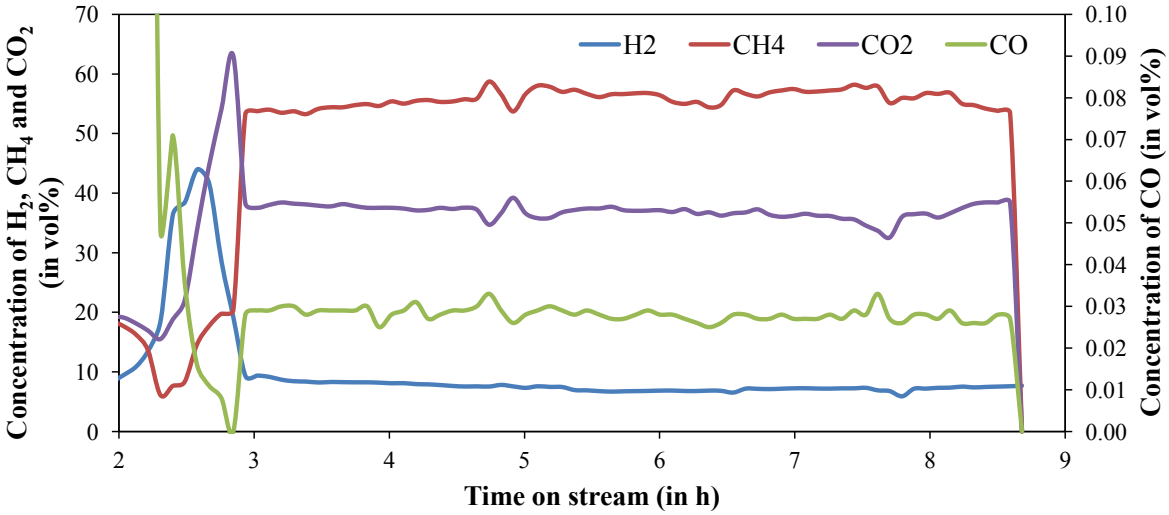

Figure 5.48: Evolution of the gas phase composition of the reactor effluent (second gasification test).

The results of the microGC measurements are depicted in Figure 5.48. It can be seen that the measurements stabilized after about 3 h and stayed quite constant during the whole experiment. A gas containing about 7% H_2, 57% CH_4, 0.03% CO and 36% CO_2 was produced, which can be expected to be close to the thermodynamic equilibrium [130]. The fact that the gas composition did not change shows that the catalyst did not deactivate. Brandenberger [2], who conducted a similar experiment with PSI's old continuous test rig but without the use of ZnO, obtained

catalyst deactivation within a few minutes. This shows again the possibility of ZnO as a sulfur adsorber under hydrothermal conditions. Unfortunately, the gas meter was not working properly, which means that neither information about the gas flow could be gained nor a carbon gasification efficiency of this experiment calculated.

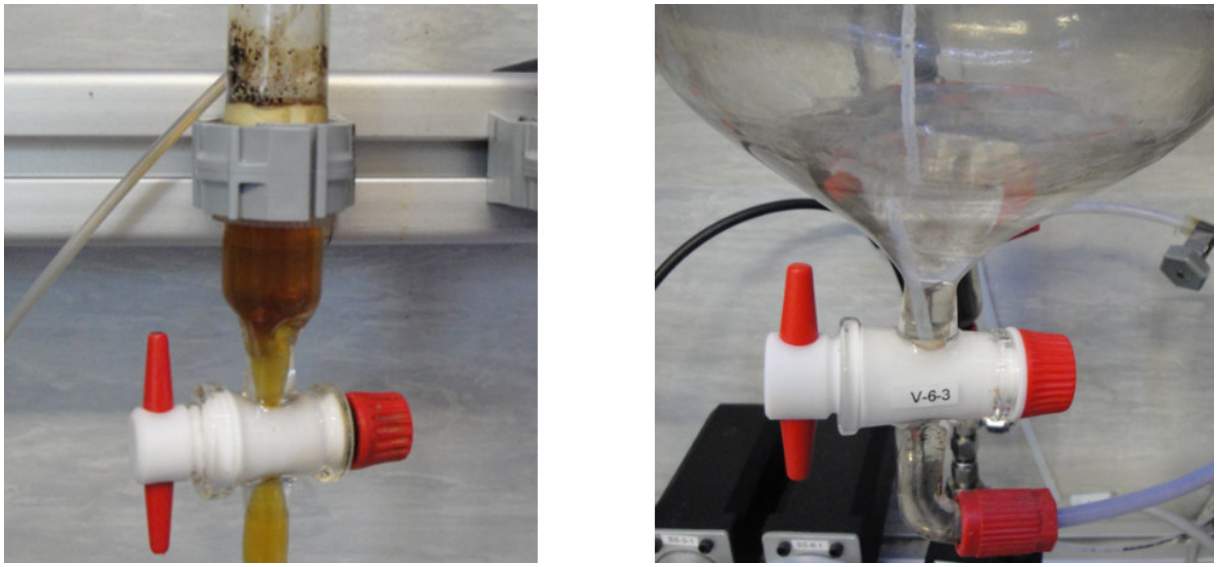

Figure 5.49: Left: Phase separator of the brine effluent (TOS: 7.6 h). Right: Phase separator of the reactor effluent (TOS: 5.3 h).

As in the first gasification experiment, the color of the brine effluent was orange-brown showing no non-liquified feed (Figure 5.49 left). A little bit of tar could be seen towards the end of the test, too, which was not withheld by the filter of the brine effluent. The reactor effluent stayed clear throughout the run (Figure 5.49 right). In comparison, Brandenberger's reactor effluent contained an oily and an aqueous phase due to catalyst deactivation and incomplete gasification [2]. The pH values of the last samples were measured, too. The one of the brine effluent had a value of 5.94, the one of the reactor effluent a value of 8.44. The basic character of the reactor effluent could be explained by the presence of ammonia. In comparison, Elliott *et al.* [1] obtained an aqueous product with a pH value in the range of 8.0 to 8.6.

5.7.3. Post-experimental observation of KONTI-C

After rinsing overnight with DI water by the use of the HPLC pump, the filters of feed, brine effluent and reactor effluent were removed, inspected and cleaned. As in the previous tests with microalgae, hardly any particles could be found on the feed filter. Compared to the first gasification test, the amount of tar on the filter of the brine effluent was higher, which could be explained by a much longer time on stream (Figure 5.50 left). The filter of the reactor effluent was very clean showing no tar, but contained a few coke particles (Figure 5.50 middle and right).

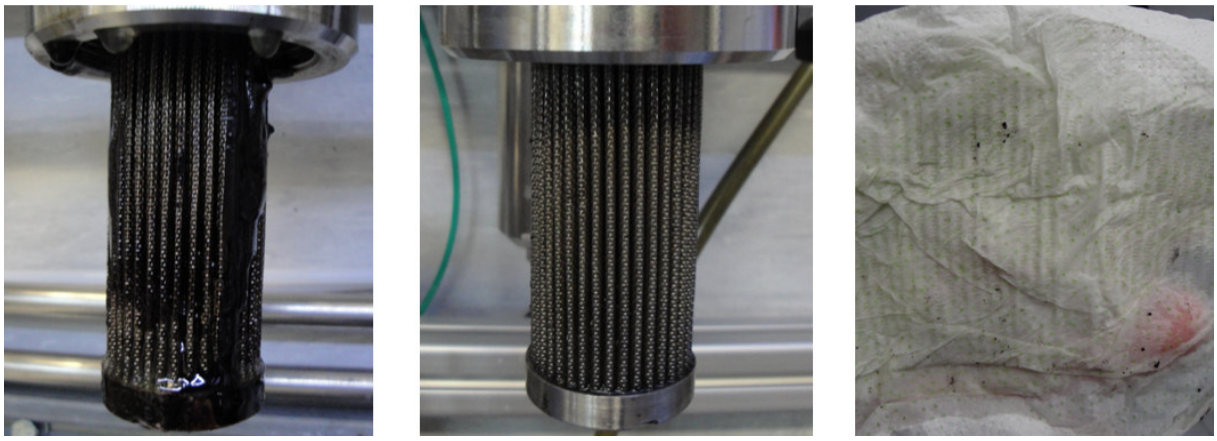

Figure 5.50: Left: Brine effluent filter after experiment. Middle: Reactor effluent filter after experiment. Right: Coke particles from reactor effluent filter.

Before rinsing KONTI-C with ethanol, the transfer pipe between the salt separator and the reactor was uncoupled so that only the salt separator and its two outlets got flushed. It was decided not to rinse the reactor yet so that the catalyst stayed untreated.

5.8. Summary of the experiments with microalgae

- Six experiments with an algal slurry containing 6.5-13.2 wt% Phaeodactylum tricornutum were performed with the use of PSI's new continuous plant (KONTI-C). Two of those tests involved hydrothermal liquefaction, further two focused on hydrothermal liquefaction with subsequent sulfur removal by ZnO and the last two combined liquefaction, sulfur removal and catalytic gasification over a 5%Ru/C catalyst.
- The temperature measurements of the salt separator indicated a very dynamic behavior of the processes inside.
- The measurements of the lance of the reactor showed a stable and narrow temperature distribution up to the top, where a transition from super- to subcritical state took place.
- The pressure sensor and the standpipe of the salt separator, the pressure regulation system and the flow controller of the brine effluent (Liquiflow) were identified as the weak points of KONTI-C. Leakage of the pressure sensor could be prohibited by welding the pressure sensor on the salt separator and the possibility of plugging inside the standpipe could be reduced through exchanging the feed filter with an original pore size of 250 µm by another one with a pore size of 25 µm. The pressure regulation system (Flowserve and pressure relief valve) was sensitive towards tar and particles. The reason for the ever and anon occurring malfunction of the Liquiflow could not be figured out.
- In contrast to the salt tests, the electrical conductivity of the reactor effluent did not stay very low and reached values up to about 30 000 µS/cm. Although nitrogen was the only

detected element with significant amount in the reactor effluent during the gasification experiments, the electrical conductivity of a corresponding aqueous NH_4OH-solution had an electrical conductivity of only 473 µS/cm. Thus, the reason for the high electrical conductivity of the reactor effluent could not be determined.

- When the conditions inside the salt separator were not harsh enough in terms of temperature, non-liquified feed could be seen in the brine effluent giving it a muddy green color. Complete liquefaction was possible for a salt separator internal temperature profile of about 300-430 °C. In such a case, the brine effluent had a clear orange-brown color.
- Tar in the brine effluent could not be prevented, which was mostly withheld by the filter of the brine effluent.
- Inspection of the inner part of the salt separator showed precipitated salts at the bottom and at the lower part of the wall in the subcritical zone, whereas the higher part of the wall in the supercritical zone was salt-free.
- During the liquefaction tests without and with ZnO, the reactor effluent contained a tarry and an aqueous phase.
- On the basis of CNS analysis, sulfur seemed to be adsorbed by ZnO.
- The gas produced from liquefaction without subsequent sulfur removal contained mostly CO_2 (92.3%), whereas the gas produced from liquefaction with subsequent sulfur removal contained high amounts of H_2 (49-56%) and CO_2 (42-50%). Therefore, ZnO had a catalytic effect by favoring steam reforming and WGS reaction rather than the methanation reactions. However, only about 5% of the carbon of the feed could be gasified.
- Cooling the reactor effluent to 25 °C led to plugging at the pressure regulation system during gasification, which was very likely caused by the formation of CH_4 hydrates. After increasing the setpoint of the chiller to 30 °C, this issue was fixed.
- Electrical conductivity measurement, CNS analysis and ICP analysis suggested that it took more than 5 h to reach steady-state regarding the composition of the brine effluent. Quite likely, the precipitated salts stayed inside the salt separator and the vessel of the filter for the brine effluent until a certain point where the broke through.
- CNS analysis showed that more than 97% of the carbon of the feed were gasified (or transformed to tar or coke), 74% of the nitrogen could be recovered in the brine- and the reactor effluent and most of the sulfur was deposited inside KONT-C.
- Separation and concentration of the inorganic substances was successful. An elemental separation efficiency in the following order could be identified: K > Na > P > S. ICP analysis suggested that the entire K and Na could be recovered in the brine effluent, whereas significant amounts of P and S stayed inside the plant.

- The reactor effluent was clear throughout the gasification tests indicating complete gasification and absence of catalyst deactivation. It contained about 4550 mg/kg nitrogen, had a TOC content of less than 1000 mg/L and a TIC content of up to about 3500 mg/L. The high TIC values might have been caused by dissolved CO_2. The last reactor effluent sample had a pH value of 8.44 suggesting the presence of ammonia, whereas the last brine effluent sample had a pH of 5.44.
- During gasification, a gas containing 7% H_2, 57% CH_4, 0.03% CO and 36% CO_2 was produced throughout the run, which was expected to be close to the thermodynamic equilibrium. Unfortunately, the gas meter was not working properly, which means that neither information about the gas flow could be gained nor a carbon gasification efficiency calculated.
- A few coke particles could be found on the filter of the reactor effluent after gasification.
- Since KONTI-C was used for further tests right after our experiments, no ZnO- or catalyst analysis could be conducted.

6. Recommendations for future work with KONTI-C

As described in Section 2.4, the aim of this project was to get familiar with the new process demonstration unit (KONTI-C) and to demonstrate the feasibility for converting microalgae to bio-methane. Although this goal could be accomplished, KONTI-C has not been optimized yet due to lack of time. Moreover, further experiments and more specific analysis are needed to evaluate the process in more detail to get a better idea of the technical and economic feasibility of a scaled up industrial plant. Based on our experience gained in this project, the following recommendations should be considered:

- The non-properly working electrical conductivity meters should be exchanged.
- The reason for the malfunction of the temperature lances should be figured out and corrected.
- The reason for the malfunction of the flow controller of the brine effluent (Liquiflow) should be figured out and corrected. Two controllers could be arranged in parallel to be able to switch from one to the other if needed.
- The gas meter should be fixed or exchanged.
- The on-line TOC analyzer should be calibrated for higher TIC concentrations.
- A flow meter for the feed would simplify operation and determination of mass balances.
- An on-line H_2S analyzer and/or an on-line sulfur analyzer for the reactor effluent would provide instantaneous monitoring of sulfur compounds.
- Long-term tests should be performed to investigate long-time activity and stability of the sulfur adsorber and the catalyst. In addition, elemental mass balances could be calculated enabling determination of salt separation-, gasification- and thermal efficiency.
- A way of hindering tar production or further treatment of the tar in the brine effluent should be developed.
- Analysis of spent sulfur adsorber and catalyst would give additional valuable information.
- The salt separator should be optimized by varying temperature, flow and type of stand-pipe (e.g. length, size of orifice).

A. Process flow diagrams of KONTI-C

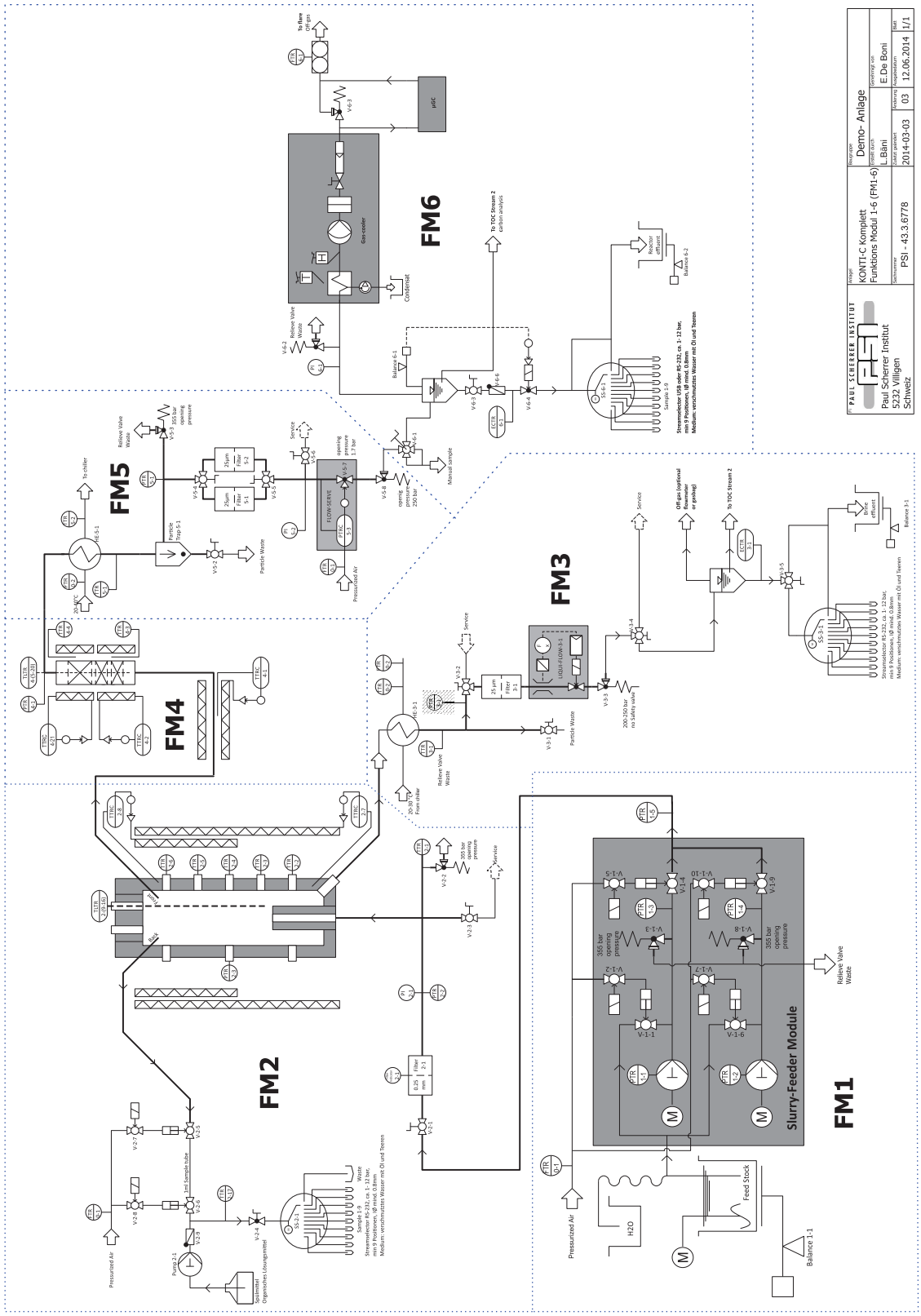

Figure A.1: Process flow diagram of KONTI-C (all sections).

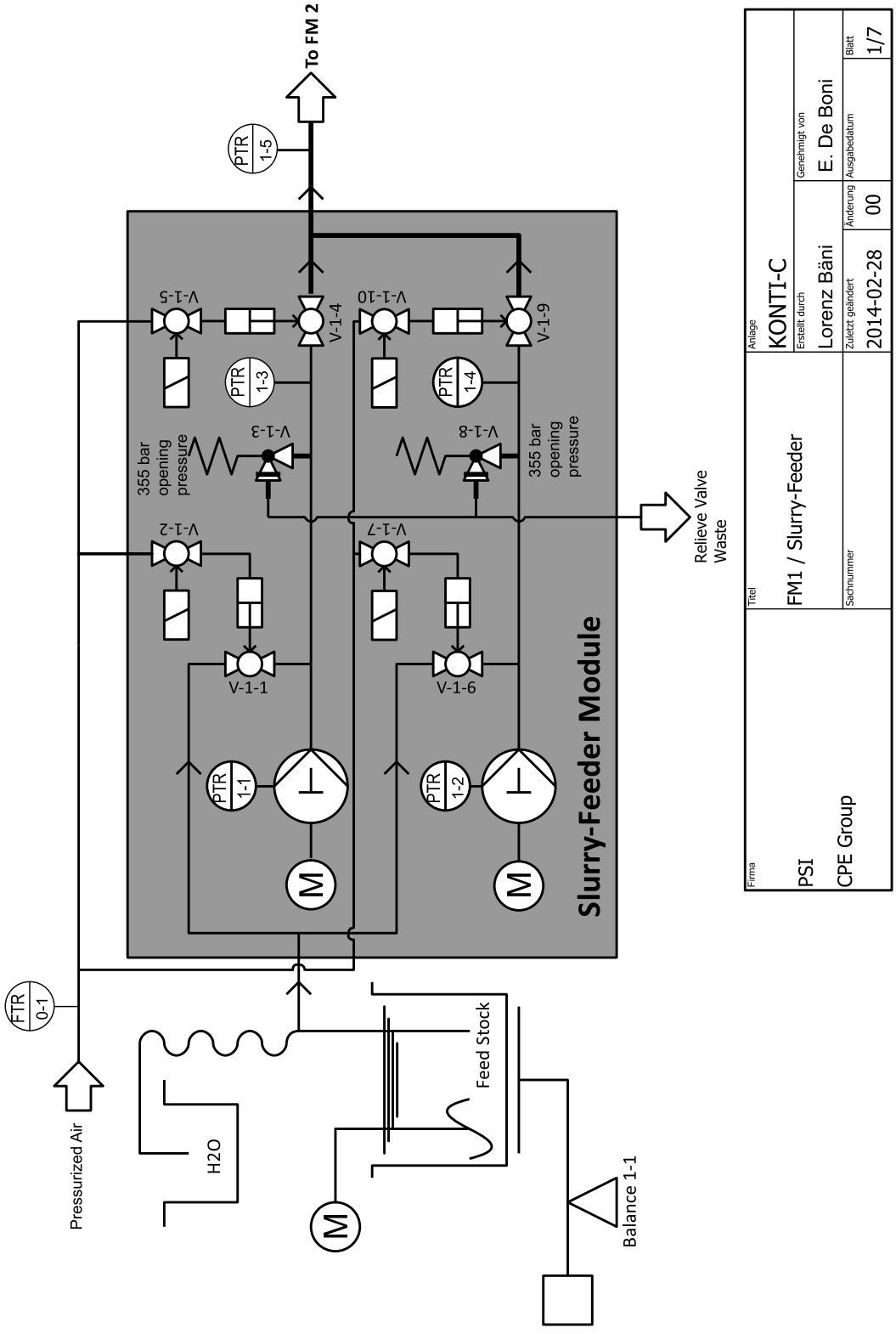

Figure A.2: Process flow diagram of KONTI-C (section FM1).

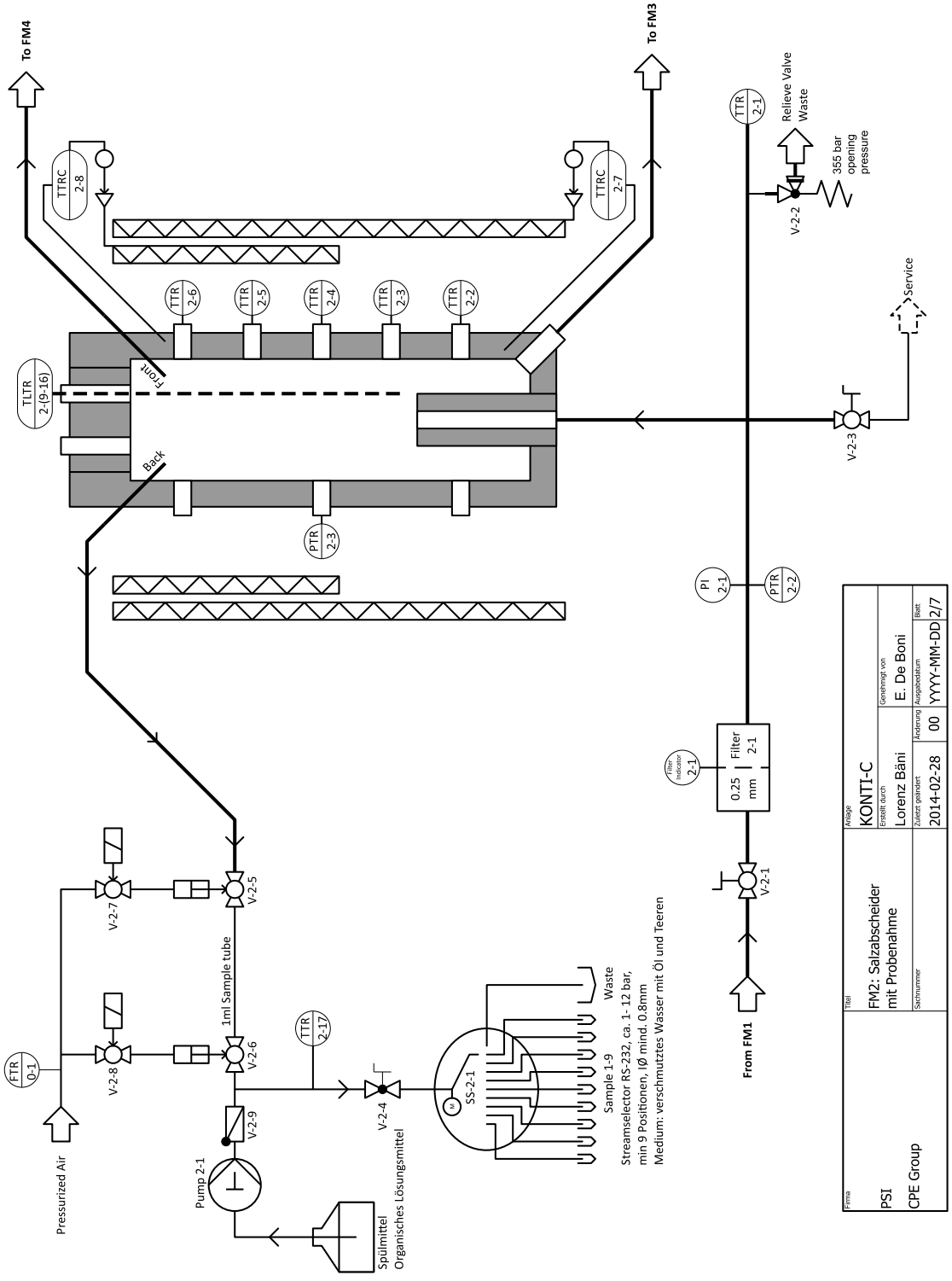

Figure A.3: Process flow diagram of KONTI-C (section FM2).

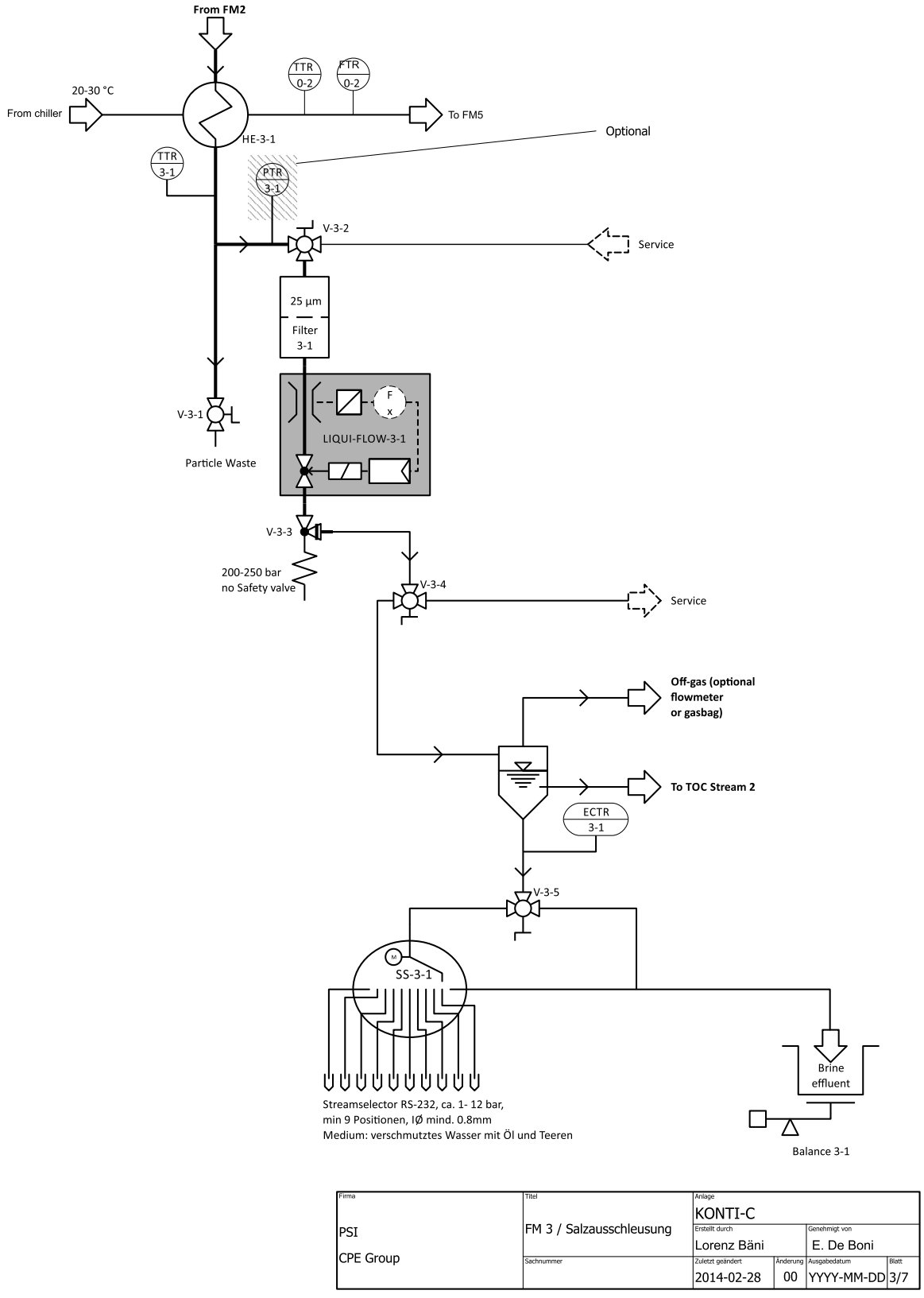

Figure A.4: Process flow diagram of KONTI-C (section FM3).

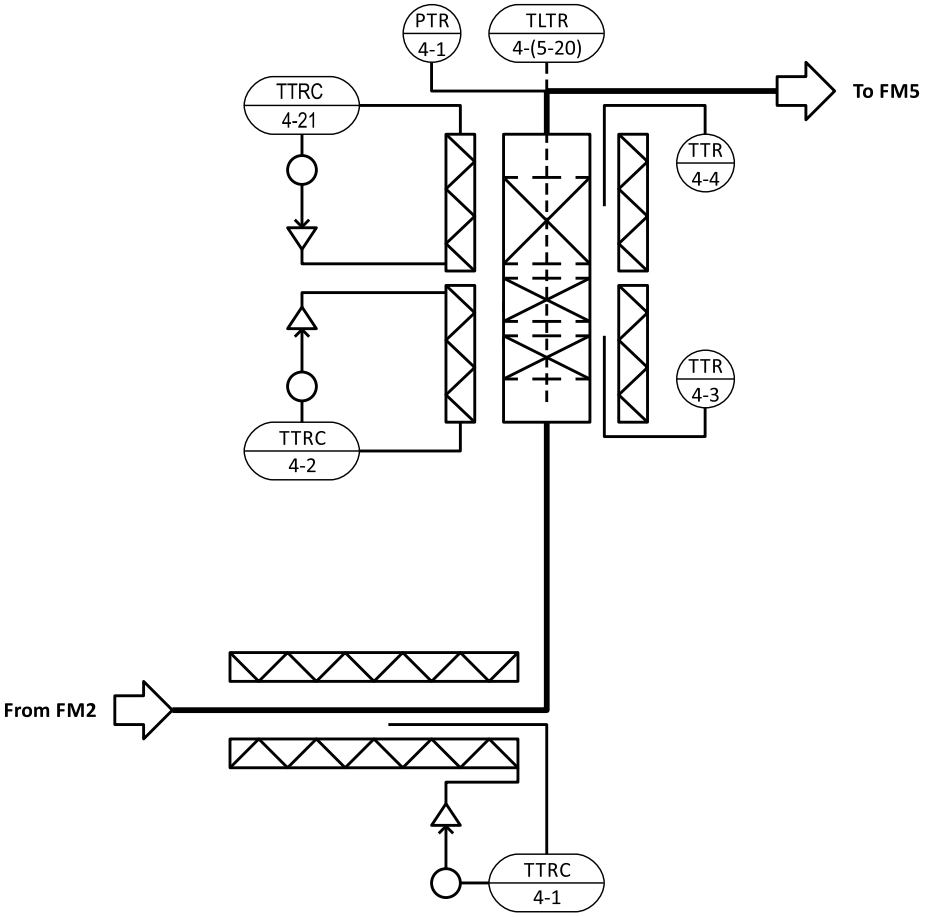

Firma	Titel	Anlage			
PSI CPE Group	FM 4: Schwefelfalle / Methanierungs-Reactor	KONTI-C			
		Erstellt durch: Lorenz Bäni		Genehmigt von: E. De Boni	
	Sachnummer	Zuletzt geändert: 2014-02-28	Änderung: 00	Ausgabedatum: YYYY-MM-DD	Blatt: 4/7

Figure A.5: Process flow diagram of KONTI-C (section FM4).

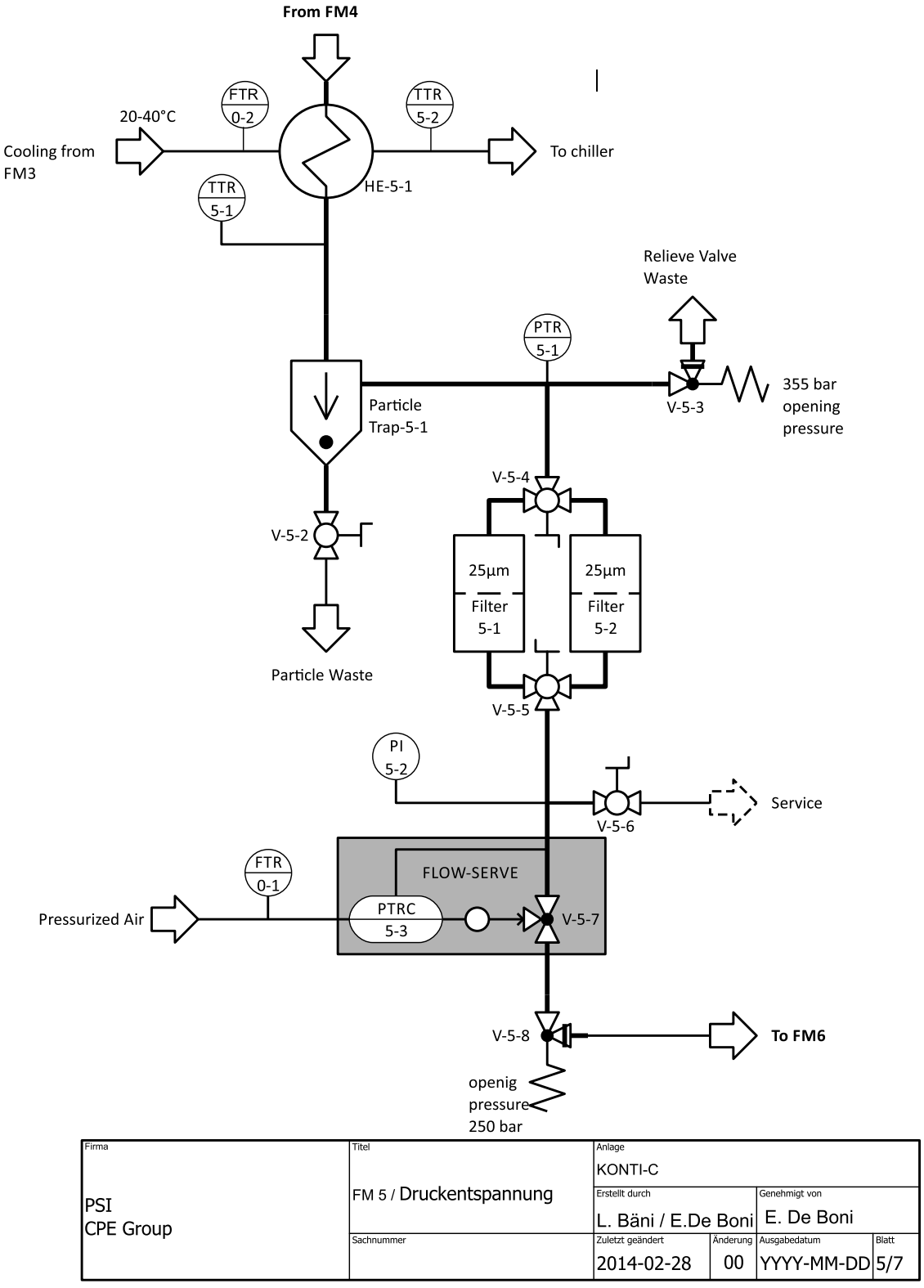

Figure A.6: Process flow diagram of KONTI-C (section FM5).

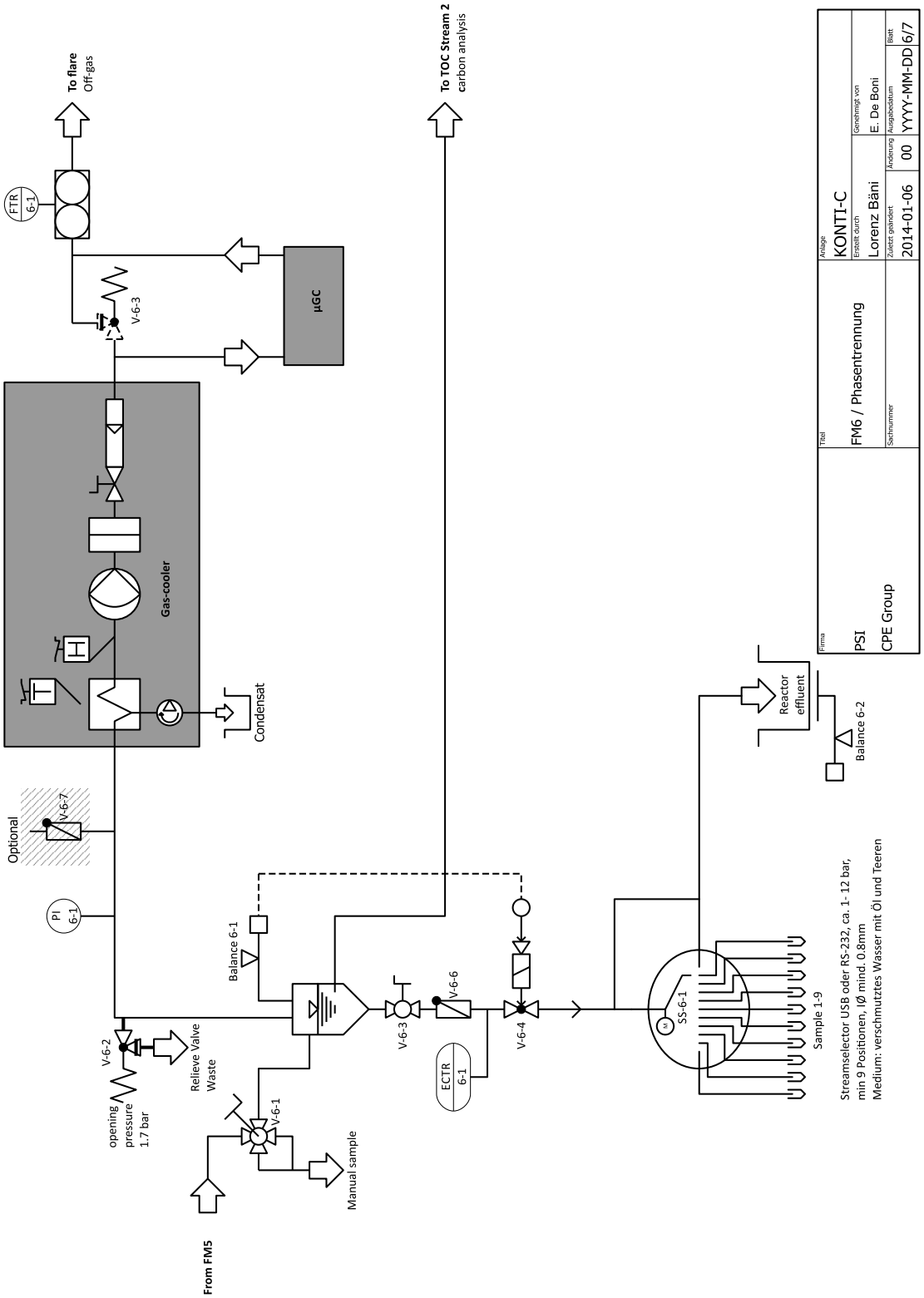

Figure A.7: Process flow diagram of KONTI-C (section FM6).

B. Screenshots of the LabVIEW based software for KONTI-C

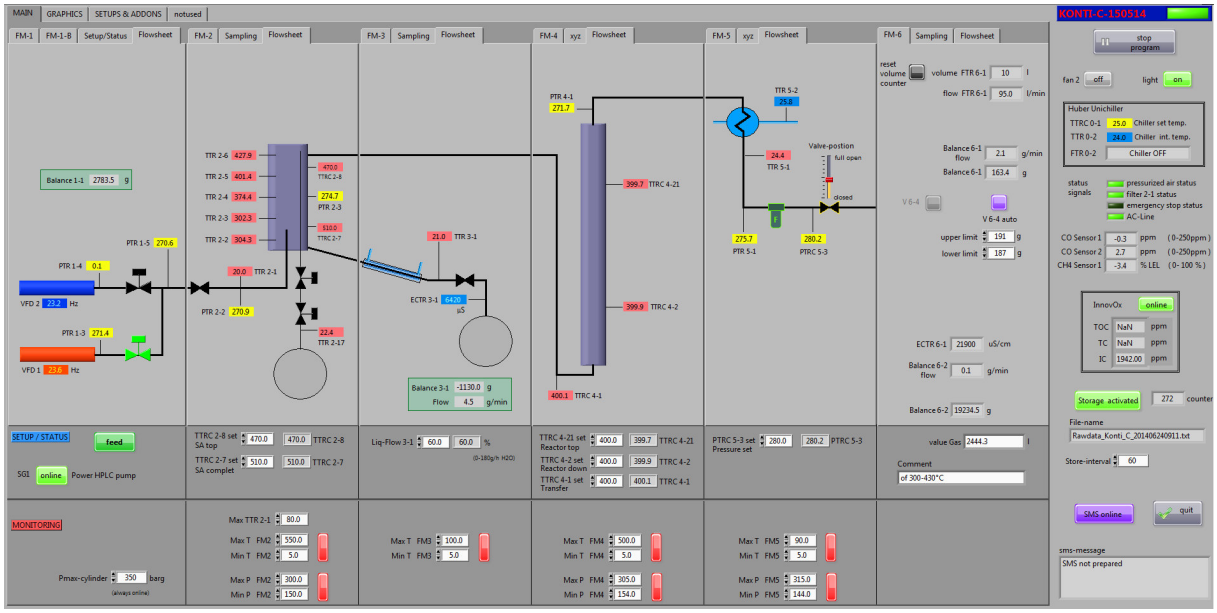

Figure B.1: LabVIEW - main screen.

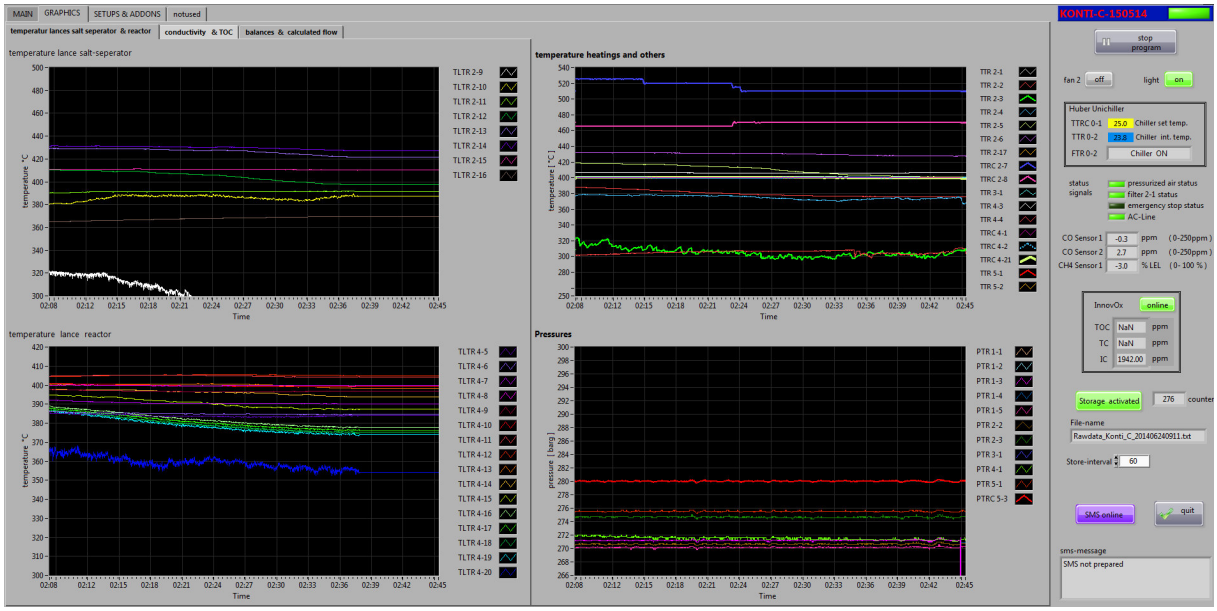

Figure B.2: LabVIEW - monitoring of temperature and pressure.

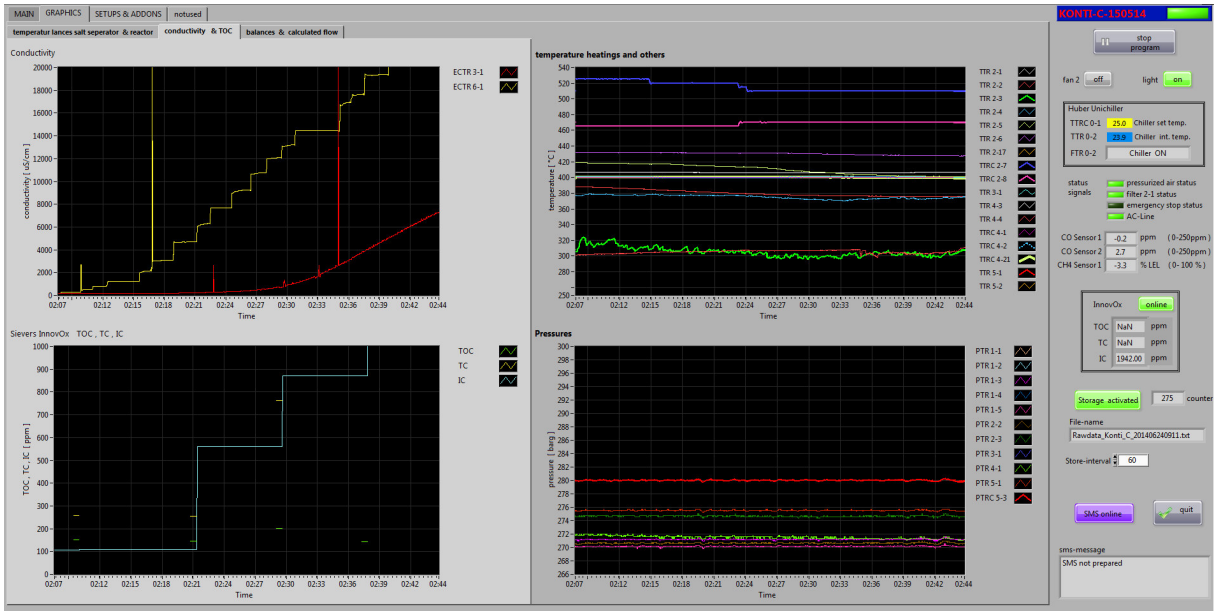

Figure B.3: LabVIEW - monitoring of conductivity, TOC/TIC, temperature and pressure.

C. Feedstock characterization

Table C.1: Feedstock characteristics of Phaeodactylum tricornutum. Adapted from [14].

Parameter	Content (in wt%)	SD
Ash	16.80	0.50
Lipids	20.00	ND
Composition		
C	37.50	0.10
H	6.47	0.01
N	7.25	0.01
S	0.83	0.01
O	27.30	0.10
P	3.27	0.01
Cl	2.96	0.24
Na	1.83	0.04
Mg	0.51	0.01
K	1.85	0.04
Ca	0.80	0.00
Fe	0.02	0.00

D. Catalyst characterization

Table D.1: Characterization of 5%-Ru/C (BASF).

BET (in m^2/g)	$V_{mesop.}$ (in cm^3/g)	$V_{microp.}$ (in cm^3/g)	D_{CO}[(a)]	$d_{P,CO}$ (in nm)[(a)]
1254	0.21	0.42	0.23	5.00

[(a)]Determined by CO pulse chemisorption.

E. Summarized results of the experiments with model solutions

Parameter	Unit	First salt separation test	Second salt separation test	Third salt separation test
Pressure	bar	280	280	280
T-profile inside salt separator	°C	239-435	243-244	240-451
Time on stream of model solution	h	2.80	4.08	3.12
Conductivity of feed	µS/cm	23600	15070	15070
Final conductivity of brine effluent	µS/cm	61700	53200	57000
Final conductivity of reactor effluent	µS/cm	55	27	14
Mass flow rate of feed	g/min	18.22	17.83	16.52
Sulfur content in feed	mg/kg	4283	6720	5468
Mass flow rate of brine effluent	g/min	3.20	3.20	1.60
Final sulfur content in brine effluent	mg/kg	11994	25100	21825
Final sulfur content in reactor effluent	mg/kg	68	ND	108
Sulfur recovery in brine effluent	%	49.18	67.04	38.66

F. Summarized results of the final (second) microalgae gasification experiment

Parameter	Unit	Value
Microalgae content (dry matter)	wt%	9.02
Setpoint for Slurry Feeder	Hz	23
Setpoint for Liquiflow	% (g/min)	60 (1.92)
Mass flow rate of feed	g/min	17.01
Mass flow rate of brine effluent	g/min	2.37
Mass flow rate of reactor effluent	g/min	12.50
Pressure	bar	280.00
T-profile inside salt separator	°C	300-430
Temperature inside reactor	°C	370-410
Time on stream of algal slurry	h	6.39
Conductivity of feed	µS/cm	16100
Final conductivity of brine effluent	µS/cm	87800
Final conductivity of reactor effluent	µS/cm	29300
C-recovery in brine- & reactor effluent	%	0.55 & 2.05
N-recovery in brine- & reactor effluent	%	12.61 & 61.15
S-recovery in brine- & reactor effluent	%	< 46.80 & < 5.15
K-recovery in brine- & reactor effluent	%	138.18 & ND
Na-recovery in brine- & reactor effluent	%	118.91 & 0.65
P-recovery in brine- & reactor effluent	%	61.92 & ND
TOC- & TIC content of reactor effluent	mg/L	< 1000 & < 3500
H_2-, CH_4-, CO_2- & CO-concentration in product gas (dry)	vol%	7, 57, 0.03 & 36
Reactor filling - amount	g	528.5 (Katalco), 443.5 (Ru/C)
WHSV[(a)]	g_{Org}/g_{Cat}-h	< 0.21[(b)]

[(a)]WHSV = weight hourly space velocity used in units of hourly rate of algae (dry matter) processed over the grams of catalyst.

[(b)]0.21, if the entire organic material from the feed left the salt separator at the top and passed the catalyst.

G. CNS analysis

Table G.1: Sulfur content of feed, brine effluent and reactor effluent (Na_2SO_4-K_2SO_4-H_2O, first salt separation test).

Sample	Time on stream (in h)	S-content (in mg/kg)	SD
4F-1	-	4283	24
4SB-1	1.51	183	26
4SB-2	1.84	882	62
4SB-3	2.18	4088	78
4SB-5	2.84	8637	127
4SB-7	3.51	10275	742
4SB-9	4.18	11994	193
4RL-1	1.51	85	10
4RL-4	2.51	80	9
4RL-7	3.51	72	4
4RL-9	4.18	68	3

Table G.2: Sulfur content of feed and brine effluent (Na_2SO_4-K_2SO_4-IPA-H_2O, second salt separation test).

Sample	Time on stream (in h)	S-content (in mg/kg)	SD
3F-1	-	6720	249
3SB-1	3.10	ND	ND
3SB-2	3.43	4680	312
3SB-3	3.76	17150	493
3SB-4	4.10	15310	971
3SB-5	4.43	20520	1678
3SB-6	4.76	21830	1950
3SB-7	5.10	25100	2524
3SB-8	5.43	25820	1691
3SB-9	5.76	25130	2082

Sulfur content in the reactor effluent samples was below the detection limit.

Table G.3: Sulfur content of feed, brine effluent and reactor effluent (Na_2SO_4-K_2SO_4-IPA-H_2O, third salt separation test).

Sample	Time on stream (in h)	S-content (in mg/kg)	SD
6F-1	-	5468	1469
6SB-1	2.58	93	11
6SB-4	3.58	2094	111
6SB-5	3.92	10193	1353
6SB-7	4.58	18800	156
6SB-8	4.92	21825	1710
6ST-2	2.92	245	61
6ST-6	4.25	136	15
6ST-8	4.92	108	2

Table G.4: Carbon-, nitrogen- and sulfur content of feed and brine effluent (first liquefaction test).

Sample	Time on stream (in h)	N-content (in mg/kg)	SD	C-content (in mg/kg)	SD	S-content (in mg/kg)	SD
7F-1	-	7700	100	49333	306	1825	85
7SB-1	3.11	35	61	211	183	359	77
7SB-3	3.66	2820	181	8843	60	645	8
7SB-5	4.33	5790	882	20052	961	1678	224
7SB-7	4.99	6894	337	22643	264	2498	29
7SB-9	5.66	6529	120	19238	159	2595	35
7SB-10	5.99	7206	104	21514	209	2113	73

Table G.5: Carbon-, nitrogen- and sulfur content in the aqueous phase of the reactor effluent (first liquefaction test).

Sample	Time on stream (in h)	N-content (in mg/kg)	SD	C-content (in mg/kg)	SD	S-content (in mg/kg)	SD
7ST-1	3.11	213	71	599	59	20	5
7ST-3	3.66	6172	47	17947	207	120	15
7ST-5	4.33	6410	59	17558	178	144	3
7ST-7	4.99	6576	58	17026	15	133	5
7ST-9	5.66	6842	23	18814	819	124	29
7ST-10	5.99	6798	166	22243	244	152	12

Table G.6: Carbon-, nitrogen- and sulfur content of feed and brine effluent (second liquefaction test).

Sample	Time on stream (in h)	N-content (in mg/kg)	SD	C-content (in mg/kg)	SD	S-content (in mg/kg)	SD
8F-1	-	4950	495	29450	71	1206	86
8SB-1	0.40	139	60	277	60	264	43
8SB-2	0.73	244	60	2791	60	188	22
8SB-3	1.07	2217	317	11224	61	387	3
8SB-4	1.40	3737	611	18687	477	616	13
8SB-5	1.73	4156	59	28094	567	894	30
8SB-6	2.07	4774	429	30910	1249	1006	7

Table G.7: Carbon-, nitrogen- and sulfur content of feed and brine effluent (third liquefaction test).

Sample	Time on stream (in h)	N-content (in mg/kg)	SD	C-content (in mg/kg)	SD	S-content (in mg/kg)	SD
9F-1	-	5650	71	32300	566	1329	63
9SB-1	4.78	615	121	289	40	378	48
9SB-2	5.12	2323	394	5548	394	467	94
9SB-3	5.45	3233	181	10012	181	627	27
9SB-5	6.12	4956	267	16179	858	920	25
9SB-7	6.78	4576	563	15916	171	850	2

Table G.8: Carbon-, nitrogen- and sulfur content of feed and brine effluent (fourth liquefaction test).

Sample	Time on stream (in h)	N-content (in mg/kg)	SD	C-content (in mg/kg)	SD	S-content (in mg/kg)	SD
10F-1	-	3700	0	24350	71	1197	102
10SB-1	3.30	105	60	314	0	213	39
10SB-3	3.97	210	0	1577	0	195	18
10SB-5	4.63	2157	162	9125	0	561	10
10SB-7	5.30	2642	0	10358	0	655	5
10SB-9	5.97	2756	280	11093	523	680	7
10SB-11	6.63	3748	373	13544	162	853	11
10SB-12	6.97	3573	590	13613	284	774	4

Table G.9: Carbon-, nitrogen- and sulfur content in the aqueous phase of the reactor effluent (fourth liquefaction test).

Sample	Time on stream (in h)	N-content (in mg/kg)	SD	C-content (in mg/kg)	SD	S-content (in mg/kg)	SD
10RL-1	3.30	108	6	388	18	16	3
10RL-3	3.97	1648	89	5294	44	19	3
10RL-5	4.63	2394	56	7340	82	26	6
10RL-7	5.30	2974	273	10294	775	36	9
10RL-9	5.97	3239	76	9169	119	35	4
10RL-11	6.63	2406	56	7000	75	30	3
10RL-12	6.97	2383	64	7837	269	34	4

Table G.10: Carbon-, nitrogen- and sulfur content of feed, brine effluent and reactor effluent (first gasification test).

Sample	Time on stream (in h)	N-content (in mg/kg)	SD	C-content (in mg/kg)	SD	S-content (in mg/kg)	SD
11F-1	-	6300	173	39567	971	1498	219
11SB-1	0.79	69	60	300	0	427	0
11SB-2	1.12	344	260	103	0	144	20
11SB-4	1.79	1888	126	5990	0	362	8
11SB-5	2.62	3386	344	10123	62	548	7
11RL-2	1.12	70	60	104	0	103	11
11RL-4	1.79	4298	104	690	120	76	11
11RL-5	2.62	4588	60	517	0	58	4

Table G.11: Carbon-, nitrogen- and sulfur content of feed, brine effluent and reactor effluent (second gasification test).

Sample	Time on stream (in h)	N-content (in mg/kg)	SD	C-content (in mg/kg)	SD	S-content (in mg/kg)	SD
12F-1	-	5467	58	33833	115	956	13
12SB-1	1.70	375	531	107	0	92	3
12SB-5	3.39	3816	184	4981	6726	678	1
12SB-9	4.80	4464	396	1325	604	809	14
12SB-11	5.80	5030	159	1526	262	1037	26
12SB-12	7.55	4946	278	1333	161	1854	33
12RL-1	1.70	69	60	104	0	85	6
12RL-5	3.39	4412	0	473	74	65	4
12RL-9	4.80	4566	60	802	60	58	7
12RL-12	7.55	4550	61	945	0	67	6

H. Off-line GC analysis

Table H.1: Composition of the gas phase of the reactor effluent (second liquefaction test).

CO_2 (in vol%)	SD	H_2 (in vol%)	SD	CH_4 (in vol%)	SD	CO (in vol%)	SD
92.32	0.08	0.00	0.00	4.79	0.09	2.89	0.01

Time: 11:38-11:57, Time on stream: 1.03-1.35 h, Volume: 1120 mL.

Table H.2: Composition of the gas phase of the reactor effluent (fourth liquefaction test).

#	CO_2 (in vol%)	SD	H_2 (in vol%)	SD	CH_4 (in vol%)	SD	CO (in vol%)	SD
1[(a)]	41.92	0.78	56.46	0.77	1.61	0.02	0.00	0.00
2[(b)]	49.75	0.24	49.05	0.31	1.19	0.06	0.00	0.00

[(a)]Time: 13:13-13:25, Time on stream: 4.37-4.57 h, Volume: 640 mL.

[(b)]Time: 14:15-14:24, Time on stream: 5.40-5.55 h, Volume: 1000 mL.

I. ICP-OES analysis

Table I.1: Potassium- and sodium content of feed, brine effluent and reactor effluent (second gasification test).

Sample	Time on stream (in h)	K-content (in mg/L)	SD	Na-content (in mg/L)	SD
12F-1	-	1161	4	2492	11
12SB-1	1.70	ND	ND	39	2
12SB-2	2.14	ND	ND	48	1
12SB-3	2.47	ND	ND	145	3
12SB-4	2.97	379	7	1552	7
12SB-5	3.39	881	2	2583	34
12SB-6	3.80	1405	17	3435	28
12SB-7	4.14	1416	15	3312	53
12SB-8	4.47	1493	8	3155	24
12SB-9	4.80	2675	206	5278	448
12SB-10	5.30	2268	1	5241	65
12SB-11	5.80	3878	7	8288	94
12SB-12	7.55	11514	59	21267	97
12RL-1	1.70	ND	ND	18	1
12RL-2	2.14	ND	ND	20	1
12RL-3	2.47	ND	ND	20	1
12RL-4	2.97	ND	ND	19	1
12RL-5	3.39	ND	ND	20	1
12RL-6	3.80	ND	ND	20	1
12RL-7	4.14	ND	ND	24	0
12RL-8	4.47	ND	ND	0	0
12RL-9	4.80	ND	ND	0	ND
12RL-10	5.30	ND	ND	22	1
12RL-11	5.80	ND	ND	23	1
12RL-12	7.55	ND	ND	22	1

Table I.2: Phosphorus- and sulfur content of feed, brine effluent and reactor effluent (second gasification test).

Sample	Time on stream (in h)	P-content (in mg/L)	SD	S-content (in mg/L)	SD
12F-1	-	1537	9	760	7
12SB-1	1.70	23	1	ND	ND
12SB-2	2.14	28	0	197	1
12SB-3	2.47	68	1	223	2
12SB-4	2.97	621	3	788	8
12SB-5	3.39	1090	4	1090	12
12SB-6	3.80	1494	13	1278	3
12SB-7	4.14	1408	10	1322	6
12SB-8	4.47	1339	4	1420	11
12SB-9	4.80	2325	162	2013	118
12SB-10	5.30	2071	13	1488	12
12SB-11	5.80	2886	3	1560	12
12SB-12	7.55	6831	51	2553	42
12RL-1	1.70	ND	ND	ND	ND
12RL-2	2.14	ND	ND	ND	ND
12RL-3	2.47	4	1	190	2
12RL-4	2.97	ND	ND	ND	ND
12RL-5	3.39	ND	ND	185	3
12RL-6	3.80	ND	ND	ND	ND
12RL-7	4.14	2	1	192	3
12RL-8	4.47	ND	ND	190	1
12RL-9	4.80	2	1	ND	ND
12RL-10	5.30	3	0	ND	ND
12RL-11	5.80	ND	ND	ND	ND
12RL-12	7.55	ND	ND	ND	ND

J. Comments on feed concentration

Since the experimental schedule was very tight, there was no time to fully analyze and evaluate each experiment in between. Therefore, it took until the fourth liquefaction test when the discontinuity of the CNS analysis of the feed was noticed. Variations of up to about 20% could be explained by inhomogeneity due to settling and difference between the sample of the feed and bulk. But the fact that the CNS values of the feed of the second and especially the fourth liquefaction experiment were much lower than the ones of the other microalgae tests, was very surprising. As described in Section 3.3.2, the dry matter content of Phaeodactylum tricornutum delivered from Subitec was only determined for the first package since it coincided with the value stated on it. However, after having discovered those CNS variations, the dry matter content of other packages was examined. Some of the determined values did not match with the stated ones. One package contained about 7.7% and another one about 5.3% instead of 13%. As a result, the algal slurries for the second, the fourth and also for the third liquefaction test were unwittingly diluted during feed preparation.

K. Pictures of brine- and reactor effluent samples

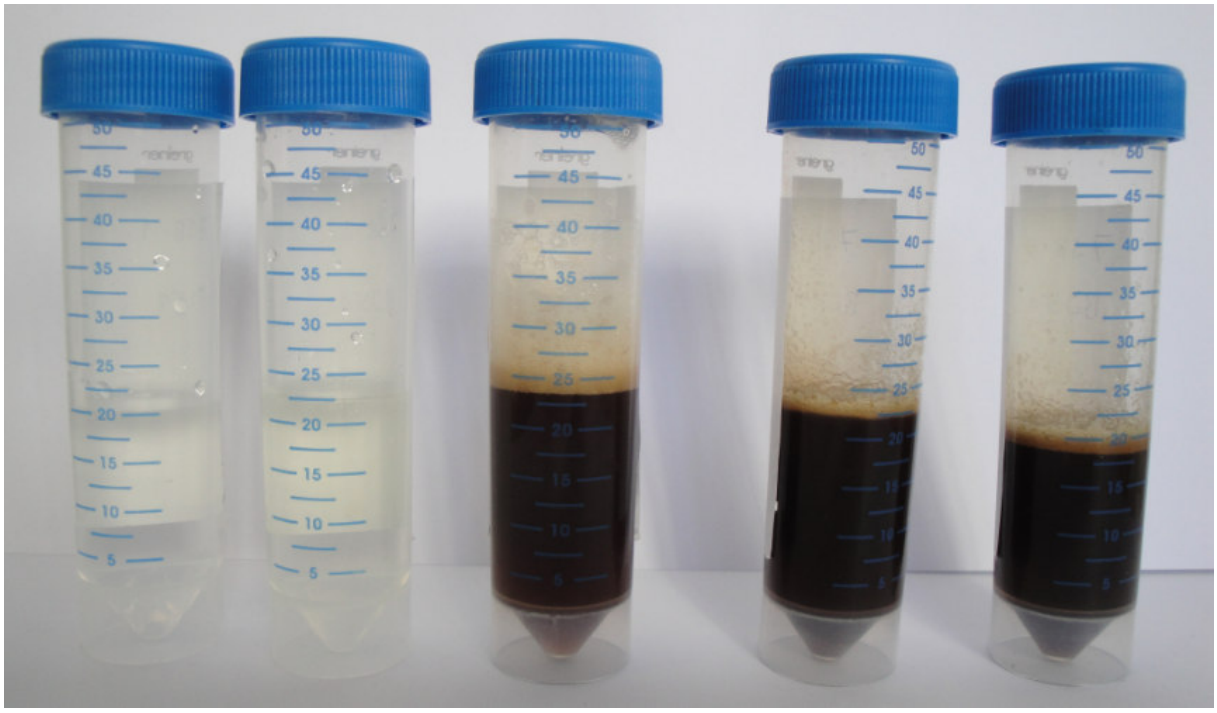

Figure K.1: Brine effluent samples of the first liquefaction test.

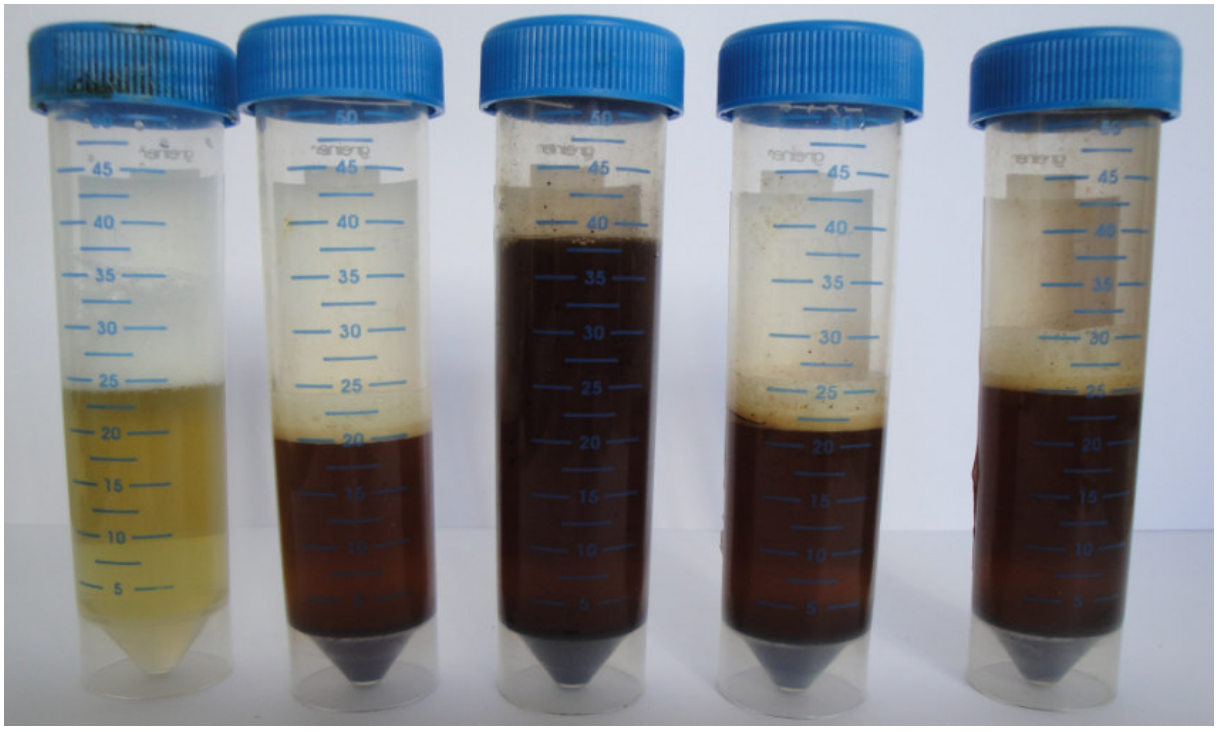

Figure K.2: Reactor effluent samples of the first liquefaction test.

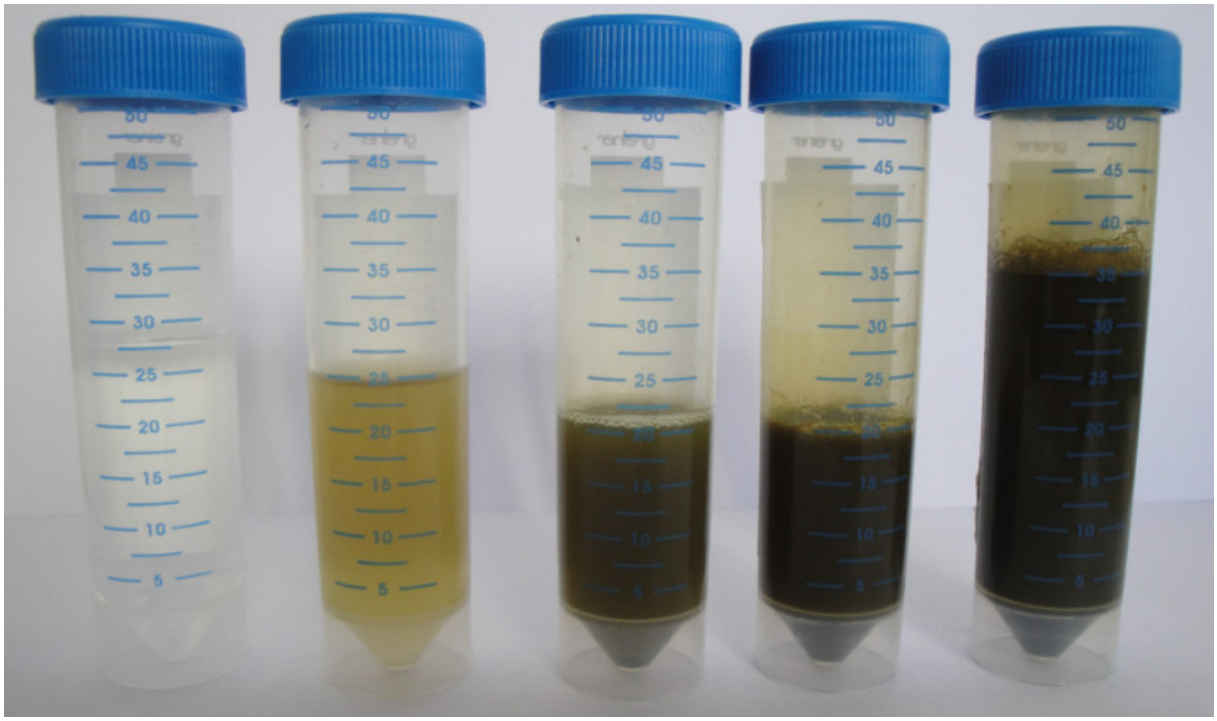

Figure K.3: Brine effluent samples of the second liquefaction test.

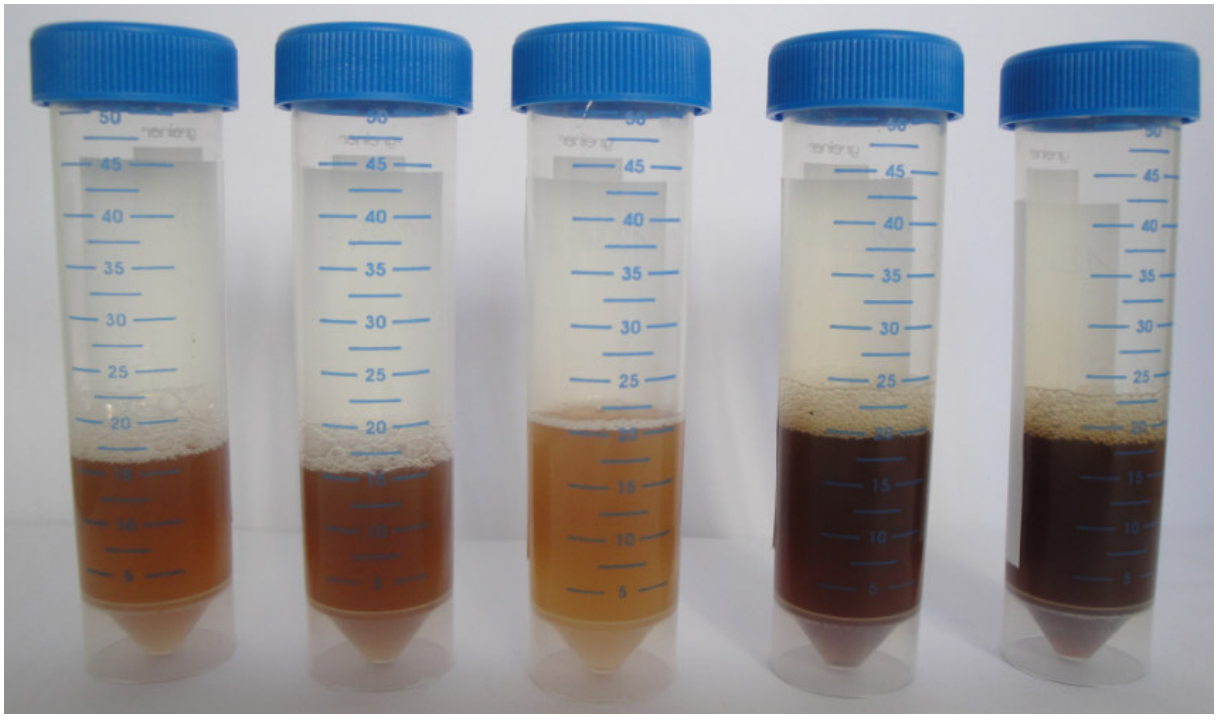

Figure K.4: Brine effluent samples of the second gasification test.

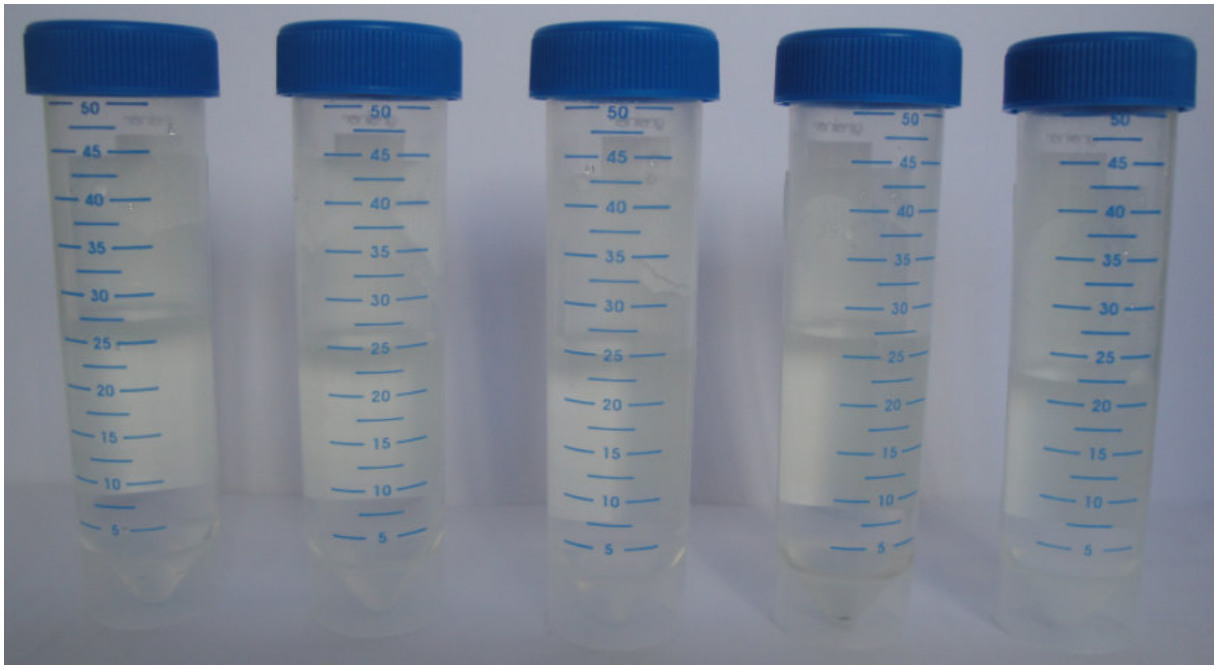

Figure K.5: Reactor effluent samples of the second gasification test.

References

[1] Douglas C Elliott, Todd R Hart, Gary G Neuenschwander, Leslie J Rotness, Mariefel V Olarte, and Alan H Zacher. Chemical processing in high-pressure aqueous environments. 9. process development for catalytic gasification of algae feedstocks. *Industrial & Engineering Chemistry Research*, 51(33):10768–10777, 2012.

[2] Martin Brandenberger. *Process Development for Catalytic Supercritical Water Gasification of Algae Feedstocks*. PhD thesis, EPFL (CH), 2014.

[3] ESRL Web Team et al. ESRL Global Monitoring Division, http://www.esrl.noaa.gov/gmd/ccgg/trends/, (retrieved May 18, 2014).

[4] *EU energy in figures 2014*. Publications office of the European Union, Luxembourg, 2014.

[5] Gordana Vunjak-Novakovic, Yoojeong Kim, Xiaoxi Wu, Isaac Berzin, and Jose C Merchuk. Air-lift bioreactors for algal growth on flue gas: mathematical modeling and pilot-plant studies. *Industrial & engineering chemistry research*, 44(16):6154–6163, 2005.

[6] BP, http://www.bp.com/en/global/corporate/about-bp/energy-economics/statistical-review-of-world-energy/review-by-energy-type/natural-gas/natural-gas-trade-movements.html, (retrieved September 17, 2014).

[7] E.W. Lemmon, M.O. McLinden, and D.G. Friend. *"Thermophysical Properties of Fluid Systems" in NIST Chemistry WebBook, NIST Standard Reference Database Number 69*. Eds. P.J. Linstrom and W.G. Mallard, National Institute of Standards and Technology, Gaithersburg MD, 20899, http://webbook.nist.gov (retrieved April 05, 2014).

[8] DP Fernandez, ARH Goodwin, Eric W Lemmon, JMH Levelt Sengers, and RC Williams. A formulation for the static permittivity of water and steam at temperatures from 238 k to 873 k at pressures up to 1200 mpa, including derivatives and debye–hückel coefficients. *Journal of Physical and Chemical Reference Data*, 26(4):1125–1166, 1997.

[9] Andrei V Bandura and Serguei N Lvov. The ionization constant of water over wide ranges of temperature and density. *Journal of physical and chemical reference data*, 35(1):15–30, 2005.

[10] Frédéric Vogel. *Catalytic Conversion of High-Moisture Biomass to Synthetic Natural Gas in Supercritical Water*. Wiley-VCH Verlag GmbH & Co. KGaA, 2010.

[11] *Biomass : green energy for Europe*. EUR-OP, Luxembourg, 2005.

[12] Anca G Haiduc, Martin Brandenberger, Sébastien Suquet, Frédéric Vogel, Rizlan Bernier-Latmani, and Christian Ludwig. SunCHem: an integrated process for the hydrothermal production of methane from microalgae and CO2 mitigation. *Journal of applied phycology*, 21(5):529–541, 2009.

[13] Andres F Clarens, Eleazer P Resurreccion, Mark A White, and Lisa M Colosi. Environmental life cycle comparison of algae to other bioenergy feedstocks. *Environmental science & technology*, 44(5):1813–1819, 2010.

[14] Per S Christensen, Gaël Peng, Frédéric Vogel, and Bo B Iversen. Hydrothermal liquefaction of the microalgae phaeodactylum tricornutum: Impact of reaction conditions on product and elemental distribution. *Energy & Fuels*, 2014.

[15] International Energy Agency, editor. *Key World Energy Statistics*. 2014.

[16] Stocker and D Qin. Climate change 2013: The physical science basis. *Working Group I Contribution to the Fifth Assessment Report of the Intergovernmental Panel on Climate Change, Summary for Policymakers, IPCC*, 2013.

[17] EC European Commission et al. Directive 2009/28/ec of the european parliament and of the council of 23 april 2009 on the promotion of the use of energy from renewable sources and amending and subsequently repealing directives 2001/77/ec and 2003/30. *Official Journal of the European Union Belgium*, 2009.

[18] Arthouros Zervos, Christine Lins, and Josche Muth. *RE-thinking 2050: a 100% renewable energy vision for the European Union*. EREC, 2010.

[19] Bram van der Drift, Serge Biollaz, Lars Waldheim, Reinhard Rauch, and Chris Manson-Whitton. Status and future of biosng in europe. *Energy*, 2012.

[20] Martin Kaltschmitt. *Energie aus Biomasse : Grundlagen, Techniken und Verfahren*. Springer-Verlag Berlin Heidelberg, 2009.

[21] AV Bridgwater and GVC Peacocke. Fast pyrolysis processes for biomass. *Renewable and Sustainable Energy Reviews*, 4(1):1–73, 2000.

[22] S Wehlte, D Meier, J Moltran, and O Faix. The impact of wood preservatives on the flash pyrolysis of biomass. In *Developments in thermochemical biomass conversion*, pages 206–219. Springer, 1997.

[23] Paul T Williams and Serpil Besler. The influence of temperature and heating rate on the slow pyrolysis of biomass. *Renewable Energy*, 7(3):233–250, 1996.

[24] Jan Kopyscinski, Tilman J Schildhauer, and Serge Biollaz. Production of synthetic natural gas (sng) from coal and dry biomass–a technology review from 1950 to 2009. *Fuel*, 89(8):1763–1783, 2010.

[25] Reinhard Rauch, Jitka Hrbek, and Hermann Hofbauer. Biomass gasification for synthesis gas production and applications of the syngas. *Wiley Interdisciplinary Reviews: Energy and Environment*, 2013.

[26] G Schuster, G Löffler, K Weigl, and H Hofbauer. Biomass steam gasification–an extensive parametric modeling study. *Bioresource technology*, 77(1):71–79, 2001.

[27] Yebo Li, Stephen Y Park, and Jiying Zhu. Solid-state anaerobic digestion for methane production from organic waste. *Renewable and sustainable energy reviews*, 15(1):821–826, 2011.

[28] Tony Bridgwater. Biomass for energy. *Journal of the Science of Food and Agriculture*, 86(12):1755–1768, 2006.

[29] Jerry R Taricska, David A Long, J Paul Chen, Yung-Tse Hung, and Shuai-Wen Zou. Anaerobic digestion. In *Biosolids Treatment Processes*, pages 135–176. Springer, 2007.

[30] Christian Stevens and Robert C Brown. *Thermochemical processing of biomass: conversion into fuels, chemicals and power*, volume 12. John Wiley & Sons, 2011.

[31] Andrew A Peterson, Frédéric Vogel, Russell P Lachance, Morgan Fröling, Michael J Antal Jr, and Jefferson W Tester. Thermochemical biofuel production in hydrothermal media: a review of sub-and supercritical water technologies. *Energy & Environmental Science*, 1(1):32–65, 2008.

[32] Yanqun Li, Mark Horsman, Nan Wu, Christopher Q Lan, and Nathalie Dubois-Calero. Biofuels from microalgae. *Biotechnology progress*, 24(4):815–820, 2008.

[33] Paul Chen, Min Min, Ylfeng Chen, Liang Wang, Yecong Li, Qin Chen, Chengguang Wang, Yiqin Wan, Xiaoquan Wang, Yanling Cheng, et al. Review of the biological and engineering aspects of algae to fuels approach. *International Journal of Agricultural & Biological Engineering*, 2(4), 2009.

[34] Rojan P John, GS Anisha, K Madhavan Nampoothiri, and Ashok Pandey. Micro and macroalgal biomass: a renewable source for bioethanol. *Bioresource Technology*, 102(1):186–193, 2011.

[35] Amos Richmond. *Handbook of microalgal culture: biotechnology and applied phycology*. John Wiley & Sons, 2008.

[36] J Masojídek, G Torzillo, J Sven Erik, and F Brian. Mass cultivation of freshwater microalgae. *Encyclopedia of ecology*, pages 2226–2235, 2008.

[37] Teresa M Mata, António A Martins, and Nidia S Caetano. Microalgae for biodiesel production and other applications: a review. *Renewable and Sustainable Energy Reviews*, 14(1):217–232, 2010.

[38] Liam Brennan and Philip Owende. Biofuels from microalgae–a review of technologies for production, processing, and extractions of biofuels and co-products. *Renewable and sustainable energy reviews*, 14(2):557–577, 2010.

[39] Razif Harun, Manjinder Singh, Gareth M Forde, and Michael K Danquah. Bioprocess engineering of microalgae to produce a variety of consumer products. *Renewable and Sustainable Energy Reviews*, 14(3):1037–1047, 2010.

[40] Chun-Yen Chen, Kuei-Ling Yeh, Rifka Aisyah, Duu-Jong Lee, and Jo-Shu Chang. Cultivation, photobioreactor design and harvesting of microalgae for biodiesel production: a critical review. *Bioresource technology*, 102(1):71–81, 2011.

[41] Shakeel A Khan, Mir Z Hussain, S Prasad, UC Banerjee, et al. Prospects of biodiesel production from microalgae in india. *Renewable and Sustainable Energy Reviews*, 13(9):2361–2372, 2009.

[42] Liliana Rodolfi, Graziella Chini Zittelli, Niccolò Bassi, Giulia Padovani, Natascia Biondi, Gimena Bonini, and Mario R Tredici. Microalgae for oil: Strain selection, induction of lipid synthesis and outdoor mass cultivation in a low-cost photobioreactor. *Biotechnology and bioengineering*, 102(1):100–112, 2009.

[43] Jon K Pittman, Andrew P Dean, and Olumayowa Osundeko. The potential of sustainable algal biofuel production using wastewater resources. *Bioresource technology*, 102(1):17–25, 2011.

[44] Martin Banse, Hans Van Meijl, Andrzej Tabeau, Geert Woltjer, Fritz Hellmann, and Peter H Verburg. Impact of eu biofuel policies on world agricultural production and land use. *Biomass and Bioenergy*, 35(6):2385–2390, 2011.

[45] Poonam Singh Nigam and Anoop Singh. Production of liquid biofuels from renewable resources. *Progress in energy and combustion science*, 37(1):52–68, 2011.

[46] Jan B van Beilen. Why microalgal biofuels won't save the internal combustion machine. *Biofuels, Bioproducts and Biorefining*, 4(1):41–52, 2010.

[47] Ryan Davis, Andy Aden, and Philip T Pienkos. Techno-economic analysis of autotrophic microalgae for fuel production. *Applied Energy*, 88(10):3524–3531, 2011.

[48] JGG Jonker and APC Faaij. Techno-economic assessment of micro-algae as feedstock for renewable bio-energy production. *Applied Energy*, 102:461–475, 2013.

[49] Martin Brandenberger, J Matzenberger, F Vogel, and Ch Ludwig. Producing synthetic natural gas from microalgae via supercritical water gasification: A techno-economic sensitivity analysis. *Biomass and Bioenergy*, 51:26–34, 2013.

[50] Christian Bach and S Lienin. Emissionsvergleich verschiedener antriebsarten in aktuellen personenwagen. *Untersuchung der Emissionen von aktuellen Personenwagen mit konventionellen und direkteingespritzten Benzinmotoren, Dieselmotoren mit und ohne Partikelfilter sowie Erdgasmotoren. Dübendorf, CH: EMPA Materials Science and Technology*, 2007.

[51] Igor Pioro and Sarah Mokry. Thermophysical properties at critical and supercritical conditions. *Heat Transfer Theoretical Analysis, Experimental Investigations and Industrial Systems. InTech, Rijeka*, 2011.

[52] Hans Baehr. *Thermodynamik Grundlagen und technische Anwendungen*. Springer Vieweg, Berlin Heidelberg, 2012.

[53] AD Chistyakov. The permittivity of water and water vapor in saturation states. *Russian Journal of Physical Chemistry*, 81(1):5–8, 2007.

[54] W. M. Haynes. *CRC Handbook of Chemistry and Physics, 94th Edition (Internet Version 2014)*. CRC Press/Taylor and Francis, Boca Raton, FL.

[55] A Kruse and E Dinjus. Hot compressed water as reaction medium and reactant: properties and synthesis reactions. *The Journal of Supercritical Fluids*, 39(3):362–380, 2007.

[56] Jefferson W Tester, Philip A Marrone, Matthew M DiPippo, Kentaro Sako, Matthew T Reagan, Tomas Arias, and William A Peters. Chemical reactions and phase equilibria of model halocarbons and salts in sub-and supercritical water (200–300 bar, 100–600 c). *The Journal of supercritical fluids*, 13(1):225–240, 1998.

[57] Michael Modell. Gasification and liquefaction of forest products in supercritical water. In *Fundamentals of thermochemical biomass conversion*, pages 95–119. Springer, 1985.

[58] Andrea Kruse. Supercritical water gasification. *Biofuels, Bioproducts and Biorefining*, 2(5):415–437, 2008.

[59] Martin Schubert, Johann W Regler, and Frédéric Vogel. Continuous salt precipitation and separation from supercritical water. part 1: Type 1 salts. *The Journal of Supercritical Fluids*, 52(1):99–112, 2010.

[60] Martin Schubert, Johann W Regler, and Frédéric Vogel. Continuous salt precipitation and separation from supercritical water. part 2. type 2 salts and mixtures of two salts. *The Journal of Supercritical Fluids*, 52(1):113–124, 2010.

[61] Martin Schubert, John Aubert, Johannes B Müller, and Frédéric Vogel. Continuous salt precipitation and separation from supercritical water. part 3: Interesting effects in processing type 2 salt mixtures. *The Journal of Supercritical Fluids*, 61:44–54, 2012.

[62] Martin Schubert. *Catalytic Hydrothermal Gasification of Biomass - Salt Recovery and Continuous Gasification of Glycerol*. PhD thesis, ETH Zürich (CH), 2010.

[63] Hermann Weingärtner and Ernst Ulrich Franck. Überkritisches wasser als lösungsmittel. *Angewandte Chemie*, 117(18):2730–2752, 2005.

[64] W Bühler, E Dinjus, HJ Ederer, A Kruse, and C Mas. Ionic reactions and pyrolysis of glycerol as competing reaction pathways in near-and supercritical water. *The Journal of Supercritical Fluids*, 22(1):37–53, 2002.

[65] Mitsumasa Osada, Takafumi Sato, Masaru Watanabe, Masayuki Shirai, and Kunio Arai. Catalytic gasification of wood biomass in subcritical and supercritical water. *Combustion Science and Technology*, 178(1-3):537–552, 2006.

[66] A Kruse and A Gawlik. Biomass conversion in water at 330-410 c and 30-50 mpa. identification of key compounds for indicating different chemical reaction pathways. *Industrial & Engineering Chemistry Research*, 42(2):267–279, 2003.

[67] Phillip E Savage, Sudhama Gopalan, Thamid I Mizan, Christopher J Martino, and Eric E Brock. Reactions at supercritical conditions: applications and fundamentals. *AIChE Journal*, 41(7):1723–1778, 1995.

[68] Saqib Sohail Toor, Lasse Rosendahl, and Andreas Rudolf. Hydrothermal liquefaction of biomass: a review of subcritical water technologies. *Energy*, 36(5):2328–2342, 2011.

[69] Andrew A Peterson, Russell P Lachance, and Jefferson W Tester. Kinetic evidence of the maillard reaction in hydrothermal biomass processing: Glucose- glycine interactions in high-temperature, high-pressure water. *Industrial & Engineering Chemistry Research*, 49(5):2107–2117, 2010.

[70] F Gelin, JK Volkman, C Largeau, S Derenne, JS Sinninghe Damsté, and JW De Leeuw. Distribution of aliphatic, nonhydrolyzable biopolymers in marine microalgae. *Organic Geochemistry*, 30(2):147–159, 1999.

[71] Diego López Barreiro, Wolter Prins, Frederik Ronsse, and Wim Brilman. Hydrothermal liquefaction (htl) of microalgae for biofuel production: State of the art review and future prospects. *Biomass and Bioenergy*, 53:113–127, 2013.

[72] Cristian Torri, Laura Garcia Alba, Chiara Samorì, Daniele Fabbri, and Derk WF Brilman. Hydrothermal treatment (htt) of microalgae: detailed molecular characterization of htt oil in view of htt mechanism elucidation. *Energy & Fuels*, 26(1):658–671, 2012.

[73] Sivamohan N Reddy, Sonil Nanda, Ajay K Dalai, and Janusz A Kozinski. Supercritical water gasification of biomass for hydrogen production. *International Journal of Hydrogen Energy*, 39(13):6912–6926, 2014.

[74] N Boukis, V Diem, W Habicht, and E Dinjus. Methanol reforming in supercritical water. *Industrial & Engineering Chemistry Research*, 42(4):728–735, 2003.

[75] LJ Guo, YJ Lu, XM Zhang, CM Ji, Y Guan, and AX Pei. Hydrogen production by biomass gasification in supercritical water: a systematic experimental and analytical study. *Catalysis Today*, 129(3):275–286, 2007.

[76] Qiuhui Yan, Liejin Guo, and Youjun Lu. Thermodynamic analysis of hydrogen production from biomass gasification in supercritical water. *Energy conversion and management*, 47(11):1515–1528, 2006.

[77] Daniele Castello and Luca Fiori. Supercritical water gasification of biomass: thermodynamic constraints. *Bioresource technology*, 102(16):7574–7582, 2011.

[78] Yousef M Alshammari and Klaus Hellgardt. Thermodynamic analysis of hydrogen production via hydrothermal gasification of hexadecane. *International Journal of Hydrogen Energy*, 37(7):5656–5664, 2012.

[79] FAP Voll, CCRS Rossi, C Silva, R Guirardello, ROMA Souza, VF Cabral, and L Cardozo-Filho. Thermodynamic analysis of supercritical water gasification of methanol, ethanol, glycerol, glucose and cellulose. *International Journal of Hydrogen Energy*, 34(24):9737–9744, 2009.

[80] Douglas C Elliott. Catalytic hydrothermal gasification of biomass. *Biofuels, Bioproducts and Biorefining*, 2(3):254–265, 2008.

[81] Y Guo, SZ Wang, DH Xu, YM Gong, HH Ma, and XY Tang. Review of catalytic supercritical water gasification for hydrogen production from biomass. *Renewable and Sustainable Energy Reviews*, 14(1):334–343, 2010.

[82] Pooya Azadi and Ramin Farnood. Review of heterogeneous catalysts for sub-and supercritical water gasification of biomass and wastes. *International Journal of Hydrogen Energy*, 36(16):9529–9541, 2011.

[83] Thomas M Yeh, Jacob G Dickinson, Allison Franck, Suljo Linic, Levi T Thompson, and Phillip E Savage. Hydrothermal catalytic production of fuels and chemicals from aquatic biomass. *Journal of Chemical Technology and Biotechnology*, 88(1):13–24, 2013.

[84] InfoMine Inc. InfoMine, http://www.infomine.com/investment/metal-prices/ruthenium/ (retrieved September 17, 2014).

[85] Zhen Ma and Francisco Zaera. Heterogeneous catalysis by metals. *Encyclopedia of Inorganic and Bioinorganic Chemistry*, 2005.

[86] Masaru Watanabe, Mitsumasa Osada, Hiroshi Inomata, Kunio Arai, and Andrea Kruse. Acidity and basicity of metal oxide catalysts for formaldehyde reaction in supercritical water at 673 k. *Applied Catalysis A: General*, 245(2):333–341, 2003.

[87] Douglas C Elliott, Todd R Hart, and Gary G Neuenschwander. Chemical processing in high-pressure aqueous environments. 8. improved catalysts for hydrothermal gasification. *Industrial & engineering chemistry research*, 45(11):3776–3781, 2006.

[88] Xiaodong Xu, Yukihiko Matsumura, Jonny Stenberg, and Michael Jerry Antal. Carbon-catalyzed gasification of organic feedstocks in supercritical water. *Industrial & Engineering Chemistry Research*, 35(8):2522–2530, 1996.

[89] Y Matsumura, X Xu, et al. Gasification characteristics of an activated carbon in supercritical water. *Carbon*, 35(6):819–824, 1997.

[90] Maurice H Waldner and Frédéric Vogel. Renewable production of methane from woody biomass by catalytic hydrothermal gasification. *Industrial & engineering chemistry research*, 44(13):4543–4551, 2005.

[91] Hideki Takahashi, Stanislav Kopriva, Mario Giordano, Kazuki Saito, and Rüdiger Hell. Sulfur assimilation in photosynthetic organisms: molecular functions and regulations of transporters and assimilatory enzymes. *Annual review of plant biology*, 62:157–184, 2011.

[92] Maurice H Waldner, Frank Krumeich, and Frédéric Vogel. Synthetic natural gas by hydrothermal gasification of biomass: selection procedure towards a stable catalyst and its sodium sulfate tolerance. *The Journal of Supercritical Fluids*, 43(1):91–105, 2007.

[93] Waldner. *Catalytic Hydrothermal Gasification of Biomass for the Production of Synthetic Natural Gas*. PhD thesis, ETH Zürich (CH), 2007.

[94] Mitsumasa Osada, Norihito Hiyoshi, Osamu Sato, Kunio Arai, and Masayuki Shirai. Reaction pathway for catalytic gasification of lignin in presence of sulfur in supercritical water. *Energy & fuels*, 21(4):1854–1858, 2007.

[95] Mitsumasa Osada, Norihito Hiyoshi, Osamu Sato, Kunio Arai, and Masayuki Shirai. Effect of sulfur on catalytic gasification of lignin in supercritical water. *Energy & fuels*, 21(3):1400–1405, 2007.

[96] Douglas C Elliott, Gary G Neuenschwander, Todd R Hart, R Scott Butner, Alan H Zacher, Mark H Engelhard, James S Young, and David E McCready. Chemical processing in high-pressure aqueous environments. 7. process development for catalytic gasification of wet biomass feedstocks. *Industrial & engineering chemistry research*, 43(9):1999–2004, 2004.

[97] Hemma Zöhrer and Frédéric Vogel. Hydrothermal catalytic gasification of fermentation residues from a biogas plant. *Biomass and Bioenergy*, 53:138–148, 2013.

[98] Hemma Zöhrer. *Hydrothermal gasification of fermentation residues for SNG-production*. PhD thesis, ETH Zürich (CH), 2013.

[99] Marian Dreher, Benjamin Johnson, Andrew A Peterson, Maarten Nachtegaal, Jörg Wambach, and Frédéric Vogel. Catalysis in supercritical water: Pathway of the methanation reaction and sulfur poisoning over a ru/c catalyst during the reforming of biomolecules. *Journal of Catalysis*, 301:38–45, 2013.

[100] Marian Dreher. *Catalysis Under Extreme Conditions: in situ Studies of the Reforming of Organic Key Compounds in Supercritical Water*. PhD thesis, ETH Zürich (CH), 2013.

[101] H Zöhrer, M Schubert, and F Vogel. Regeneration methods for sulfur-poisoned catalysts in supercritical water gasification. *Chemie Ingenieur Technik*, 84(8):1305–1305, 2012.

[102] Marian Dreher, Matthias Steib, Maarten Nachtegaal, Jörg Wambach, and Frédéric Vogel. On-stream regeneration of a sulfur-poisoned ruthenium–carbon catalyst under hydrothermal gasification conditions. *ChemCatChem*, 2013.

[103] Tamer Karayıldırım, A Sınağ, and Andrea Kruse. Char and coke formation as unwanted side reaction of the hydrothermal biomass gasification. *Chemical engineering & technology*, 31(11):1561–1568, 2008.

[104] J Müller. *Hydrothermal gasification of biomass-investigation on coke formation and continuous salt separation with pure substrates and real biomass*. PhD thesis, ETH Zürich (CH), 2012.

[105] Peter Kritzer. Corrosion in high-temperature and supercritical water and aqueous solutions: a review. *The Journal of Supercritical Fluids*, 29(1):1–29, 2004.

[106] Philip A Marrone and Glenn T Hong. Corrosion control methods in supercritical water oxidation and gasification processes. *The Journal of Supercritical Fluids*, 51(2):83–103, 2009.

[107] Chunwen Sun, Rob Hui, Wei Qu, and Sing Yick. Progress in corrosion resistant materials for supercritical water reactors. *Corrosion Science*, 51(11):2508–2523, 2009.

[108] Jeremy S Luterbacher, Morgan Fröling, Frederic Vogel, François Maréchal, and Jefferson W Tester. Hydrothermal gasification of waste biomass: process design and life cycle asessment. *Environmental science & technology*, 43(5):1578–1583, 2009.

[109] Vaclav Smil. Phosphorus in the environment: natural flows and human interferences. *Annual review of energy and the environment*, 25(1):53–88, 2000.

[110] V.M. Valyashko. Chapter 15 - Phase equilibria of water-salt systems at high temperatures and pressures. In Donald A. Palmer, Roberto Fernández-Prini, and Allan H. Harvey, editors, *Aqueous Systems at Elevated Temperatures and Pressures*, pages 597 – 641. Academic Press, London, 2004.

[111] Andrew A Peterson, Peter Vontobel, Frédéric Vogel, and Jefferson W Tester. Normal-phase dynamic imaging of supercritical-water salt precipitation using neutron radiography. *The Journal of Supercritical Fluids*, 49(1):71–78, 2009.

[112] Herschel Hunt and HT Briscoe. The conductivity of solutions of some aliphatic organic acids in water and ethyl alcohol. *The Journal of Physical Chemistry*, 33(2):190–199, 1929.

[113] Tylisha M Brown, Peigao Duan, and Phillip E Savage. Hydrothermal liquefaction and gasification of nannochloropsis sp. *Energy & Fuels*, 24(6):3639–3646, 2010.

[114] Peigao Duan and Phillip E Savage. Hydrothermal liquefaction of a microalga with heterogeneous catalysts. *Industrial & Engineering Chemistry Research*, 50(1):52–61, 2011.

[115] Peter J Valdez, Jacob G Dickinson, and Phillip E Savage. Characterization of product fractions from hydrothermal liquefaction of nannochloropsis sp. and the influence of solvents. *Energy & Fuels*, 25(7):3235–3243, 2011.

[116] Umakanta Jena, KC Das, and JR Kastner. Effect of operating conditions of thermochemical liquefaction on biocrude production from spirulina platensis. *Bioresource technology*, 102(10):6221–6229, 2011.

[117] Laura Garcia Alba, Cristian Torri, Chiara Samorì, Jaapjan van der Spek, Daniele Fabbri, Sascha RA Kersten, and Derk WF Brilman. Hydrothermal treatment (htt) of microalgae:

evaluation of the process as conversion method in an algae biorefinery concept. *Energy & fuels*, 26(1):642–657, 2011.

[118] Douglas C Elliott, Todd R Hart, Andrew J Schmidt, Gary G Neuenschwander, Leslie J Rotness, Mariefel V Olarte, Alan H Zacher, Karl O Albrecht, Richard T Hallen, and Johnathan E Holladay. Process development for hydrothermal liquefaction of algae feedstocks in a continuous-flow reactor. *Algal Research*, 2(4):445–454, 2013.

[119] Christopher Jazrawi, Patrick Biller, Andrew B Ross, Alejandro Montoya, Thomas Maschmeyer, and Brian S Haynes. Pilot plant testing of continuous hydrothermal liquefaction of microalgae. *Algal Research*, 2(3):268–277, 2013.

[120] Ali Sınağ, Tuğrul Yumak, Volkan Balci, and Andrea Kruse. Catalytic hydrothermal conversion of cellulose over sno2 and zno nanoparticle catalysts. *The Journal of Supercritical Fluids*, 56(2):179–185, 2011.

[121] Sandra Sá, Hugo Silva, Lúcia Brandão, José M Sousa, and Adélio Mendes. Catalysts for methanol steam reforming - a review. *Applied Catalysis B: Environmental*, 99(1):43–57, 2010.

[122] Ahmed Bshish, Zahira Yaakob, Binitha Narayanan, Resmi Ramakrishnan, and Ali Ebshish. Steam-reforming of ethanol for hydrogen production. *Chemical Papers*, 65(3):251–266, 2011.

[123] Weijie Cai, Pilar Ramírez de la Piscina, and Narcis Homs. Oxidative steam reforming of bio-butanol for hydrogen production: effects of noble metals on bimetallic com/zno catalysts (m= ru, rh, ir, pd). *Applied Catalysis B: Environmental*, 145:56–62, 2014.

[124] AB Ross, P Biller, ML Kubacki, H Li, A Lea-Langton, and JM Jones. Hydrothermal processing of microalgae using alkali and organic acids. *Fuel*, 89(9):2234–2243, 2010.

[125] Jixiang Zhang and Yuanhui Zhang. Hydrothermal liquefaction of microalgae in an ethanol–water co-solvent to produce biocrude oil. *Energy & Fuels*, 28(8):5178–5183, 2014.

[126] Dong Zhou, Liang Zhang, Shicheng Zhang, Hongbo Fu, and Jianmin Chen. Hydrothermal liquefaction of macroalgae enteromorpha prolifera to bio-oil. *Energy & Fuels*, 24(7):4054–4061, 2010.

[127] Chao Gai, Yuanhui Zhang, Wan-Ting Chen, Yan Zhou, Lance Schideman, Peng Zhang, Giovana Tommaso, Chih-Ting Kuo, and Yuping Dong. Characterization of aqueous phase from the hydrothermal liquefaction of chlorella pyrenoidosa. *Bioresource Technology*, 2014.

[128] Wan-Ting Chen, Yuanhui Zhang, Jixiang Zhang, Guo Yu, Lance C Schideman, Peng Zhang, and Mitchell Minarick. Hydrothermal liquefaction of mixed-culture algal biomass from wastewater treatment system into bio-crude oil. *Bioresource technology*, 152:130–139, 2014.

[129] Amir H Mohammadi, Ross Anderson, and Bahman Tohidi. Carbon monoxide clathrate hydrates: equilibrium data and thermodynamic modeling. *AIChE journal*, 51(10):2825–2833, 2005.

[130] Mariluz Bagnoud-Velásquez, Martin Brandenberger, Frédéric Vogel, and Christian Ludwig. Continuous catalytic hydrothermal gasification of algal biomass and case study on toxicity of aluminum as a step toward effluents recycling. *Catalysis Today*, 223:35–43, 2014.